

January 01, 2011

## Connecting string theory to particle physics at the LHC

Ismet Baris Altunkaynak

---

### Recommended Citation

Altunkaynak, Ismet Baris, "Connecting string theory to particle physics at the LHC" (2011). *Physics Dissertations*. Paper 22.  
<http://hdl.handle.net/2047/d20000897>

This work is available open access, hosted by Northeastern University.

# Connecting String Theory to Particle Physics at the LHC

A dissertation presented

by

Ismet Baris Altunkaynak

to

The Department of Physics

In partial fulfillment of the requirements for the degree of

Doctor of Philosophy

in the field of

Physics

Northeastern University

Boston, Massachusetts

May, 2011

©Ismet Baris Altunkaynak, 2011

ALL RIGHTS RESERVED

# Connecting String Theory to Particle Physics at the LHC

by

Ismet Baris Altunkaynak

## ABSTRACT OF DISSERTATION

Submitted in partial fulfillment of the requirement  
for the degree of Doctor of Philosophy in Physics  
in the Graduate School of Arts and Sciences of  
Northeastern University, May, 2011

# Abstract

The Large Hadron Collider (LHC) has recently turned on and started collecting invaluable physics data. The particle physics community is eager to see which of the recent beyond the Standard Model theories will be discovered at the LHC. Supersymmetry is one of the strongest candidate for the physics beyond the Standard Model. In this thesis, first, we study the possibilities of discovering supersymmetry at the LHC running at 7 TeV center of mass energy and carry out a reach analysis within the mSUGRA parameter space. We generate nonuniversal mSUGRA benchmark models with nonuniversities in the gaugino sector which satisfy all the current collider, non-collider, as well as dark matter constraints and at the same time are also discoverable with as low as  $1 - 2 \text{ fb}^{-1}$  of integrated luminosity. In the second part of the thesis, we develop a method to determine if the gaugino masses are unified with the help of the LHC data. As a framework to study gaugino masses, we utilize the mirage mediation model which is a string motivated construction that includes mixed gravity and anomaly mediation. We show that up to a 30% non-universality is measurable after just one year of LHC data running at 14 TeV center of mass energy. Finally, we study the collider phenomenology of another string theory motivated model known as deflected mirage mediation. Deflected mirage mediation is an extension of mirage mediation in which gauge-mediated supersymmetry breaking terms are also present and competitive in size to the gravity-mediated and anomaly-mediated soft terms. We compare and show the phenomenological differences between mirage and deflected mirage mediation at the LHC and study the mass hierarchies of the lightest four sparticles within the deflected mirage unification framework.

# Acknowledgements

First and foremost, I would like to thank my advisor Professor Brent Nelson from whom I have learned so much during the past couple of years. This thesis would not be possible without his guidance and support.

I would like to thank the other members of my committee, Professor Pran Nath, Professor Tomasz Taylor and Professor Darien Wood for their help and support.

I would like to thank my collaborators Professor Pran Nath, Professor Lisa Everett, Professor Gordon Kane, Dr. Michael Holmes, Dr. Ian-Woo Kim, Dr. Phillip Grajek, and last but not least Gregory Peim.

I would not enjoy the past couple of years without the friendship of so many great friends. Thank you all, but especially thank you Anish Mokashi, Arda Halu, Ashenafi Dadi, Ata Karakci, Cagdas Kafali, Daniel Feldman, Elif Nilay Yilmaz, Evin Gultepe, Gabriel Facini, Gina Escobar, Gregory Peim, Michael Holmes, Rasim Tumer, Saltuk Kurtoglu, Sinem Dogu-Tumer, Susmita Basak, Tanmoy Das, Tuhin Roy, Umut Kemiktarak, Utku Kemiktarak, Wael Al-Sawai, Zeynep Damla Ok and Zuowei Liu.

I would like to thank Kimberly Ferzoco for being with me and bringing joy to my life.

Finally and most of all I thank my family for their encouragement and their endless support.

**İsmet Barış Altunkaynak**

*April 2011*

# Contents

<b>Abstract</b>	<b>3</b>
<b>Acknowledgements</b>	<b>5</b>
<b>1 Introduction</b>	<b>8</b>
<b>2 Standard Model</b>	<b>11</b>
2.1 Yang-Mills theory . . . . .	12
2.2 SM Lagrangian . . . . .	13
2.3 Challenges . . . . .	15
<b>3 Supersymmetry</b>	<b>17</b>
3.1 Minimal Supersymmetric Standard Model . . . . .	18
3.2 Global and local supersymmetry . . . . .	21
3.3 mSUGRA . . . . .	23
3.4 Electroweak symmetry breaking and the Higgs . . . . .	24
3.5 Gaugino sector . . . . .	25
3.6 Squarks and sleptons . . . . .	27
<b>4 SUSY Discovery Potential and Benchmarks for Early Runs at <math>\sqrt{s} = 7</math> TeV at the LHC</b>	<b>29</b>
4.1 Standard Model at $\sqrt{s} = 7$ TeV . . . . .	29
4.2 SUSY models, constraints and collider signatures . . . . .	33
4.3 Sparticle production and LHC reach in mSUGRA . . . . .	35
4.4 Nonuniversal mSUGRA and benchmark models . . . . .	38
4.5 Summary . . . . .	45

<b>5</b>	<b>Studying Gaugino Mass Unification at the LHC</b>	<b>46</b>
5.1	Mirage pattern of gaugino masses . . . . .	47
5.2	Setting up the problem . . . . .	50
5.3	Signature selection . . . . .	52
5.4	Signatures . . . . .	58
5.5	Results . . . . .	65
5.6	Summary . . . . .	67
<b>6</b>	<b>Phenomenology of Deflected Mirage Mediation</b>	<b>68</b>
6.1	DMM framework . . . . .	69
6.2	Comparison with mirage unification . . . . .	72
6.3	Influence of $\alpha_g$ on LHC Phenomenology . . . . .	79
6.4	Comparison with mSUGRA and sparticle landscape . . . . .	81
6.5	Impact of Progressive Cuts . . . . .	87
6.6	Hierarchy Patterns in mSUGRA and DMM . . . . .	93
6.7	Focusing on DMM Hierarchy Patterns . . . . .	101
6.8	DMM Higgsino/mixed LSP patterns: Higgs LSP . . . . .	103
6.9	DMM patterns: mSP2 and mSP3' . . . . .	105
6.10	mSUGRA-like DMM patterns: mSP6' . . . . .	110
6.11	Summary . . . . .	111
<b>7</b>	<b>Conclusions</b>	<b>114</b>
	<b>Appendix</b>	<b>116</b>
<b>A</b>	<b>Benchmark models for early discovery of SUSY at the LHC</b>	<b>117</b>
<b>B</b>	<b>Anomalous dimensions in the DMM framework</b>	<b>120</b>
	<b>Bibliography</b>	<b>122</b>

# Chapter 1

## Introduction

After years of design and construction, the Large Hadron Collider (LHC) has finally started collecting invaluable physics data. This biggest and one of the most expensive experiments in the history of science will open the doors to the unknown new physics beyond the Standard Model. The Standard Model is regarded as a triumph of particle physics although it falls short of being a complete theory of fundamental interactions. Among many problems it has, some of the important ones are worth emphasizing. It does not include gravity, it does not have a dark matter candidate and it requires fine tuning in the Higgs sector (also known as the hierarchy problem). Many theories exist that offer an explanation for the physics beyond the Standard Model, and supersymmetry (SUSY) is one of the best motivated candidates. It provides a theoretically attractive framework that resolves many of the long standing problems of the Standard Model. It also predicts the unification of gauge couplings which is often considered to be a sign of a grand unification where all three interactions are merged into one single interaction characterized by a larger gauge symmetry group.

The Minimal Supersymmetric Standard Model (MSSM) introduces 32 new particles and 105 new parameters in addition to the Standard Model. This generality allows a very rich LHC phenomenology but also suffers from the “LHC inverse Problem,” that is the inverse map from the signature space to the parameter space is not one to one. The maximum number of uncorrelated observables puts a limit on the maximum information we can collect from a collider experiment.\* One can focus on a smaller set of 19 parameters, called as pMSSM or phenomenological MSSM, by ignoring the ones less relevant for the LHC, but the problem still persists as shown by Arkani-Hamed et al. in [2].

---

\*See [1] for an example of how to use non-collider results, specifically direct and indirect detection of dark matter in conjunction with the collider data to reduce the degeneracies.

This raises the importance of exploring possible mediation mechanisms for supersymmetry breaking. Most models of supersymmetry breaking involve one of the three most popular mediation mechanisms; gravity mediation, gauge mediation and anomaly mediation. String motivated scenarios of mixed mediation mechanisms also exist. One example is Kachru-Kallosh-Linde-Trivedi (KKLT) motivated mirage mediation, where the tree-level gravity (modulus)-mediated terms and the (loop-suppressed) anomaly-mediated terms are comparable in size, contrary to naive expectations. Another example is the deflected mirage mediation scenario (DMM) which is an extension of mirage mediation in which gauge-mediated supersymmetry breaking terms are also present and competitive in size to the gravity-mediated and anomaly-mediated soft terms. Deflected mirage mediation provides a general framework in which to explore mixed supersymmetry breaking scenarios at the LHC, where well-known single mediation mechanism models can be recovered by judiciously adjusting dimensionless parameters in the theory. This suggests that one can learn much more by studying the phenomenology of deflected mirage mediation instead of its special limits. We will discuss the LHC phenomenology of deflected mirage mediation in Chapter 6 and compare it to the pure mirage mediation. We will also study the similarities and differences in the hierarchy of lightest four supersymmetric states in the DMM and mSUGRA paradigms.

Evidence for gaugino unification at the supersymmetry breaking scale is one of the most important pieces of information a string theorist would like to learn from the LHC [3]. One common feature of both pure and deflected mirage mediations is that gaugino masses always unify at a scale determined by the dimensionless parameters of the models. We discuss how to determine the signs of this unification at the LHC in Chapter 5.

Obviously the first step that we must take, before exploring the details of the specific supersymmetric theory that nature will reveal us, is to actually discover supersymmetry in the first place. This has been studied for the center of mass energy of 14 TeV. We attack the same problem for half the design energy and determine benchmark points that will be observable within one or two years at the LHC as well as at the near future dark matter experiments.

The organization of this thesis is as follows. In Chapter 2, we briefly review the Standard Model.

In Chapter 3, we discuss the properties of supersymmetry and of the Minimal supersymmetric Standard Model. Chapter 4 analyzes the discovery potential of supersymmetry in the early runs of the LHC at its half design center of mass energy of 7 TeV. Chapter 5 focuses on studying the gaugino mass unification at the LHC. Chapter 6 introduces the deflected mirage mediation (DMM) scenario and focuses on the LHC phenomenology of DMM as well as its sparticle landscape.

## Chapter 2

### Standard Model

The Standard Model of particle physics is a unified field theory combining electromagnetic, weak and strong interactions. The weakest of the four known interactions, gravity, is not included in the theory. It is one of the greatest achievements in particle physics, and has been tested very extensively and shown that it agrees perfectly with experiments so far.

The development of the Standard Model took place between 1960-1974. The electroweak part of the theory was finalized by Sheldon Glashow, Steven Weinberg and Abdus Salam [4, 5, 6], and the strong interaction part, i.e. quantum chromodynamics (QCD), was finalized by Murray Gell-Mann, David Gross, David Politzer and Frank Wilczek [7, 8, 9, 10, 11, 12].

Particle content of the Standard Model can be grouped into 3 categories: matter particles, force carriers, and the Higgs particle. Matter particles consist of three families of fermions that are divided into two subgroups of quarks and leptons. Interactions are mediated by vector bosons. The only scalar particle in the theory is the Higgs particle, which is yet to be discovered, that is assumed to give mass to the massive particles of the theory.

quarks	<i>u</i>	<i>c</i>	<i>t</i>	$\gamma$	force carriers	+ <i>H</i>
	<i>d</i>	<i>s</i>	<i>b</i>	<i>g</i>		
leptons	$\nu_e$	$\nu_\mu$	$\nu_\tau$	<i>Z</i>		
	<i>e</i>	$\mu$	$\tau$	<i>W</i>		

Table 2.1: Particle content of the Standard Model. Quarks: up, down, charm, strange, top, bottom. Leptons: electron, muon, tau and their neutrinos. Force carriers: photon, gluon, Z and W bosons. And the scalar Higgs particle.



Figure 2.1: Nobel laureates of the electroweak theory: Sheldon Glashow, Abdus Salam and Steven Weinberg. Courtesy of the Nobel Foundation.

## 2.1 Yang-Mills theory

A modern formulation of the Standard Model can be constructed in terms of Yang-Mills theory which is a local gauge theory with non-abelian gauge group such as  $SU(N)$ . The generators  $T^a$  of the gauge group satisfy the algebra

$$[T^a, T^b] = if^{abc}T^c, \quad (2.1)$$

where  $f^{abc}$  are the structure constants of the group. We define the covariant derivative, which generates the gauge interactions, as

$$D_\mu = \partial_\mu - igT^a A_\mu^a, \quad (2.2)$$

where  $g$  is the coupling constant and  $A_\mu^a$  are the gauge fields (or gauge connection) that transform under the adjoint representation of the gauge group. The covariant derivatives satisfy the following commutation relations

$$[D_\mu, D_\nu] = -gT^a F_{\mu\nu}^a, \quad (2.3)$$

where  $F_{\mu\nu}^a$  are the the field strength tensors associated with the gauge fields, and they are given by

$$F_{\mu\nu}^a = \partial_\mu A_\nu^a - \partial_\nu A_\mu^a + gf^{abc}A_\mu^b A_\nu^c. \quad (2.4)$$

We can couple the gauge fields to a fermion field and write down an interaction Lagrangian as

$$\mathcal{L}_{YM} = \bar{f}(x)(i\not{D} - m)f(x) - \frac{1}{4}F_{\mu\nu}^a(x)F^{a\mu\nu}(x), \quad (2.5)$$

where  $m$  is the mass of the fermion in the theory.

With this general recipe, we can easily obtain the QED and QCD Lagrangians by choosing the appropriate gauge groups and coupling the theory to a fermion field. For QED, the gauge group is simply  $U(1)$  with the generators being just the identity, the coupling constant becomes the electric charge and the gauge field is the massless photon field. For QCD, the gauge group becomes  $SU(3)$  which gives 8 massless gluon fields in the adjoint representation.

## 2.2 SM Lagrangian

The gauge group of the Standard Model is  $SU(3)_C \times SU(2)_L \times U(1)_Y$ , where subscripts denote the color, weak isospin and hypercharge respectively. We can use the general Yang-Mills Lagrangian to construct the Standard Model Lagrangian. Our gauge bosons fall in the adjoint representations of each of the 3 gauge groups of the Standard Model. Hence we have 8  $SU(3)_C$  gluon fields  $G_\mu^a$ , 3  $SU(2)_L$  fields  $W_\mu^a$  and 1 hypercharge field  $B_\mu$ . The matter fields consist of three generation of quarks and leptons given by

$$q = (u_L, d_L)^T, u_R, d_R \quad ; \quad l = (v_L, e_L)^T, e_R \quad (2.6)$$

The covariant derivative is given by

$$D_\mu = \partial_\mu - ig_3 \frac{\lambda^a}{2} G_\mu^a - ig_2 \frac{\sigma^a}{2} W_\mu^a - ig_1 \frac{Y}{2} B_\mu, \quad (2.7)$$

where  $\lambda^a$  are the Gell-Mann matrices,  $\sigma^a$  are the Pauli spin matrices and  $Y$  is the hypercharge generator. Note that this covariant derivative acts differently on the fields. For example right handed  $SU(2)_L$  singlet fields do not feel the  $SU(2)$  interaction,  $SU(3)_C$  singlet fields do not feel the  $SU(3)$  interaction and a field with vanishing hypercharge does not feel the  $U(1)_Y$  interaction. The

electric charge is given by the weak isospin and the hypercharge as

$$Q = T_3 + \frac{Y}{2}. \quad (2.8)$$

Interactions are generated by the term  $\bar{\psi}i\mathcal{D}\psi$  in the Lagrangian but an explicit mass term is not gauge invariant hence is not allowed. Mass is generated by Yukawa interactions and spontaneous symmetry breaking through the Higgs mechanism which breaks the  $SU(2)_L \times U(1)_Y$  group to  $U(1)_{EM}$ . The scalar Higgs field is an  $SU(2)_L$  doublet which is given by

$$\Phi = (\phi^+ \ \phi^0)^T \quad (2.9)$$

and the symmetry breaking Lagrangian is given by

$$\mathcal{L}_{SSB} = (D_\mu \Phi)^\dagger (D^\mu \Phi) - V(\Phi), \quad (2.10)$$

where  $V(\Phi)$  is the Higgs potential given by

$$V(\Phi) = \mu^2 \Phi^\dagger \Phi + \lambda (\Phi^\dagger \Phi)^2. \quad (2.11)$$

Fermion masses are generated by the broken  $SU(2)_L \times U(1)_Y$  symmetry via the Higgs coupling to the fermions with the Yukawa interaction given by the Lagrangian

$$\mathcal{L}_Y = \lambda_e \bar{l}_L \Phi e_R + \lambda_u \bar{u}_L \Phi u_R + \lambda_d \bar{d}_L \Phi d_R + h.c. \quad (2.12)$$

When  $\mu^2$  becomes negative, the Higgs field gets a vacuum expectation value (VEV) which can be parametrized by

$$\langle 0|\Phi|0\rangle = \frac{1}{\sqrt{2}} \begin{pmatrix} 0 \\ v \end{pmatrix} \quad \text{where} \quad v = \sqrt{\mu^2/\lambda} = 246 \text{ GeV} \quad (2.13)$$

Before the spontaneous symmetry breaking we have 4 massless gauge bosons  $W_\mu^{1,2,3}$  and  $B_\mu$  and 4 massless scalars  $\phi_{1,\dots,4}$  which are the component of the Higgs doublet. After the spontaneous

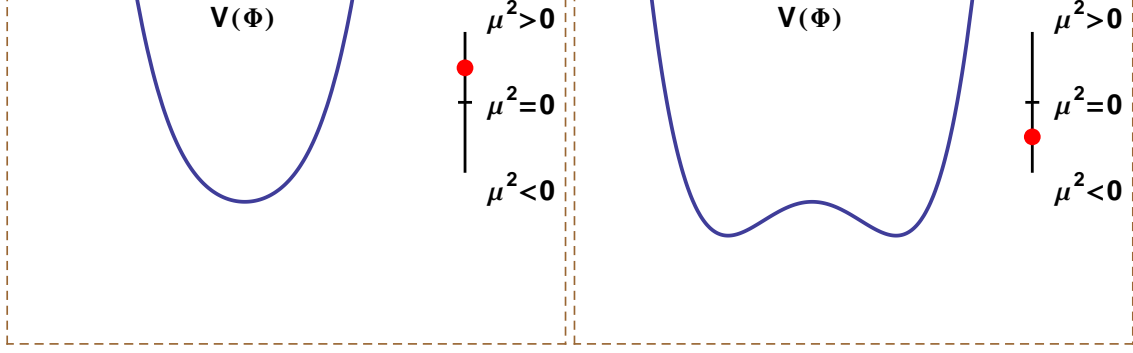


Figure 2.2: Higgs potential as a function of  $\mu$ . Note that this is only a cross section and the full shape of the potential can be obtained by rotating the curve around its symmetry axis which is also called as the Mexican hat potential.

symmetry breaking occurs we get the physical vector gauge bosons and the scalar Higgs boson. These physical states are given by the electroweak interaction eigenstates as

$$\begin{aligned}
 W^\pm &= \frac{1}{\sqrt{2}} (W_\mu^1 \mp i W_\mu^2) \\
 Z_\mu &= c_w W_\mu^3 - s_w B_\mu \\
 A_\mu &= s_w W_\mu^3 + c_w B_\mu,
 \end{aligned}
 \tag{2.14}$$

where  $\theta_W$  is the Weinberg angle,  $c_W = \cos \theta_W$ ,  $s_W = \sin \theta_W$  and the masses of the gauge bosons in terms of the Higgs VEV,  $SU(2)_L$  coupling constant and the Weinberg angle are given by

$$M_W = \frac{g_2 v}{2} \quad , \quad M_Z = \frac{M_W}{\cos \theta_W}.
 \tag{2.15}$$

## 2.3 Challenges

The Standard Model is the best tested quantum theory of elementary particles and interactions. Some theoretical predictions agree with the experimental measurements with better than 1 part in a billion precision. Nevertheless there are unaccounted for observations and theoretical problems with the Standard Model. Here, we list some those problems and give a brief explanation.

- **Cold dark matter:** The existence of cold dark matter has been confirmed by many indepen-

dent observations, such as the anomaly in the galactic rotation curves or by gravitational lensing effects. The Standard Model does not include a particle which can make up the dark matter.

- **Neutrino masses and mixings:** Atmospheric and solar neutrino experiments proved that neutrinos oscillate from one flavor to another. This implies that they have small but non zero masses. Neutrinos are massless in the Standard Model. To account for these latest observation, we can extend the Standard Model to include Dirac neutrino masses but then the Yukawa couplings must be really tiny which will clearly require an explanation.
- **Matter-antimatter asymmetry:** The apparent imbalance of matter and antimatter in our universe requires an explanation. Standard Model does not differentiate between matter and antimatter, so it is very difficult to understand why the universe is matter dominated within the Standard Model.
- **Fine tuning in the Higgs sector:** The quantum corrections to the square of the Higgs mass goes like the square of the cutoff scale, i.e.  $m_H^2(\Lambda) = m_H^2 + c\Lambda^2$ . For the Higgs mass to be in the order of 100 GeV which is required by the electroweak theory, the bare mass term  $m_H^2$  needs to cancel the correction term up to 35 digits, leaving a non zero value of desired size. This is of course a very large fine tuning problem.

We will see in the next chapter that supersymmetry offers solutions to some of the above problems. In particular the dark matter and the fine tuning problem are naturally solved in supersymmetric theories.

## Chapter 3

### Supersymmetry

Supersymmetry offers a link between fermions and bosons by extending the Poincaré algebra to include spinorial generators that connect the fermionic degrees of freedom to the bosonic degrees of freedom. Exploration of the possible symmetries of the scattering matrix showed the maximum extension of such symmetries are obtained by introducing supersymmetry [13, 14]. The first realization of the four dimensional supersymmetric Lagrangian [15, 16] was followed by the first realistic supersymmetric extension of the Standard Model [17]. Local supersymmetry provided a natural way to include gravity into the supersymmetric theories [18, 19, 20, 21, 22].

Supersymmetry is realized by introducing a spinorial generator, or a supercharge  $Q$  which is an anticommuting spinor with the properties

$$Q|\text{Boson}\rangle = |\text{Fermion}\rangle \quad , \quad Q|\text{Fermion}\rangle = |\text{Boson}\rangle. \quad (3.1)$$

The generator  $Q$  satisfies the following super-Poincaré algebra

$$\begin{aligned} \{Q_\alpha, Q_\alpha^\dagger\} &= 2\sigma_{\alpha\dot{\alpha}}^\mu P_\mu \\ \{Q_\alpha, Q_\beta\} &= \{Q_\alpha^\dagger, Q_\beta^\dagger\} = 0 \\ [Q_\alpha, P^\mu] &= [Q_\alpha^\dagger, P^\mu] = 0, \end{aligned} \quad (3.2)$$

where  $\sigma^\mu = (1, \vec{\sigma})$  are the Pauli spin matrices,  $\alpha, \beta$  are the spinor indices and  $P_\mu$  is the generator of spacetime translations. Because of this algebraic structure, anticommuting supersymmetry transformation  $Q$  can be thought as the “square root” of the spacetime translations.

In a supersymmetric theory, single particle states fall into irreducible representations of the supersymmetry algebra that are called supermultiplets. Each supermultiplet contains fermion

and boson states that are superpartners of each other. One can show that, in a supermultiplet, the fermionic degrees of freedom is equal in number to the bosonic degrees of freedom. Particles in a supermultiplet share the same quantum numbers and have the same mass. In a renormalizable supersymmetric gauge theory with only one distinct copy of supersymmetry generators  $Q, Q^\dagger$  ( $\mathcal{N} = 1$ ), and massless gauge bosons, the simplest combinations we can have in a supermultiplet all contain two fermionic and bosonic degrees of freedom. The first combination is a chiral/matter/scalar supermultiplet which contains a spin 1/2 Weyl fermion and a complex scalar. The other combination is a gauge/vector supermultiplet which contains a massless spin 1 vector boson and its superpartner, a spin 1/2 Weyl fermion. If we also include quantum gravity, then we have the gravity supermultiplet which contains a spin 2 graviton and a spin 3/2 superpartner called the gravitino. In a supermultiplet, spin 0 superpartners are named with an 's' prefix such as squarks and sleptons. Spin 1/2 superpartners are named with an 'ino' suffix such as Higgsino, gluino, etc. One can also have extended supersymmetry with more than one distinct copy of supersymmetry generators but these theories fail to satisfy basic phenomenological constraints such as chiral fermions and parity violation.

As we mentioned before, supersymmetry solves the fine tuning problem of the Higgs sector. Thanks to the cancellation of the terms due to fermionic and bosonic degrees of freedom, in a supersymmetric theory the quantum corrections to the physical Higgs mass do not go like the square of the cutoff scale but changes logarithmically as  $m_H^2(\Lambda) = m_H^2 + c' \ln \Lambda$ . Another nice feature of supersymmetry is gauge coupling unification. As opposed to the Standard Model, in MSSM gauge couplings unify at the so called grand unified theory (GUT) scale which is approximately  $10^{16}$  GeV. Figure 3.1 shows the running of the gauge couplings in both frameworks.

### 3.1 Minimal Supersymmetric Standard Model

The simplest ( $\mathcal{N} = 1$ ) extension of the Standard Model which contains only one distinct copy of supersymmetry generators  $Q, Q^\dagger$  is the Minimal Supersymmetric Standard Model (MSSM). In Table 3.1, we display the chiral and gauge supermultiplets of the MSSM. In addition to the superpartners of quarks and leptons, which are squarks and sleptons, the MSSM contains two

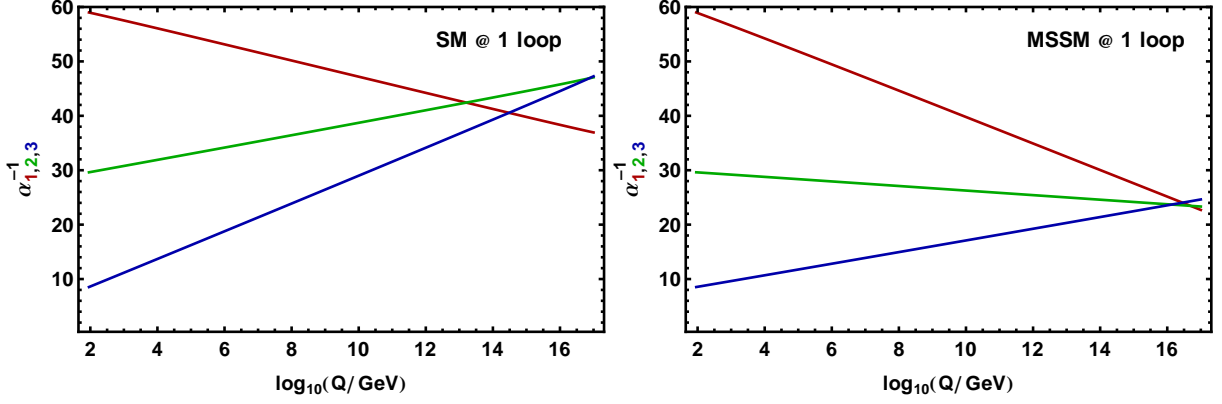


Figure 3.1: One loop renormalization group evolution of the  $SU(3)_C$ ,  $SU(2)_L$  and  $U(1)_Y$  gauge couplings in SM and MSSM.

Higgs doublets and corresponding Higgsino doublets, as well gauginos which are the partners of the gauge bosons of the Standard Model. The reason for two Higgs doublets is two-fold: to cancel the gauge anomalies, and to give mass to up and down type quarks.

In total, the MSSM introduces 32 new supersymmetric mass eigenstates which are

- **Higgs bosons:**  $h^0, H^0, A^0, H^\pm$

These states are the mixture of the spin 0 gauge eigenstates  $H_u^0, H_d^0, H_u^+, H_d^-$ .  $h^0$  and  $H^0$  are CP even states,  $A$  is CP odd, and  $H^\pm$  is the charged Higgs state.

- **Neutralinos:**  $\tilde{\chi}_1^0, \tilde{\chi}_2^0, \tilde{\chi}_3^0, \tilde{\chi}_4^0$

These states are the mixture of the binos, winos and Higgsinos  $\tilde{B}^0, \tilde{W}^0, \tilde{H}_u^0, \tilde{H}_d^0$ . In R-parity conserving models  $\tilde{\chi}_1^0$  is a dark matter candidate.

- **Charginos:**  $\tilde{\chi}_1^\pm, \tilde{\chi}_2^\pm$

These states are the mixtures of charged winos and Higgsinos  $\tilde{W}^\pm, \tilde{H}_u^\pm, \tilde{H}_d^\pm$ .

- **Gluino:**  $\tilde{g}$

- **Squarks:**  $\tilde{u}_{L,R}, \tilde{d}_{L,R}, \tilde{c}_{L,R}, \tilde{s}_{L,R}, \tilde{t}_{1,2}, \tilde{b}_{1,2}$

First and second generation mass eigenstates are assumed to be same as the gauge eigenstates due to small mixing. Third generation squarks, i.e. stop and sbottom states, are the mixtures of the gauge eigenstates.

		Names	spin 0	spin 1/2	spin 1	$SU(3)_C$	$SU(2)_L$	$U(1)_Y$
chiral	squarks, quarks × 3 families	$Q$	$(\widetilde{u}_L \ \widetilde{d}_L)$	$(u_L \ d_L)$		<b>3</b>	<b>2</b>	$\frac{1}{6}$
		$\bar{u}$	$\widetilde{u}_R^*$	$u_R^+$		$\bar{\mathbf{3}}$	<b>1</b>	$-\frac{2}{3}$
		$\bar{d}$	$\widetilde{d}_R^*$	$d_R^+$		$\bar{\mathbf{3}}$	<b>1</b>	$\frac{1}{3}$
	sleptons, leptons × 3 families	$L$	$(\widetilde{\nu}_L \ \widetilde{e}_L)$	$(\nu \ e_L)$		<b>1</b>	<b>2</b>	$-\frac{1}{2}$
		$\bar{e}$	$\widetilde{e}_R^*$	$e_R^+$		<b>1</b>	<b>1</b>	<b>1</b>
	Higgs, higgsinos	$H_u$	$(H_u^+ \ H_u^0)$	$(\widetilde{H}_u^+ \ \widetilde{H}_u^0)$		<b>1</b>	<b>2</b>	$+\frac{1}{2}$
$H_d$		$(H_d^0 \ H_d^-)$	$(\widetilde{H}_d^0 \ \widetilde{H}_d^-)$		<b>1</b>	<b>2</b>	$-\frac{1}{2}$	
gauge	gluino, gluon			$\widetilde{g}$	$g$	<b>8</b>	<b>1</b>	<b>0</b>
	winos, W bosons			$\widetilde{W}^\pm \ \widetilde{W}^0$	$W^\pm \ W^0$	<b>1</b>	<b>3</b>	<b>0</b>
	bino, B boson			$\widetilde{B}^0$	$B^0$	<b>1</b>	<b>1</b>	<b>0</b>

Table 3.1: Chiral and gauge supermultiplets in the Minimal Supersymmetric Standard Model.

- **Sleptons:**  $\widetilde{e}_{L,R}, \widetilde{\nu}_e, \widetilde{\mu}_{L,R}, \widetilde{\nu}_\mu, \widetilde{\tau}_{1,2}, \widetilde{\nu}_\tau$

Similar to the squarks, there is no mixing in the first and second generation gauge eigenstates.

Third generation gauge eigenstates mix to give the stau and sneutrino states.

We know that supersymmetry must be a broken symmetry because the superpartners of the Standard Model particles have not been observed which implies they need to have higher masses than their Standard Model partners. The question of how supersymmetry is broken does not have a definitive answer yet. Many models have been proposed that will break the supersymmetry by including new particles and interactions which are usually hidden from us below the symmetry breaking scale. We can avoid the question of how supersymmetry is broken by parameterizing the most general soft supersymmetry breaking terms [23]. In the MSSM these terms are given by

$$\begin{aligned}
\mathcal{L}_{soft}^{MSSM} = & -\frac{1}{2} (M_3 \widetilde{g}\widetilde{g} + M_2 \widetilde{W}\widetilde{W} + M_1 \widetilde{B}\widetilde{B} + c.c.) \\
& - (\widetilde{u}\mathbf{a}_u \widetilde{Q}H_u - \widetilde{d}\mathbf{a}_d \widetilde{Q}H_d - \widetilde{e}\mathbf{a}_e \widetilde{L}H_d + c.c.) \\
& - \widetilde{Q}^\dagger \mathbf{m}_Q^2 \widetilde{Q} - \widetilde{L}^\dagger \mathbf{m}_L^2 \widetilde{L} - \widetilde{d}^\dagger \mathbf{m}_d^2 \widetilde{d} - \widetilde{e}^\dagger \mathbf{m}_e^2 \widetilde{e} \\
& - m_{H_u}^2 H_u^* H_u - m_{H_d}^2 H_d^* H_d - (\mu H_u H_d + c.c.),
\end{aligned} \tag{3.3}$$

where  $M_{1,2,3}$  are the bino, wino and gluino mass terms,  $\mathbf{a}_{u,d,e}$  are related to the Yukawa couplings,  $\mathbf{m}_{Q,L,\bar{u},\bar{d},\bar{e}}^2$  are squark and slepton mass terms,  $m_{H_u,H_d}^2$  are the mass terms for up and down type Higgs and finally  $\mu$  is the supersymmetric Higgs mass parameter.

### 3.2 Global and local supersymmetry

We start by introducing the superfields. A superfield  $\Phi(x, \theta, \bar{\theta})$  is a function of not only the spacetime coordinate  $x$  but also a function of Grassmann variables  $\theta$  and  $\bar{\theta}$  satisfying the following anticommutation relation:

$$\{\theta_\alpha, \bar{\theta}_{\dot{\alpha}}\} = 0, \quad (3.4)$$

where  $\alpha$  and  $\dot{\alpha}$  are spinor indices. Because of their anticommutation property, expansion of a function of these variables is finite and given by

$$f(\theta) = f_0 + f_1\theta \quad (3.5)$$

$$f(\bar{\theta}) = f_0^* + f_1^*\bar{\theta} \quad (3.6)$$

and a function of both  $\theta$  and  $\bar{\theta}$  is given by

$$f(\theta, \bar{\theta}) = f_0 + f_1\theta + f_2^*\bar{\theta} + f_3\theta\bar{\theta}, \quad (3.7)$$

where  $f_0, f_1, f_2, f_3$  are complex numbers.

Then by using the above properties we can write any chiral or vector superfield in the following way

$$\Phi(x, \theta) = \phi(x) + \theta\psi(x) + \theta\theta F(x) \quad (3.8)$$

$$V^a(x, \theta, \bar{\theta}) = -\theta\sigma^\mu\bar{\theta}A_\mu^a(x) + i\theta\theta\bar{\theta}\lambda^a(x) - i\bar{\theta}\bar{\theta}\theta\lambda^a(x) + \frac{1}{2}\theta\theta\bar{\theta}\bar{\theta}D^a(x), \quad (3.9)$$

where  $\phi$  are scalar fields and  $\psi$  are their fermionic superpartners. Also in the above expression,  $F$  and  $D$  are auxiliary fields which are introduced to close the supersymmetry algebra. They can be

eliminated using the equation of motions which imply

$$F_i = \frac{\partial F}{\partial \phi_i} = W^i \quad (3.10)$$

$$D^a = -g_a(\phi_i^* T^a \phi_i), \quad (3.11)$$

where  $W(\Phi)$  is the superpotential which is a holomorphic function of  $\Phi$ . The scalar potential can be written in terms of these F and D terms as

$$V = \sum_i \left| \frac{\partial W}{\partial \phi_i} \right|^2 + \frac{1}{2} \sum_a g_a^2 \left( \sum_i \phi_i^* T^a \phi_i \right)^2. \quad (3.12)$$

By using the superfields and the Grassmann algebra, we can write a general Lagrangian in the following form

$$L = \int d^4x \left\{ \int d^2\theta d^2\bar{\theta} \mathcal{L}_D + \int d^2\theta \mathcal{L}_F + h.c. \right\}, \quad (3.13)$$

where  $\mathcal{L}_F$  is a sum of scalar superfields and  $\mathcal{L}_D$  is a sum of vector superfields. This can be expressed in terms of the superfields  $\Phi$ ,  $V^a$  and the superpotential  $W(\Phi)$ , as

$$L_{SUSY} = \int d^4x \left\{ \int d^2\theta d^2\bar{\theta} \left[ \Phi^\dagger e^{g_a T^a V^a} \Phi + h.c. \right] + \int d^2\theta \left[ \frac{1}{4} W^{a\alpha} W_\alpha^a + W(\Phi) + h.c. \right] \right\}, \quad (3.14)$$

where the field strength superfield is defined as

$$W^a = -i\lambda^a + \theta D^a - \sigma^{\mu\nu} \theta F_{\mu\nu}^a - \theta \theta \sigma^\mu D_\mu \lambda^{a\dagger} \quad (3.15)$$

By promoting global supersymmetry to be a local symmetry we can obtain supergravity (SUGRA). This will introduce the gravity superfield which includes the spin 2 massless graviton and its superpartner spin 3/2 gravitino. The resulting Lagrangian depends only on 2 functions: the Kähler potential  $\mathcal{G}$  (mass dimension 2) and the gauge kinetic function  $f_{ab}$  (dimensionless). In SUGRA, the Kähler potential can be written as

$$\mathcal{G} = \kappa^2 K + \ln \left[ \kappa^6 |W|^2 \right] \quad (3.16)$$

where  $K(\phi_i, \phi_i^\dagger)$  is a real function (sometimes also called the Kähler potential) and  $\kappa = M_{\text{PL}}^{-1}$  where  $M_{\text{PL}} = \sqrt{\hbar c^5/8\pi G} = 2.43 \times 10^{18}$  GeV is the reduced Planck energy.

If the supersymmetry is broken spontaneously, the gravitino acquires mass by eating the goldstino in a similar way to the Standard Model Higgs mechanism. In this context, it is called the super-Higgs mechanism and the gravitino mass after the symmetry breaking becomes

$$m_{3/2} = M_{\text{PL}} e^{-\langle \mathcal{G} \rangle / 2M_{\text{PL}}^2} \quad (3.17)$$

where  $\langle \mathcal{G} \rangle$  is the VEV of the Kähler potential.

### 3.3 mSUGRA

The simplest ansatz for the form of the Kähler metric is to make it symmetric under the permutation of the superfields. As the result of this ansatz, soft supersymmetry breaking parameters are universal. This leads to minimal supergravity (mSUGRA) [22].

In mSUGRA, all the sparticle spectrum and mixing angles are determined by four parameters and a sign specified at the GUT scale which is approximately  $10^{16}$  GeV. These are

$m_0$	universal scalar mass	
$m_{1/2}$	universal gaugino mass	
$A_0$	universal trilinear coupling	(3.18)
$\tan \beta$	ratio of Higgs VEVs	
$\text{sgn } \mu$	sign of the $\mu$ parameter.	

With tree level renormalization group running, the unified boundary conditions implies that the gaugino masses at the electroweak scale obtain the ratios:

$$M_1 : M_2 : M_3 = 1 : 2 : 6 \quad (3.19)$$

### 3.4 Electroweak symmetry breaking and the Higgs

In the MSSM, the classical scalar potential for the Higgs scalar field is given by

$$V = (|\mu|^2 + m_{H_u}^2)|H_u^0|^2 + (|\mu|^2 + m_{H_d}^2)|H_d^0|^2 - (bH_u^0H_d^0 + c.c.) + \frac{1}{8}(g^2 + g'^2)(|H_u^0|^2 - |H_d^0|^2)^2, \quad (3.20)$$

where we set  $H_u^+ = 0$  by using an  $SU(2)_L$  gauge transformation which also implies  $H_d^- = 0$  without any loss of generality. For the scalar potential to have a minimum, we need to make sure it is bounded from below. Quartic interactions guarantee that bound except for the  $D$ -flat directions ( $|H_u^0| = |H_d^0|$ ) for which we need to impose the following conditions:

$$\begin{aligned} 2b &< 2|\mu|^2 + m_{H_u}^2 + m_{H_d}^2 \\ b^2 &> (|\mu|^2 + m_{H_u}^2)(|\mu|^2 + m_{H_d}^2). \end{aligned} \quad (3.21)$$

If these conditions are not satisfied, the origin  $H_u^0 = H_d^0 = 0$  will be a stable minimum of the scalar potential and electroweak symmetry breaking cannot occur. For the models with unified boundary conditions  $m_{H_u}^2 = m_{H_d}^2$  such as mSUGRA, renormalization group evolution due to quantum corrections pushes  $m_{H_u}^2$  to be below  $m_{H_d}^2$  at the electroweak scale, and hence breaks the electroweak symmetry. Because of these quantum corrections, this mechanism is known as radiative electroweak symmetry breaking.

We now define the Higgs VEVs as  $v_{u,d} = \langle H_{u,d}^0 \rangle$  and the ratio of the VEVs as  $\tan \beta = v_u/v_d$  where  $0 < \beta < \pi/2$ . The Z boson mass and the electroweak gauge couplings can be written in terms of these VEVs as

$$v^2 = v_u^2 + v_d^2 = 2m_Z^2/(g^2 + g'^2) \approx (174 \text{ GeV})^2. \quad (3.22)$$

Since we made sure the scalar potential is bounded from below, to minimize it we simply impose

the conditions  $\partial V/\partial H_u^0 = \partial V/\partial H_d^0 = 0$  which imply

$$\begin{aligned} m_{H_u}^2 + |\mu|^2 - b \cot \beta - (m_Z^2/2) \cos(2\beta) &= 0 \\ m_{H_d}^2 + |\mu|^2 - b \tan \beta + (m_Z^2/2) \cos(2\beta) &= 0. \end{aligned} \quad (3.23)$$

We can eliminate  $b$  and  $|\mu|$  by using these equations, but sign of  $\mu$  remains free. In these equations different types of parameters mix. The  $\mu$  parameter is the *supersymmetric* Higgs mass parameter, but  $b$  and  $m_{H_{u,d}}^2$  are *supersymmetry breaking* parameters. For the above system of equations to be valid, these parameters need to be of the same order of magnitude. It is difficult to understand this cancellation since those terms have different origins. This is known as the  $\mu$  problem in supersymmetry.

Below the electroweak symmetry breaking scale, electroweak gauge bosons  $Z^0$  and  $W^\pm$  get mass and the remaining degrees of freedom in the Higgs doublet form neutral and charged Higgs states  $h^0, H^0, A^0, H^\pm$ . We can write these masses in terms of the Lagrangian parameters as

$$m_{A^0}^2 = 2|\mu|^2 + m_{H_u}^2 + m_{H_d}^2 \quad (3.24)$$

$$m_{h^0, H^0}^2 = \frac{1}{2} \left( m_{A^0}^2 + m_Z^2 \mp \sqrt{(m_{A^0}^2 - m_Z^2)^2 + 4m_Z^2 m_{A^0}^2 \sin^2(2\beta)} \right) \quad (3.25)$$

$$m_{H^\pm}^2 = m_{A^0}^2 + m_W^2 \quad (3.26)$$

and the mixing angle between the CP-even Higgs states  $h^0$  and  $H^0$  is given by

$$\frac{\sin 2\alpha}{\sin 2\beta} = -\frac{m_{H^0}^2 + m_{h^0}^2}{m_{H^0}^2 - m_{h^0}^2}, \quad \tan 2\alpha = \frac{m_{A^0}^2 + m_Z^2}{m_{A^0}^2 - m_Z^2}. \quad (3.27)$$

### 3.5 Gaugino sector

We can write the mass terms of the MSSM Lagrangian for the gaugino sector as

$$\mathcal{L}_{\text{gaugino}} = -\frac{1}{2} M_3 \widetilde{g\widetilde{g}} - \frac{1}{2} (\psi^0)^T \mathbf{M}_{\widetilde{N}} \psi^0 - \frac{1}{2} (\psi^\pm)^T \mathbf{M}_{\widetilde{C}} \psi^\pm + \text{c.c.}, \quad (3.28)$$

where  $\psi'$ s are in the gauge-eigenstate basis and given by

$$\begin{aligned}\psi^0 &= (\widetilde{B}, \widetilde{W}^0, \widetilde{H}_d^0, \widetilde{H}_u^0) \\ \psi^\pm &= (\widetilde{W}^+, \widetilde{H}_u^+, \widetilde{W}^-, \widetilde{H}_d^-) \quad , \quad \psi^+ = (\widetilde{W}^+, \widetilde{H}_u^+) \quad , \quad \psi^- = (\widetilde{W}^-, \widetilde{H}_d^-)\end{aligned}\tag{3.29}$$

Here  $\mathbf{M}_{\widetilde{N}}$  and  $\mathbf{M}_{\widetilde{C}}$  are neutralino and chargino mass matrices, respectively. At tree level, they are given by

$$\mathbf{M}_{\widetilde{N}} = \begin{pmatrix} M_1 & 0 & -c_\beta s_W m_Z & s_\beta s_W m_Z \\ 0 & M_2 & c_\beta c_W m_Z & -s_\beta c_W m_Z \\ -c_\beta s_W m_Z & c_\beta c_W m_Z & 0 & -\mu \\ s_\beta s_W m_Z & -s_\beta c_W m_Z & -\mu & 0 \end{pmatrix} \quad , \quad \mathbf{M}_{\widetilde{C}} = \begin{pmatrix} \mathbf{0} & \mathbf{X}^T \\ \mathbf{X} & \mathbf{0} \end{pmatrix}\tag{3.30}$$

where  $s_\beta = \sin \beta$ ,  $c_\beta = \cos \beta$ ,  $s_W = \sin \theta_W$ ,  $c_W = \cos \theta_W$ , and  $\theta_W$  is the Weinberg angle. The chargino mass matrix is block diagonal and  $\mathbf{X}$  is a  $2 \times 2$  matrix given by

$$\mathbf{X} = \begin{pmatrix} M_2 & \sqrt{2} s_\beta m_W \\ \sqrt{2} c_\beta m_W & \mu \end{pmatrix}.\tag{3.31}$$

Now we can introduce a  $4 \times 4$  unitary matrix  $\mathbf{N}$  and two  $2 \times 2$  unitary matrices  $\mathbf{U}$  and  $\mathbf{V}$  to diagonalize the mass matrices  $\mathbf{M}_{\widetilde{N}}$  and  $\mathbf{M}_{\widetilde{C}}$  and obtain mass eigenstates as follows

$$\widetilde{N}_i = \mathbf{N}_{ij} \psi_j^0 \quad , \quad \widetilde{C}_i^+ = \mathbf{V}_{ij} \psi_j^+ \quad , \quad \widetilde{C}_i^- = \mathbf{U}_{ij} \psi_j^-\tag{3.32}$$

such that

$$\mathbf{M}_{\widetilde{N}}^{\text{diag}} = \mathbf{N}^* \mathbf{M}_{\widetilde{N}} \mathbf{N}^{-1} = \begin{pmatrix} m_{\widetilde{N}_1} & 0 & 0 & 0 \\ 0 & m_{\widetilde{N}_2} & 0 & 0 \\ 0 & 0 & m_{\widetilde{N}_3} & 0 \\ 0 & 0 & 0 & m_{\widetilde{N}_4} \end{pmatrix} \quad (3.33)$$

$$\mathbf{M}_{\widetilde{C}}^{\text{diag}} = \mathbf{U}^* \mathbf{X} \mathbf{V}^{-1} = \begin{pmatrix} m_{\widetilde{C}_1} & 0 \\ 0 & m_{\widetilde{C}_2} \end{pmatrix}.$$

At tree level, we can see from the Lagrangian given in Eqn. 3.28 that the gluino mass is equal to  $M_3$ . If we include one-loop corrections due to gluon exchange and quark-squark loops, we obtain the result given in [24] as

$$m_{\widetilde{g}} = M_3(Q) \left( 1 + \frac{\alpha_s}{4\pi} \left\{ 15 + 6 \ln(Q/M_3) + \sum_{\widetilde{q}} A_{\widetilde{q}} \right\} \right), \quad (3.34)$$

where

$$A_{\widetilde{q}} = \int_0^1 dx x \ln \left( x m_{\widetilde{q}}^2 M_3^2 + (1-x) m_q^2 / M_3^2 - x(1-x) - i\epsilon \right). \quad (3.35)$$

### 3.6 Squarks and sleptons

In the Cabibbo-Kobayashi-Maskawa (CKM) basis defined by the transformation  $K = V_1 V_2$  where  $V_1$  and  $V_2$  rotate the left handed up and down quarks to the mass eigenstates, we can write the general  $6 \times 6$  squark mass matrices as

$$M_u^2 = \begin{pmatrix} M_Q^2 + m_u^\dagger m_u + \Delta_L^u & -m_u^\dagger (A_u^\dagger + \mu^* \cot \beta) \\ -(A_u + \mu \cot \beta) m_u & M_U^2 + m_u m_u^\dagger + \Delta_R^u \end{pmatrix} \quad (3.36)$$

$$M_d^2 = \begin{pmatrix} K^\dagger M_Q^2 K + m_d m_d^\dagger + \Delta_R^u & -m_d^\dagger (A_d^\dagger + \mu^* \tan \beta) \\ -(A_d + \mu \tan \beta) m_d & M_D^2 + m_u m_u^\dagger + \Delta_R^u \end{pmatrix} \quad (3.37)$$

and the general slepton matrices as

$$M_{\tilde{\nu}}^2 = M_L^2 + \Delta_L^\mu \quad (3.38)$$

$$M_{\tilde{e}}^2 = \begin{pmatrix} M_L^2 + m_e m_e^\dagger + \Delta_L^e & -m_e^\dagger (A_e^\dagger + \mu^* \tan \beta) \\ -(A_e + \mu \tan \beta) m_e & M_E^2 + m_e^\dagger m_e + \Delta_R^e \end{pmatrix}, \quad (3.39)$$

where  $\Delta_{L,R}^f$  is given by

$$\Delta_L^f = m_Z^2 \cos 2\beta (T_{3f} - e_f \sin^2 \theta_W) \quad (3.40)$$

$$\Delta_R^f = m_Z^2 \cos 2\beta e_f \sin^2 \theta_W \quad (3.41)$$

So in summary, the MSSM is the minimal extension ( $\mathcal{N} = 1$ ) of the Standard Model that includes supersymmetry. It has extra fermionic and bosonic degrees of freedom which are the superpartners of the Standard Model particles that will be probed at the LHC. In the following chapters we are going to study how we can discover supersymmetry in the early runs at 7 TeV center of mass energy at the LHC, and how to obtain information about string theory by studying the low energy phenomenology of string theory motivated models.

## Chapter 4

# SUSY Discovery Potential and Benchmarks for Early Runs at $\sqrt{s} = 7$ TeV at the LHC\*

As of the writing of this thesis, the LHC is running at 7 TeV center of mass energy and collecting physics data. CERN has recently decided to continue running the LHC for a longer time period and this increases the chances of discovering supersymmetry before an upgrade which will allow the LHC to run at its design center of mass energy of 14 TeV. In this chapter, we focus on SUSY discovery in this early run at the LHC, i.e., at 7 TeV center of mass energy with up to  $2 \text{ fb}^{-1}$  of integrated luminosity. We also generate candidate benchmark models that can be studied further with an emphasis on the next to lightest superpartner (NLSP) such as the chargino ( $\tilde{\chi}_1^\pm$ ), the stau ( $\tilde{\tau}_1$ ), the gluino ( $\tilde{g}$ ), the CP odd Higgs ( $A^0$ ), and the stop ( $\tilde{t}_1$ ).

### 4.1 Standard Model at $\sqrt{s} = 7$ TeV

The determination of the relevant Standard Model backgrounds is an important part for the discovery studies of new physics. Previous works were on early discovery at higher energies [26, 27, 28, 29, 30]. One analysis at 7 TeV has already appeared in the literature [31] before this work got published.

In our analysis, we use MadGraph/MadEvent 4.4 [32] for parton level processes, Pythia 6.4 [33] for hadronization, and PGS 4 [34] for detector simulation and Parvicursor [35] for the signature analysis. We used MLM matching [36, 37] with a  $k_T$  jet clustering scheme to prevent double counting of final states, CTEQ6L1 [38] parton distribution functions, and we required all final state partons (except the top quarks) to have  $p_T > 40$  GeV. For a better sampling of the phase space we

---

\*This chapter is based on the work that has been published in Physical Review D [25].

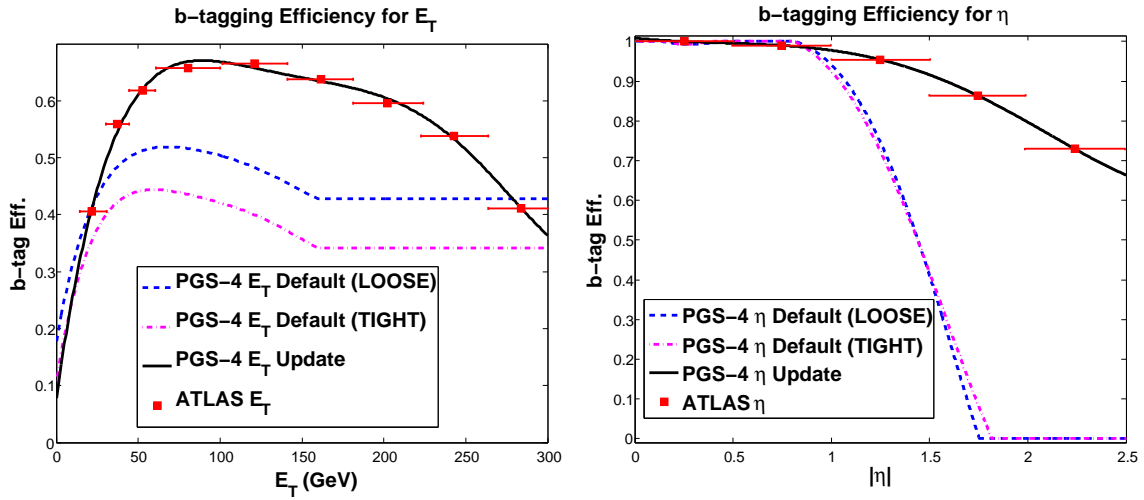
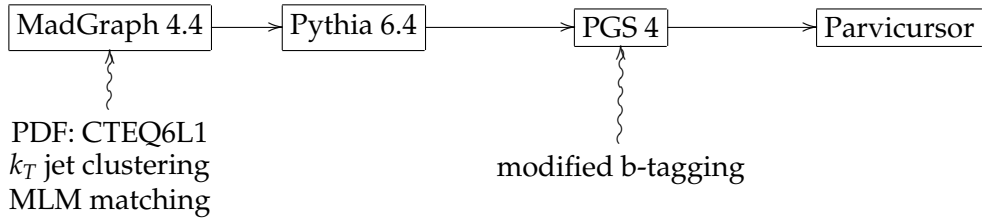


Figure 4.1: Left panel: A comparison of the  $b$ -tagging efficiency of ATLAS and the loose and tight efficiencies of PGS 4 as a function of  $E_T$ . Right panel: A comparison of the  $b$ -tagging efficiency of ATLAS and the loose and tight efficiencies of PGS 4 as a function of  $\eta$ . Ours fits to the efficiency of ATLAS as a function of  $E_T$ , and  $\eta$  as parametrized by Eq. (4.1) are also exhibited. Note that the total  $b$ -tagging efficiency is the product of the  $E_T$  and  $\eta$  efficiency functions.

partitioned the QCD jet production into 4 bins according to the energy of the hardest jet.



We also updated the  $b$ -tagging efficiency of PGS 4 to better represent the detector characteristics of the LHC which was by default based off of the Tevatron  $b$ -tagging efficiency. In Fig. (4.1) we compare the  $b$ -tagging efficiencies given in the ATLAS Expected Performance Report (EPR) [39] with the one implemented in PGS 4. The left/right panel of Fig. (4.1) gives the  $b$ -tagging efficiencies as a function of  $E_T/\eta$  for ATLAS and the so called “tight” and “loose” efficiencies as defined in PGS 4. There is a significant difference between these and those expected in the ATLAS and CMS [40] detectors. In PGS 4,  $b$ -tagging efficiencies were assumed to approach a constant value for  $E_T \geq 160$  GeV. We have extended this  $E_T$  value to 300 GeV following the EPRs of both

detectors. Thus we have updated the  $b$ -tagging efficiencies as given in Eq. (4.1) where we have kept the same degree polynomial as in PGS 4 originally. Here we make no modification to the default PGS 4 rate for mistagging  $b$  jets. Our revised  $b$ -tagging efficiencies have the following form where  $\tilde{E}_T = E_T/100$  GeV and the total  $b$ -tagging efficiency is the product of the  $E_T$  and  $\eta$  efficiency functions.

$$\begin{aligned}
 b_{E_T} &= 0.0781391 + 2.02661 \tilde{E}_T - 2.59664 \tilde{E}_T^2 + 1.5509 \tilde{E}_T^3 - 0.446698 \tilde{E}_T^4 + 0.047995 \tilde{E}_T^5 \\
 b_\eta &= 1.00885 - 0.0497485 \eta + 0.693036 \eta^2 - 0.0361142 \eta^3 - 0.0222204 \eta^4 + 0.00797621 \eta^5
 \end{aligned}
 \tag{4.1}$$

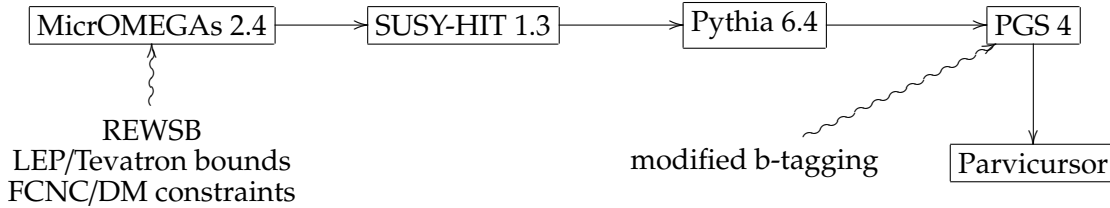
We show the Standard Model processes and their corresponding cross sections in Tab. (4.1) as well as the number of events we have generated for each process. The reason for different numbers of events for different processes is to better sample the more relevant part of the phase space. It is not possible to generate at least  $1 \text{ fb}^{-1}$  of data for each process, so while trying to sample every part of the phase space with sufficient precision, we focused more on the processes that might result in a reasonable number of events after we apply our global cuts. That is also why we chose to limit our background sample with the processes given in Tab. (4.1). For example, although the single top production cross section is approximately half the  $t\bar{t}$  production cross section, our post-trigger cuts ( $\cancel{E}_T \geq 200$  GeV and a minimum transverse sphericity of 0.2) perform very well and eliminate most of that background. Our analysis compares well with the analysis of [31]. The differences between the two analyses can be explained by the different jet clustering methods used ( $k_T$ -based versus cone-based). See [41] for further details on how different jet clustering methods compare.

SM process	Cross section (fb)	Number of events	Luminosity ( $\text{fb}^{-1}$ )
QCD 2,3,4 jets [ $40 \geq E_T(j_1)/\text{GeV} \geq 100$ ]	$2.0 \times 10^{10}$	74 M	0.0037
QCD 2,3,4 jets [ $100 \geq E_T(j_1)/\text{GeV} \geq 200$ ]	$7.0 \times 10^8$	98 M	0.14
QCD 2,3,4 jets [ $200 \geq E_T(j_1)/\text{GeV} \geq 500$ ]	$4.6 \times 10^7$	40 M	0.88
QCD 2,3,4 jets [ $500 \geq E_T(j_1)/\text{GeV} \geq 3000$ ]	$3.9 \times 10^5$	1.7 M	4.4
$t\bar{t} + 0, 1, 2$ jets	$1.6 \times 10^5$	4.8 M	30
$b\bar{b} + 0, 1, 2$ jets	$9.5 \times 10^7$	95 M	1.0
$Z/\gamma (\rightarrow \ell\bar{\ell}, \nu\bar{\nu}) + 0, 1, 2, 3$ jets	$6.2 \times 10^6$	6.2 M	1.0
$W^\pm (\rightarrow \ell\nu) + 0, 1, 2, 3$ jets	$1.9 \times 10^7$	21 M	1.1
$Z/\gamma (\rightarrow \ell\bar{\ell}, \nu\bar{\nu}) + t\bar{t} + 0, 1, 2$ jets	56	1.0 M	17,000
$Z/\gamma (\rightarrow \ell\bar{\ell}, \nu\bar{\nu}) + b\bar{b} + 0, 1, 2$ jets	$2.8 \times 10^3$	0.1 M	36
$W^\pm (\rightarrow \ell\nu) + b\bar{b} + 0, 1, 2$ jets	$3.2 \times 10^3$	0.6 M	180
$W^\pm (\rightarrow \ell\nu) + t\bar{t} + 0, 1, 2$ jets	70	4.6 M	65,000
$W^\pm (\rightarrow \ell\nu) + t\bar{b} (\bar{t}b) + 0, 1, 2$ jets	$2.4 \times 10^2$	2.1 M	8,700
$t\bar{t}\bar{t}$	0.5	0.09 M	180,000
$t\bar{t}b\bar{b}$	$1.2 \times 10^2$	0.32 M	2,700
$b\bar{b}b\bar{b}$	$2.2 \times 10^4$	0.22 M	1.0
$W^\pm (\rightarrow \ell\nu) + W^\pm (\rightarrow \ell\nu)$	$2.0 \times 10^3$	0.05 M	25
$W^\pm (\rightarrow \ell\nu) + Z (\rightarrow \text{all})$	$1.1 \times 10^3$	1.3 M	1,100
$Z (\rightarrow \text{all}) + Z (\rightarrow \text{all})$	$7.3 \times 10^2$	2.6 M	3,600
$\gamma + 1, 2, 3$ jets	$1.5 \times 10^7$	16 M	1.1

Table 4.1: An exhibition of the Standard Model backgrounds computed in this work at  $E_{CM} = 7$  TeV. All processes were generated using MadGraph 4.4 [32]. Our notation here is that  $\ell = e, \mu, \tau$ , and  $\text{all} = \ell, \nu, \text{jets}$ . In the background analysis we eliminate double counting between the process  $W^\pm + t\bar{b} (\bar{t}b)$  and  $t\bar{t}$  by subtracting out double resonant diagrams of  $t\bar{t}$  when calculating  $W^\pm + t\bar{b} (\bar{t}b)$ .

## 4.2 SUSY models, constraints and collider signatures

To generate candidate models we use a multi-step procedure. We first set the GUT scale parameters which determines a model at the high scale, then through the renormalization group evolution we evolve the symmetry breaking parameters down to the electroweak scale, by using MicrOMEGAs 2.4 [42], which eventually determines the low scale spectrum. After checking all the constraints and bounds to see if it is a physically allowed model, we feed the spectrum into SUSY-HIT 1.3 [43] to calculate the sparticle branching ratios and then into Pythia 6.4 [33] by using the SLHA interface [44]. Then the output file which contains the event record is analyzed within Parvicursor [35].



As we mentioned, not all the models are physically allowed. The most important constraint is the radiative electroweak symmetry breaking (REWSB) which turns on the Higgs mechanism that gives masses to all fermions. Then we impose particle mass bounds obtained from LEP and the Tevatron, the  $g_\mu - 2$  constraint, FCNC constraints from the rare decays of  $B_s \rightarrow \mu^+ \mu^-$  and  $b \rightarrow s + \gamma$ , the relic density constraint and finally recent constraints on the spin independent neutralino-proton cross sections due to non-observation of a dark matter particle in direct detection experiments.

LEP and Tevatron put bounds [45] on the sparticle masses and on the Higgs masses, these are  $m_A > 85$  GeV,  $m_{H^\pm} > 79.3$  GeV,  $m_{\tilde{t}_1} > 101.5$  GeV, and  $m_{\tilde{\tau}_1} > 98.8$  GeV where  $A$  is the CP odd Higgs and  $H^\pm$  is the charged Higgs. We also impose a bound [46] on the lightest CP even Higgs mass,  $m_{h_1} > (93.5 + 15x + 54.3x^2 - 48.4x^3 - 25.7x^4 + 24.8x^5 - 0.5)$  GeV where  $x = \sin^2(\beta - \alpha)$ ,  $\tan \beta$  is the ratio of the Higgs VEVs and  $\alpha$  is the Higgs mixing angle. The final term in the bound represents a theoretical error of 0.5 GeV in the calculation of  $m_{h_1}$  and  $m_A$ . Additionally we use the constraints  $m_{\chi_1^\pm} > 104.5$  GeV if  $|m_{\chi_1^\pm} - m_{\chi_1^0}| > 3$  GeV for the chargino mass and  $m_{\tilde{g}} > 309$  GeV for the gluino

mass [47].

Recent analysis of the hadronic corrections indicate a significant deviation in  $g_\mu - 2$  around  $3.9\sigma$  between the SM prediction and experiment [48]. Such a contribution can arise from supersymmetry [49, 50, 51, 52] and the size of the correction indicates a light sparticle spectrum. On the other hand, data from semileptonic  $\tau$  decays agrees pretty well with the SM prediction. In order to reflect this uncertainty, we use a rather conservative bound  $-11.4 \times 10^{-10} \leq (g_\mu - 2)_{\text{SUSY}} \leq 9.4 \times 10^{-9}$  to constrain the SUSY contribution to the muon's anomalous magnetic moment.

Rare decays of B-mesons also constrain the SUSY parameter space. We use the bounds  $\mathcal{BR}(B_s \rightarrow \mu^+ \mu^-) < 5.8 \times 10^{-8}$  [53, 47] and  $\mathcal{BR}(b \rightarrow s\gamma) = (352 \pm 34) \times 10^{-6}$  [54, 55]. There is currently a small discrepancy between the SM prediction and the measured decay rate of  $b \rightarrow s\gamma$  which is a possible hint for the SUSY contribution [56, 57, 58] and hence another indication of possible light superpartners. Thus this discrepancy along with the reported  $g_\mu - 2$  result is encouraging for an early SUSY discovery [59].

After 7 years of operation, WMAP has measured the dark matter relic density to a great accuracy with  $\Omega_{DM} h^2 = 0.1109 \pm 0.0056$  [60]. However, to account for the errors in the theoretical computations and possible variations in the computation of the relic density using different codes we take a rather wide range in the relic density constraints, i.e.,  $0.06 < \Omega_{DM} h^2 < 0.16$ , in our analysis.

Finally, we also consider the recent negative results of the direct dark matter detection experiments CDMS-II [61, 62] and XENON-100 [63]. These experiments put the best known limits on the spin independent neutralino-proton cross sections. Furthermore, we compare our results to the expected sensitivity for XENON-100 of  $6000 \text{ kg} \times \text{day}$  and for XENON-1Ton of  $1 \text{ ton} \times \text{year}$  [64] as well as the expected sensitivity for SuperCDMS [65]. We summarize all the constraints and bounds we used in Table (4.2).

There are already a number of works which analyze the signatures for supersymmetry at  $E_{CM} = 10, 14 \text{ TeV}$ . See [26, 28, 29, 66, 67, 68, 69, 70] for a small sample. The signatures we looked at consist of a combination of multijets, b-tagged jets, multileptons, jets and leptons, and photons with a variety of cuts designed to reduce the Standard Model background and enhance the SUSY signal

	Constraints / Bounds
REWSB	Radiative electroweak symmetry breaking
LEP/Tevatron	$m_A > 85 \text{ GeV}, m_{H^\pm} > 79.3 \text{ GeV}$ $m_h > (93.5 + 15x + 54.3x^2 - 48.4x^3 - 25.7x^4 + 24.8x^5 - 0.5) \text{ GeV}$ $m_{\tilde{\tau}_1} > 101.5 \text{ GeV}, m_{\tilde{\tau}_1} > 98.8 \text{ GeV}$ $m_{\tilde{\chi}_1^\pm} > 104.5 \text{ GeV}$ if $ m_{\tilde{\chi}_1^\pm} - m_{\tilde{\chi}_1^0}  > 3 \text{ GeV}, m_{\tilde{g}} > 309 \text{ GeV}$
$\mu$ 's anomalous magnetic moment	SUSY contribution: $-11.4 \times 10^{-10} \leq (g_\mu - 2)_{\text{SUSY}} \leq 9.4 \times 10^{-9}$
FCNC	$\mathcal{BR}(B_s \rightarrow \mu^+ \mu^-) < 5.8 \times 10^{-8}, \mathcal{BR}(b \rightarrow s\gamma) = (352 \pm 34) \times 10^{-6}$
WMAP	$0.06 < \Omega_{DM} h^2 < 0.16$
CDMS-II / XENON-100	Bounds on the spin independent neutralino-proton cross section

Table 4.2: A display of constraints and bounds used in our analysis.

with and without missing transverse energy. We use these signatures in the following sections to compute the LHC reach in the framework of mSUGRA and also to determine benchmark models that will be observable in the early run of the LHC. Table (4.3) summarizes the collider signatures we have used in our analysis.

### 4.3 Sparticle production and LHC reach in mSUGRA

In this section we study sparticle production cross sections within the framework of mSUGRA and look at the LHC reach at 7 TeV center of mass energy with  $1 \text{ fb}^{-1}$  of data.

In Fig. (4.2) we show the sparticle production cross sections as a function of the universal gaugino mass  $m_{1/2}$  at the GUT scale. For this we set  $m_0 = 500 \text{ GeV}, A_0 = 0, \tan \beta = 20, \mu > 0$  and generated 5,000 events for multiple  $m_{1/2}$  values. The left panel of Fig. (4.2) shows the cross sections for the production of  $\tilde{g}\tilde{g}$  (solid red line),  $\tilde{g}\tilde{q}$  (dashed green line),  $\tilde{q}\tilde{q}$  (dashed blue line) as a function of  $m_{1/2}$ . The middle panel gives the cross sections for the production of  $\tilde{g}\chi^\pm$  (solid red line),  $\tilde{g}\chi^0$  (dashed green line), and the right panel gives the production cross section for  $\chi^\pm\chi^\pm$  (solid red line),  $\chi^\pm\chi^0$  (dashed green line),  $\chi^0\chi^0$  (dashed blue line). We see that these cross sections are significant

	Signature name	Description of the signature	
1	monojets	$n(\ell) = 0$	$p_T(j_1) \geq 100 \text{ GeV}, p_T(j_2) < 20 \text{ GeV}$
2	multi-jets200	$n(\ell) = 0$	$p_T(j_1) \geq 200 \text{ GeV}, p_T(j_2) \geq 150 \text{ GeV}, p_T(j_4) \geq 50 \text{ GeV}$
3	multi-jets100	$n(\ell) = 0$	$p_T(j_1) \geq 100 \text{ GeV}, p_T(j_2) \geq 80 \text{ GeV}, p_T(j_4) \geq 40 \text{ GeV}$
4	hard-jets500	$n(\ell) = 0$	$p_T(j_2) \geq 500 \text{ GeV}$
5	hard-jets350	$n(\ell) = 0$	$p_T(j_2) \geq 350 \text{ GeV}$
6	multi-bjets1	$n(\ell) = 0, n(b) \geq 1$	
7	multi-bjets2	$n(\ell) = 0, n(b) \geq 2$	
8	multi-bjets3	$n(\ell) = 0, n(b) \geq 3$	
9	$H_T500$	$n(\ell) + n(j) \geq 4$	$p_T(1) \geq 100 \text{ GeV}, \sum_{i=1}^4 p_T(i) + \cancel{E}_T \geq 500 \text{ GeV}$
10	$H_T400$	$n(\ell) + n(j) \geq 4$	$p_T(1) \geq 100 \text{ GeV}, \sum_{i=1}^4 p_T(i) + \cancel{E}_T \geq 400 \text{ GeV}$
11	1-lepton100	$n(\ell) = 1$	$p_T(\ell_1) \geq 20 \text{ GeV}, p_T(j_1) \geq 100 \text{ GeV}, p_T(j_2) \geq 50 \text{ GeV}$
12	1-lepton40	$n(\ell) = 1$	$p_T(\ell_1) \geq 20 \text{ GeV}, p_T(j_2) \geq 40 \text{ GeV}$
13	OS-dileptons100	$n(\ell^+) = n(\ell^-) = 1$	$p_T(\ell_2) \geq 20 \text{ GeV}, p_T(j_1) \geq 100 \text{ GeV}, p_T(j_2) \geq 50 \text{ GeV}$
14	OS-dileptons40	$n(\ell^+) = n(\ell^-) = 1$	$p_T(\ell_2) \geq 20 \text{ GeV}, p_T(j_2) \geq 40 \text{ GeV}$
15	SS-dileptons100	$n(\ell^+   \ell^-) = n(\ell) = 2$	$p_T(\ell_2) \geq 20 \text{ GeV}, p_T(j_1) \geq 100 \text{ GeV}, p_T(j_2) \geq 50 \text{ GeV}$
16	SS-dileptons40	$n(\ell^+   \ell^-) = n(\ell) = 2$	$p_T(\ell_2) \geq 20 \text{ GeV}, p_T(j_2) \geq 40 \text{ GeV}$
17	3-leptons100	$n(\ell) = 3$	$p_T(\ell_3) \geq 20 \text{ GeV}, p_T(j_1) \geq 100 \text{ GeV}, p_T(j_2) \geq 50 \text{ GeV}$
18	3-leptons40	$n(\ell) = 3$	$p_T(\ell_3) \geq 20 \text{ GeV}, p_T(j_2) \geq 40 \text{ GeV}$
19	4 <sup>+</sup> -leptons	$n(\ell) \geq 4$	$p_T(\ell_4) \geq 20 \text{ GeV}, p_T(j_2) \geq 40 \text{ GeV}$
20	1-tau100	$n(\tau) = 1$	$p_T(\tau_1) \geq 20 \text{ GeV}, p_T(j_1) \geq 100 \text{ GeV}, p_T(j_2) \geq 50 \text{ GeV}$
21	1-tau40	$n(\tau) = 1$	$p_T(\tau_1) \geq 20 \text{ GeV}, p_T(j_2) \geq 40 \text{ GeV}$
22	OS-ditaus100	$n(\tau^+) = n(\tau^-) = 1$	$p_T(\tau_2) \geq 20 \text{ GeV}, p_T(j_1) \geq 100 \text{ GeV}, p_T(j_2) \geq 50 \text{ GeV}$
23	OS-ditaus40	$n(\tau^+) = n(\tau^-) = 1$	$p_T(\tau_2) \geq 20 \text{ GeV}, p_T(j_2) \geq 40 \text{ GeV}$
24	SS-ditaus100	$n(\tau^+   \tau^-) = n(\tau) = 2$	$p_T(\tau_2) \geq 20 \text{ GeV}, p_T(j_1) \geq 100 \text{ GeV}, p_T(j_2) \geq 50 \text{ GeV}$
25	SS-ditaus40	$n(\tau^+   \tau^-) = n(\tau) = 2$	$p_T(\tau_2) \geq 20 \text{ GeV}, p_T(j_2) \geq 40 \text{ GeV}$
26	3 <sup>+</sup> -taus100	$n(\tau) \geq 3$	$p_T(\tau_3) \geq 20 \text{ GeV}, p_T(j_1) \geq 100 \text{ GeV}, p_T(j_2) \geq 50 \text{ GeV}$
27	3 <sup>+</sup> -taus40	$n(\tau) \geq 3$	$p_T(\tau_4) \geq 20 \text{ GeV}, p_T(j_2) \geq 40 \text{ GeV}$
28	1 <sup>+</sup> -photon	$n(\gamma) \geq 1$	$p_T(j_2) \geq 40 \text{ GeV}$

Table 4.3: List of signatures and cuts used in the early discovery analysis. Our notation is as follows:  $\ell = e, \mu$ ,  $n(x)$  is the number of object  $x$  in the event, and  $p_T(x_n)$  is the transverse momentum of the  $n^{\text{th}}$  hardest object  $x$ . For the case of  $p_T(\tau)$  we take this to mean the visible part of the  $p_T$  from a hadronically decaying tau. The symbol  $|$  should be read as the logic “or”: i.e. the cut  $n(\tau^+ | \tau^-) = 2$  would be read “the number of  $\tau^+$  equals 2 or the number of  $\tau^-$  equals 2.” We required a global cut of  $\cancel{E}_T \geq 200 \text{ GeV}$  and a minimum transverse sphericity of 0.2.

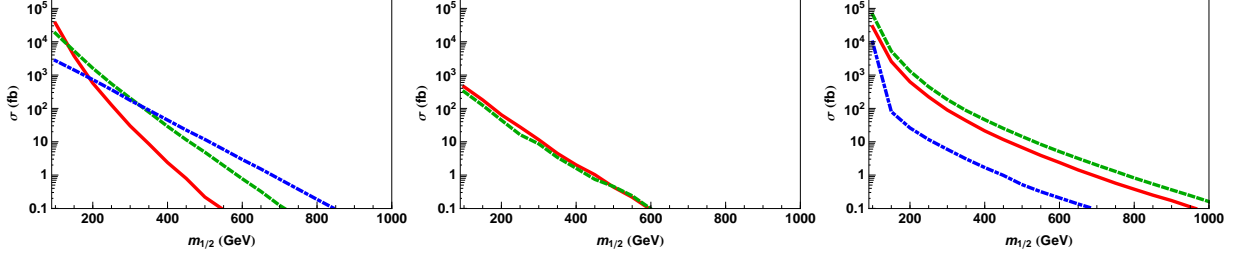


Figure 4.2: An exhibition of the sparticle production cross sections at the LHC at  $\sqrt{s} = 7$  TeV for mSUGRA as a function of the universal gaugino mass  $m_{1/2}$  at the GUT scale. Left panel: production cross sections of  $\tilde{g}\tilde{g}$ ,  $\tilde{g}\tilde{q}$ ,  $\tilde{q}\tilde{q}$  (solid red, dashed green, dashed blue lines). Middle panel: production cross sections for  $\tilde{g}\chi^\pm$ ,  $\tilde{g}\chi^0$  (solid red, dashed green lines). Right panel: production cross sections for  $\chi^\pm\chi^\pm$ ,  $\chi^\pm\chi^0$ ,  $\chi^0\chi^0$  (solid red, dashed green, dashed blue lines).

and  $10^4$  or more SUSY events might get produced with  $1 \text{ fb}^{-1}$  of integrated luminosity at the LHC. Hence even at half of its design center of mass energy, it will be possible to discover SUSY at the early runs of the LHC.

We also studied the reach of the LHC in mSUGRA by using the Standard Model backgrounds given in Table (4.1) and collider signatures given Table (4.3). We assumed an integrated luminosity of  $1 \text{ fb}^{-1}$ . The mSUGRA parameters used are  $A_0 = 0$ ,  $\tan\beta = 45$ ,  $\text{sign}(\mu) = 1$ . The analysis is done under the conditions of REWSB and the LEP and Tevatron constraints but without the imposition of the relic density and FCNC constraints. The condition used for a signal to be observable is  $S > \max(5\sqrt{SM}, 10)$  where  $SM$  stands for the Standard Model background. Early LHC reaches at  $1 \text{ fb}^{-1}$  for the gluino ( $\tilde{g}$ ), the chargino ( $\tilde{\chi}_1^\pm$ ), the neutralino ( $\chi_1^0$ ), the stau ( $\tilde{\tau}_1$ ), and the stop ( $\tilde{t}_1$ ) are exhibited in the inset where the y axis is plotted on a logarithmic scale.

We see from Fig. (4.3) that the LHC will be able to probe up to about 400 GeV in  $m_{1/2}$  at low values of  $m_0$  and up to about 2 TeV in  $m_0$  for low values of  $m_{1/2}$  with  $1 \text{ fb}^{-1}$  of integrated luminosity. If CERN decides to run at half the design center of mass energy for a longer time and accumulate  $2 \text{ fb}^{-1}$  of integrated luminosity, the reach can be extended up to 450-500 GeV in  $m_{1/2}$ .

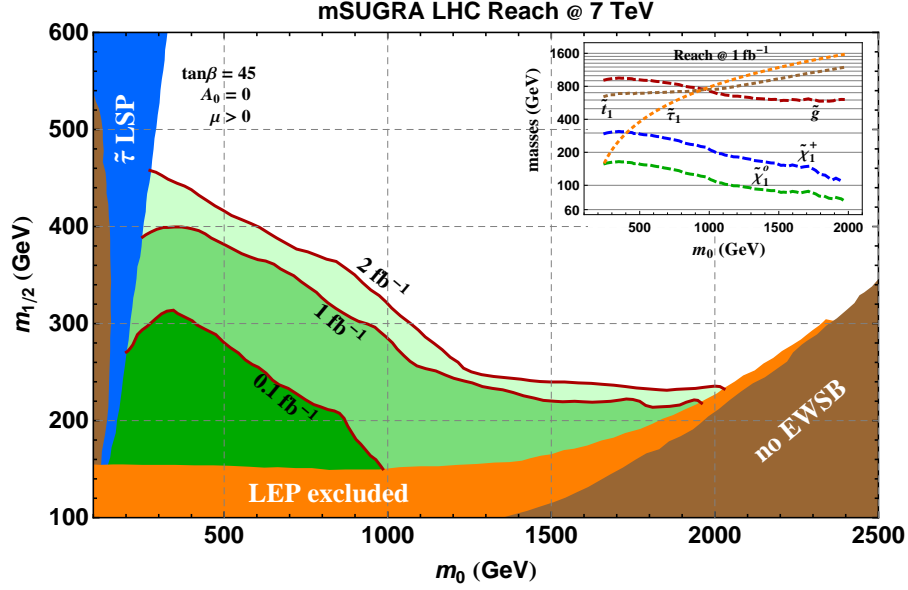


Figure 4.3: LHC reach in the framework of mSUGRA at 7 TeV center of mass energy.

#### 4.4 Nonuniversal mSUGRA and benchmark models

Since the nature of physics at the Planck scale is still largely unknown, one may extend mSUGRA to include nonuniversalities and one of the most widely used extensions is the nonuniversality in the gaugino sector [71, 72, 73, 74, 75, 76, 77, 78, 79, 1, 80, 81, 82, 83, 84, 85, 86, 87, 88, 89, 90]. With this extension, we specify each gaugino mass  $m_i$  separately or equivalently via the relations  $m_i = m_{1/2}(1 + \delta_i)$  ( $i=1,2,3$ ) corresponding to the gauge groups  $U(1)$ ,  $SU(2)_L$ , and  $SU(3)_C$ . Hence the space is extended to six parameters and a sign.

An analysis of cross sections similar to Fig (4.2) for the case of nonuniversalities in the gaugino sector is given in Fig. (4.4), where we give contour plots in the  $m_{\tilde{g}} - m_{\tilde{\chi}^\pm}$  mass plane with other parameters as stated in the caption of the figure. The plots give contours of constant  $\log(\sigma_{SUSY}/\text{fb})$  in the range 1 – 3.5. The result is that a chargino mass up to about 500 GeV and a gluino mass up to roughly 1 TeV would produce up to 1,000 or more events with  $1 \text{ fb}^{-1}$  of integrated luminosity.

Nonuniversality in the gaugino sector implies that we cannot use the  $m_{1/2} - m_0$  plane to show the LHC reach as we did for the universal case. In general, as the number of free GUT scale

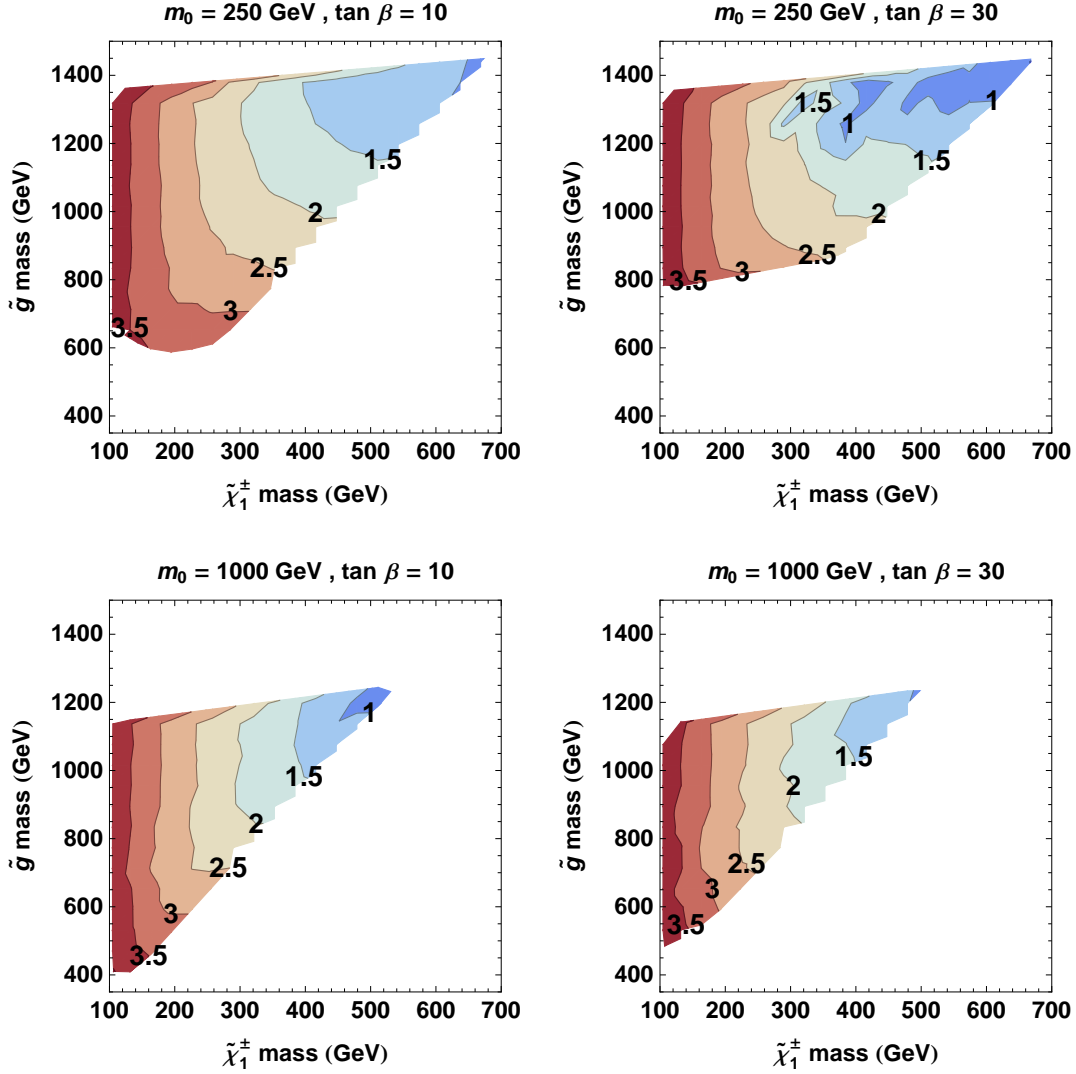


Figure 4.4: Contour plots with constant values of  $\log(\sigma_{SUSY}/\text{fb})$  for  $\sigma_{SUSY}$  in  $m_{\tilde{g}} - m_{\tilde{\chi}^\pm}$  mass plane for the case with nonuniversalities in the gaugino sector. We vary the gaugino masses  $m_{1,2,3}$  up to 1 TeV and keep  $A_0 = 0$  and  $\text{sign}(\mu)=+1$ .  $m_0$  and  $\tan\beta$  are given on the figures.

parameters increases, it gets harder to find a plane similar to  $m_{1/2} - m_0$  which will allow the drawing of a smooth reach curve. One way of dealing with this difficulty is to produce enough benchmark models that will capture the characteristics of the theory we consider and to categorize them according to a unified feature. Then one can study these models in further detail. This was done in the past for the design center of mass energy of 14 TeV of the LHC. Following [69, 79], we

accomplish the same task by using the mass of the next to lightest sparticle (NLSP) as our guide for the models we look at. This method also captures the rich LHC phenomenology better than previous methods of producing benchmark models which simply focused on covering a wider range of GUT scale parameters than mass hierarchies. Hence we categorize our models according to their NLSP's which can be a chargino ( $\chi^\pm$ ), a stau ( $\tilde{\tau}$ ), a gluino ( $\tilde{g}$ ), a CP odd Higgs ( $A^0$ ), or a stop ( $\tilde{t}$ ).

We generated  $O(10^6)$  random models and selected the ones with a neutralino LSP and that satisfy all the constraints and bounds given previously in Table (4.2) including the mass bounds of sparticles,  $g_\mu - 2$  constraint, FCNC constraints and relic density constraints. Then these models are grouped according to their NLSP's and tested for visibility in at least one of the channels given in Table (4.3) at the LHC with  $1(2) \text{ fb}^{-1}$  of integrated luminosity. The condition we used for a signal to be observable is  $S > \max(5\sqrt{SM}, 10)$  where  $SM$  stands for the Standard Model background. We also required that our models be visible at future dark matter direct detection experiments. The benchmark models we determined are displayed in Table (4.4), and the light sparticle masses are displayed in Appendix (A.1).

We see that for some of the benchmarks the SUSY production cross section can be as large as 10-20 pb or more, implying that as many as  $1 - 2 \times 10^3$  SUSY events will be produced at the LHC with  $1 \text{ fb}^{-1}$  of integrated luminosity. So there is a good chance of discovering these models with properly tuned signatures that will reduce the Standard Model background but will keep enough SUSY events. In Fig. (4.5) we display discovery channels for which the benchmark models produce enough events to be visible above background at 7 TeV center of mass energy with  $0.1/1/2 \text{ fb}^{-1}$  of integrated luminosity. In fact for most of the benchmark models of Table (4.4) there are as many as five channels and often more where the SUSY signal will become visible, thus providing important cross-checks for the discovery of supersymmetry.

For early detection, the most effective and most studied discovery channels of SUSY, i.e. jets + missing energy signatures, should be as inclusive as possible to increase the number of signal events since the number of SUSY signal events will be small at low integrated luminosities of  $< 1 \text{ fb}^{-1}$ . As Fig. (4.5) and Table (4.5) indicate four of five chargino NLSP benchmarks can actually

Label	NLSP	$m_0$	$m_{1/2}$	$A_0$	$\tan\beta$	$\delta_2$	$\delta_3$	$\sigma_{SUSY}$ (pb)	$\sigma_{SI}$ ( $10^{-8}$ pb)
C1	$\tilde{\chi}_1^\pm$	1663	309	1508	32.9	0.553	-0.687	24.3	7.0
C2	$\tilde{\chi}_1^\pm$	449	330	176	20.3	-0.382	-0.151	2.4	3.7
C3	$\tilde{\chi}_1^\pm$	1461	361	1327	30.3	-0.241	-0.702	14.8	4.5
C4	$\tilde{\chi}_1^\pm$	1264	445	1775	24.7	0.718	-0.736	11.3	4.7
C5	$\tilde{\chi}_1^\pm$	240	313	-522	5.48	-0.376	-0.106	3.5	0.7
G1	$\tilde{g}$	1694	755	-2128	45.7	0.745	-0.803	2.2	4.9
G2	$\tilde{g}$	2231	639	2710	18.0	0.543	-0.850	24.2	3.0
G3	$\tilde{g}$	2276	615	-2407	47.2	0.631	-0.784	3.1	2.6
G4	$\tilde{g}$	2180	651	-2271	47.1	0.680	-0.817	5.8	8.3
G5	$\tilde{g}$	2126	683	2924	38.0	0.580	-0.849	19.4	4.8
G6	$\tilde{g}$	1983	749	-2332	46.3	0.562	-0.824	3.7	2.7
H1	$A^0$	2225	674	-2531	47.3	0.783	-0.703	0.3	0.9
S1	$\tilde{\tau}_1$	117	394	0	15.9	-0.327	-0.177	1.4	1.4
S2	$\tilde{\tau}_1$	101	446	-153	6.1	0.607	-0.207	0.4	0.5
S3	$\tilde{\tau}_1$	102	470	183	15.3	0.603	-0.266	0.5	3.0
S4	$\tilde{\tau}_1$	309	581	-613	27.7	0.839	-0.400	0.6	1.6
S5	$\tilde{\tau}_1$	135	688	-184	5.7	-0.052	-0.499	0.4	1.6
S6	$\tilde{\tau}_1$	114	404	27	13.0	-0.369	-0.267	2.0	3.0
S7	$\tilde{\tau}_1$	114	518	87	10.4	0.266	-0.247	0.2	0.6
T1	$\tilde{t}_1$	1726	548	4197	21.2	0.132	-0.645	2.3	0.005
T2	$\tilde{t}_1$	1590	755	3477	23.4	0.805	-0.803	3.8	0.094

Table 4.4: Benchmarks for *models discoverable at the  $5\sigma$  level at the LHC at  $\sqrt{s} = 7$  TeV with  $2 \text{ fb}^{-1}$  of integrated luminosity. The model inputs are given at  $M_{GUT} = 2 \times 10^{16}$  GeV,  $\mu > 0$ , and  $\delta_1 = 0$ . The displayed masses are in GeV. All models satisfy the constraints/bounds given in Table (4.2). The spin independent neutralino-proton cross section,  $\sigma_{SI}$ , is exhibited as well as the cross section  $\sigma_{SUSY}$  for the production of supersymmetric particles at  $\sqrt{s} = 7$  TeV.*

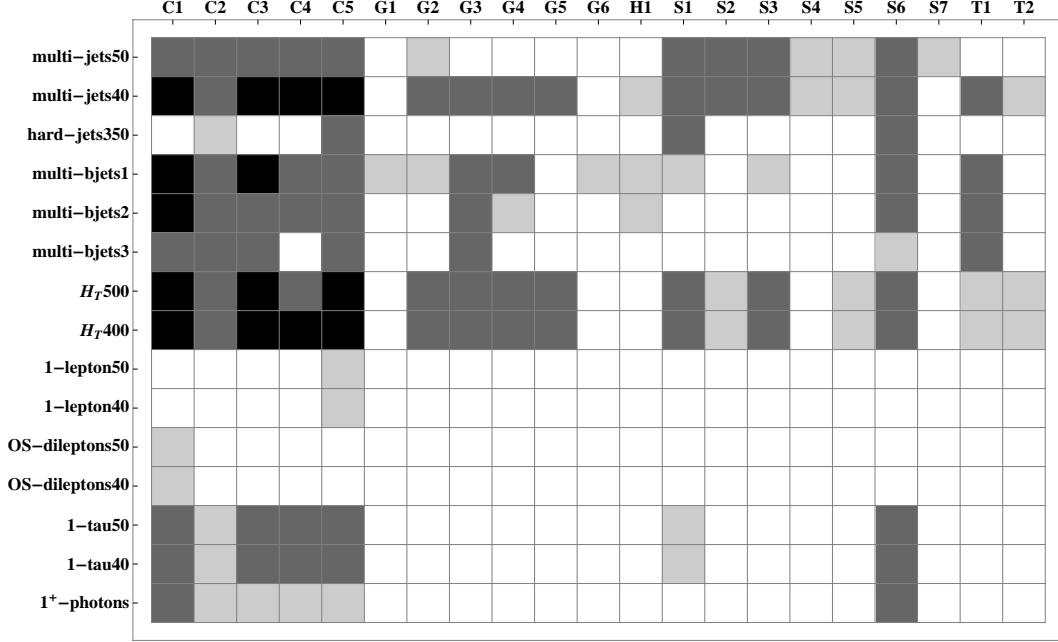


Figure 4.5: An exhibition of the visible discovery channels for  $0.1 \text{ fb}^{-1}$  (black squares),  $1 \text{ fb}^{-1}$  (dark gray squares) and  $2 \text{ fb}^{-1}$  (light gray squares) at  $\sqrt{s} = 7 \text{ TeV}$ . The discovery channels are listed in Table (4.3).

Signature Name		SM	C1	C4	C5	G2	G3	S3	S6	T1
Multi-jets200	Events	47	91	68	105	28	16	49	88	12
	$S/\sqrt{B}$	...	13.3	9.9	15.2	4.1	2.4	7.2	12.7	1.8
Multi-jets100	Events	180	401	225	213	114	83	77	171	69
	$S/\sqrt{B}$	...	29.9	16.8	15.9	8.5	6.2	5.8	12.8	5.2
Multi-jets40	Events	215	497	316	218	135	107	77	176	85
	$S/\sqrt{B}$	...	33.9	21.6	14.9	9.2	7.3	5.3	12.0	5.8
$H_T400$	Events	965	1035	501	496	286	183	156	419	143
	$S/\sqrt{B}$	...	33.3	16.1	16.0	9.2	5.9	5.0	13.5	4.6
Multi-bjets1	Events	188	460	188	175	51	126	50	102	86
	$S/\sqrt{B}$	...	33.5	13.7	12.8	3.7	9.2	3.6	7.5	6.3
Multi-bjets2	Events	46	157	49	69	7	57	19	39	45
	$S/\sqrt{B}$	...	23.1	7.3	10.1	...	8.4	2.8	5.7	6.6
1-lepton40	Events	367	45	20	74	0	0	30	38	27
	$S/\sqrt{B}$	...	2.4	1.0	3.9	...	...	1.6	2.0	1.4

Table 4.5: LHC discovery channels after  $1 \text{ fb}^{-1}$  of integrated luminosity for selected benchmark models. We have also included a much weaker multijet signature (multijets40) in which the four jets are all required merely to satisfy  $p_T^{\text{jet}} \geq 40 \text{ GeV}$  to channels listed previously in Table (4.3).

be discovered via jet-based signatures within the first  $100 \text{ pb}^{-1}$  of data, with the remainder (C2) reaching a five-sigma significance in the multijets100 channel within  $200 \text{ pb}^{-1}$ . By contrast, because of a heavier spectrum with a heavier gluino producing long cascades with moderately energetic jets, our stau NLSP benchmark models favor traditional multijet signatures such as multijets200 and  $H_T 500$  which involve much harder jet- $p_T$  requirements. And finally our Higgs, stop and gluino NLSP models favor discovery signatures with looser jet requirements including  $H_T 400$ , multi-bjets1 and multi-bjets2. The effectiveness of b-jet based signatures for these models can be explained with the rather small mass gaps between the lightest  $SU(3)$ -charged state (i.e. the gluino or squark) and the LSP which eventually appears at the end of the cascade [91]. An example would be a light stop with the following decay chain producing a bjet:  $\tilde{t}_1 \rightarrow \tilde{\chi}^+ + b \rightarrow W^+ + b + \tilde{\chi}_1^0$ .

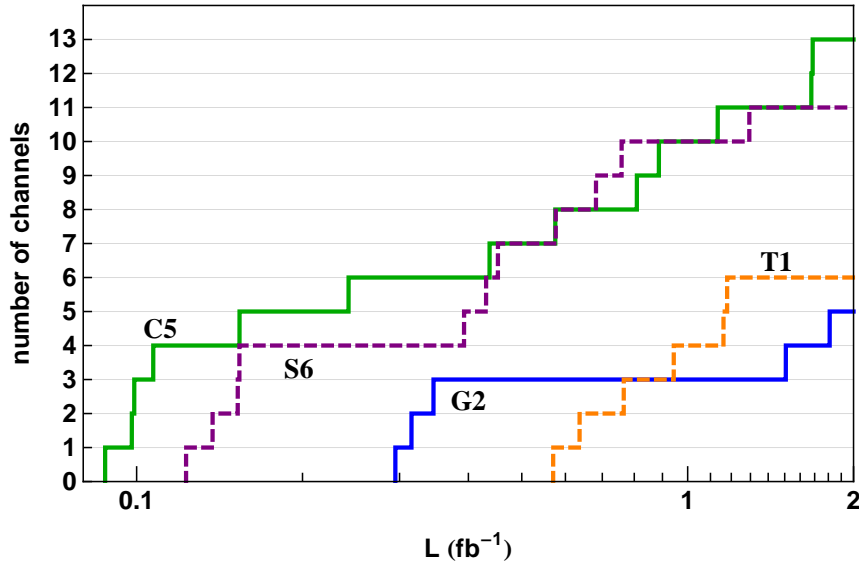


Figure 4.6: An exhibition of the rapid rise in the number of discovery channels vs integrated luminosity for four early discovery benchmarks given in Table (4.4). The number of discovery channels for supersymmetry in each case is in excess of five and in some cases as large as 10 or above at  $1 \text{ fb}^{-1}$  of data at  $\sqrt{s} = 7 \text{ TeV}$ .

It is also interesting to ask how the number of visible signatures depends on the integrated luminosity. Fig. (4.6) answers this question by showing the number of signature channels where the SUSY signal becomes visible as a function of the integrated luminosity. The figure shows that

the number of discovery channels increases rather sharply with luminosity and can become as large as 10 or more at  $1 \text{ fb}^{-1}$  of integrated luminosity. We again see the analysis of Fig. (4.6) also exhibits that a SUSY discovery can occur with an integrated luminosity as low as  $100 \text{ pb}^{-1}$  still with several available discovery channels.

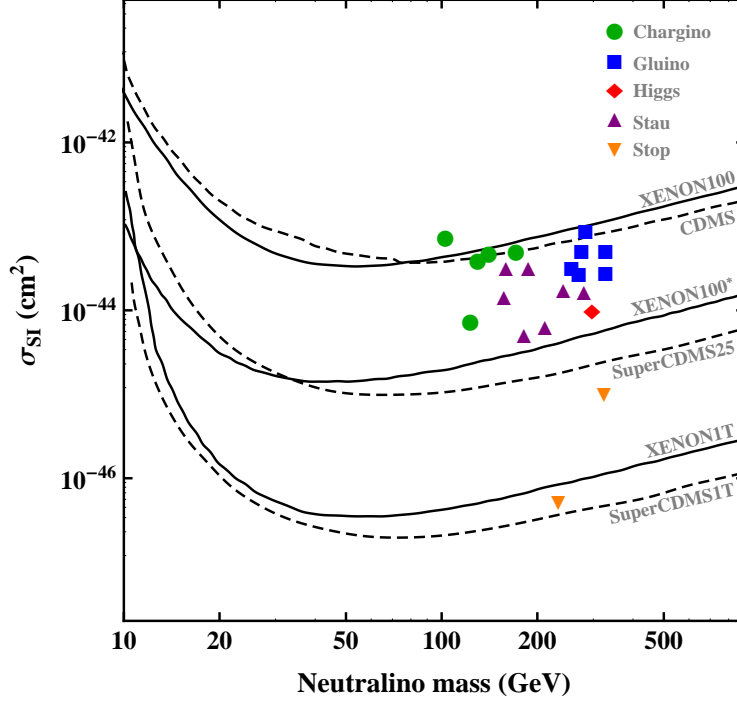


Figure 4.7: An exhibition of the spin independent neutralino-proton cross section,  $\sigma_{SI}$ , for the benchmark models. In the plot the curve labeled XENON100\* is the expected sensitivity of XENON100 with  $6000 \text{ kg} \times \text{days}$  of data, the curve labeled XENON1T is the expected sensitivity for  $1 \text{ ton} \times \text{year}$  of data and the curves labeled SuperCDMS25 and SuperCDMS1T are the expected sensitivities for the two SuperCDMS experiments.

As we mentioned earlier the benchmark models given in Table (4.4) will all be visible in at least one channel at the early run of the LHC and further, as shown in Fig. (4.7), all of them are also consistent with the current limits on the spin independent neutralino-proton cross sections from CDMS-II and XENON-100. We also show the expected sensitivity of the next generation of xenon and germanium experiments. One can see that our benchmark models will all be visible by direct detection dark matter experiments in the future. In this sense our benchmark models constitute a perfect set of models to study for the early detection of SUSY at the LHC and at direct detection of

dark matter experiments. Finally in Figs (A.1, A.2) we exhibit the sparticle spectra of a subset of the benchmark models given in Table (4.4).

## 4.5 Summary

We studied the SUSY discovery potential of the early LHC run at 7 GeV center of mass energy with up to  $2 \text{ fb}^{-1}$  of data. As a first step we worked on generating a good representation of the Standard Model background at the LHC which is generally consistent with a previous study [31]. We then looked into mSUGRA and nonuniversal mSUGRA frameworks with a nonuniversality in the gaugino sector. Specifically we analyzed the LHC reach in the mSUGRA framework and showed a reach of  $m_{1/2} \approx 400 \text{ GeV}$  (for low  $m_0$ ) and  $m_0 \approx 2000 \text{ GeV}$  (for low  $m_{1/2}$ ) is possible within the first inverse femtobarn of data. We then studied nonuniversal mSUGRA and generated the benchmark models given in Table (4.4) satisfying both the theoretical and the experimental constraints. These benchmark models are grouped according to their next to lightest sparticles and represent different phenomenological properties which can be studied further for the early detection of supersymmetry at the LHC as well as in direct detection experiments of dark matter.

## Chapter 5

### Studying Gaugino Mass Unification at the LHC\*

As we approach the end of the second year of its operation, the LHC has already collected enough physics data for analyses aimed at New Physics discoveries to be performed. So far there is no sign of physics beyond the Standard Model but a fraction of the allowed parameter space of supersymmetry (SUSY) is ruled out [94]. We continue to believe that SUSY is the best-motivated extension to the Standard Model for physics at the LHC energy scale and there are many reasons to expect that its presence will be established relatively early on in the LHC program [95]. It will be even possible to determine some of the masses and spins of lighter sparticles with little integrated luminosity [96, 26, 97].

After determining the presence of SUSY, the focus will be on interpreting these results. For a high energy theorist interested in correlating the low scale supersymmetric theory to a high energy theory, for example string theory, one of the most important properties would be the presence of gaugino mass universality. The gauginos of the MSSM are said to be universal if they all acquire soft masses of the same magnitude at the energy scale at which the SUSY breaking is transmitted to the observable sector. This question is also related to the wave function of the LSP which is the lightest neutralino for R parity conserving theories where the LSP is also a dark matter candidate. Furthermore low energy phenomenology, the nature of the SUSY breaking, and the structure of the underlying physics Lagrangian are all related strongly to the question of gaugino mass universality [3]. Unfortunately the soft supersymmetry breaking masses of the gauginos are not directly measurable at the LHC, as opposed to the physical superpartner masses [98]. Quantum corrections to the gluino bare mass can be large and are related to a large set of other MSSM soft parameters [24, 99] which are also not directly measurable at the LHC.

---

\*This chapter is based on the work that has been published in JHEP [84], AIP Conf.Proc. [92] and Nucl.Phys.Proc.Suppl. [93].

To study the gaugino masses, one can assume some particular model either with universal gaugino masses such as mSUGRA [100] or with fixed, nonuniversal gaugino mass ratios [101, 81] then make a fit to see if the model in hand explains the LHC data. But we are more interested in knowing if gaugino mass universality is a property of the underlying physics or not, rather than a feature of a particular theory. To accomplish our goal we consider a concrete parametrization of nonuniversalities in soft gaugino masses. Among many such frameworks, we choose the so-called “mirage pattern” of gaugino masses which is a string theory motivated parametrization by Choi and Nilles [83]. In this paradigm gaugino masses unify at some high energy scale but this unification has nothing to do with grand unification of gauge groups and the gauge couplings will in general not unify at this particular energy scale. In the following section we give a brief introduction to Mirage unification.

## 5.1 Mirage pattern of gaugino masses

We will now derive the mirage mass pattern here without making any reference to how it arises from string-theoretic constructions. We begin by assuming there are two contributions to the soft supersymmetry breaking gaugino masses that arise at some effective high-energy scale  $\Lambda_{UV}$  at which supersymmetry breaking is transmitted from some hidden sector to the observable sector. In string constructions, one might choose  $\Lambda_{UV}$  to be different and possibly higher than the GUT scale such that the supergravity approximation for the effective Lagrangian becomes valid. We also assume that one of these contributions to gaugino masses is universal and the other one is proportional to the beta-function coefficient of the Standard Model gauge group. Hence the universal piece is given by

$$M_a^1(\Lambda_{UV}) = M_u, \quad (5.1)$$

where  $a = 1, 2, 3$  labels the Standard Model gauge group factors  $\mathcal{G}_a$  and  $M_u$  represents some mass scale in the theory. The second piece is the so-called anomaly mediated piece, which arises from loop diagrams involving the auxiliary scalar field of supergravity [102, 103]. It has the following

form

$$M_a^2(\Lambda_{\text{UV}}) = g_a^2(\Lambda_{\text{UV}}) \frac{b_a}{16\pi^2} M_g, \quad (5.2)$$

where  $M_g$  is related to the gravitino mass and the  $b_a$  are the beta-function coefficients for the Standard Model gauge groups which are given by

$$b_a = -(3C_a - \sum_i C_a^i), \quad (5.3)$$

where  $C_a, C_a^i$  are the quadratic Casimir operators for the gauge group  $\mathcal{G}_a$ , respectively, in the adjoint representation and in the representation of the matter field charged under that group. For the MSSM these are

$$\{b_1, b_2, b_3\} = \left\{ \frac{33}{5}, 1, -3 \right\}. \quad (5.4)$$

Note that if we take  $\Lambda_{\text{UV}} = \Lambda_{\text{GUT}}$  then we have

$$g_1^2(\Lambda_{\text{UV}}) = g_2^2(\Lambda_{\text{UV}}) = g_3^2(\Lambda_{\text{UV}}) = g_{\text{GUT}}^2 \simeq \frac{1}{2}. \quad (5.5)$$

The full gaugino masses at the high energy boundary condition scale are therefore given by

$$M_a(\Lambda_{\text{UV}}) = M_a^1(\Lambda_{\text{UV}}) + M_a^2(\Lambda_{\text{UV}}) = M_u + g_a^2(\Lambda_{\text{UV}}) \frac{b_a}{16\pi^2} M_g. \quad (5.6)$$

Now we can evolve the above boundary conditions to some low-energy scale  $\Lambda_{\text{EW}}$  via the (one-loop) renormalization group equations (RGEs). Each contribution can be evolved separately and for the universal piece we can use the fact that  $M_a/g_a^2$  is a constant for the one-loop RGEs. After some manipulation this yields

$$M_a^1(\Lambda_{\text{EW}}) = M_u \left[ 1 - g_a^2(\Lambda_{\text{EW}}) \frac{b_a}{8\pi^2} \ln \left( \frac{\Lambda_{\text{UV}}}{\Lambda_{\text{EW}}} \right) \right]. \quad (5.7)$$

For the anomaly-generated piece of (5.2) we can simply replace the gauge coupling with the value at the appropriate scale

$$M_a^2(\Lambda_{\text{EW}}) = g_a^2(\Lambda_{\text{EW}}) \frac{b_a}{16\pi^2} M_g, \quad (5.8)$$

Combining these two pieces gives the low scale expression

$$M_a(\Lambda_{EW}) = M_u \left\{ 1 - g_a^2(\Lambda_{EW}) \frac{b_a}{8\pi^2} \ln\left(\frac{\Lambda_{UV}}{\Lambda_{EW}}\right) \left[ 1 - \frac{1}{2} \frac{M_g}{M_u \ln\left(\frac{\Lambda_{UV}}{\Lambda_{EW}}\right)} \right] \right\}. \quad (5.9)$$

For gaugino masses to be unified at the low scale  $\Lambda_{EW}$  then the quantity in the square brackets in the above expression must vanish. For a given  $\Lambda_{UV}$  (such as the GUT scale) and a given overall scale  $M_u$ , this gives a one-parameter family of models defined by the choice  $M_g$ . There is a more convenient parametrization of the family of gaugino mass patterns which is realized by the parameter  $\alpha$  defined as

$$\alpha = \frac{M_g}{M_u \ln(\Lambda_{UV}/\Lambda_{EW})}, \quad (5.10)$$

so that (5.9) becomes

$$M_a(\Lambda_{EW}) = M_u \left[ 1 - \left(1 - \frac{\alpha}{2}\right) g_a^2(\Lambda_{EW}) \frac{b_a}{8\pi^2} \ln\left(\frac{\Lambda_{UV}}{\Lambda_{EW}}\right) \right] \quad (5.11)$$

and the requirement of universality at the scale  $\Lambda_{EW}$  now implies  $\alpha = 2$ . Normalizing the three gaugino masses by  $M_1(\Lambda_{EW})|_{\alpha=0}$  and evaluating the gauge couplings at a scale  $\Lambda_{EW} = 1$  TeV we obtain the mirage ratios

$$\begin{aligned} M_1 : M_2 : M_3 &= (1.0 + 0.66\alpha) : (1.93 + 0.19\alpha) : (5.87 - 1.76\alpha) \\ &\simeq (1 + 0.66\alpha) : (2 + 0.2\alpha) : (6 - 1.8\alpha), \end{aligned} \quad (5.12)$$

for  $\Lambda_{UV} = \Lambda_{GUT}$ , in good agreement with the expression in [83].

We can also generalize the parametrization in (5.10) to use mass scales of the theory itself instead of the starting and stopping points in the RG evolution of the gaugino mass parameters. Following the convention of Choi et al. [104] we define

$$\alpha \equiv \frac{M_g}{M_u \ln(M_{PL}/M_g)}, \quad (5.13)$$

where  $M_{PL}$  is the reduced Planck mass  $M_{PL} = 2.4 \times 10^{18}$  GeV. Our parametrization is now free

from the boundary condition scales of the RG flow and can be fixed in advance. Inserting (5.13) into (5.9) yields

$$\begin{aligned}
M_a(\Lambda_{EW}) &= M_u \left\{ 1 - g_a^2(\Lambda_{EW}) \frac{b_a}{8\pi^2} \left[ \ln\left(\frac{\Lambda_{UV}}{\Lambda_{EW}}\right) - \frac{\alpha}{2} \ln\left(\frac{M_{PL}}{M_g}\right) \right] \right\} \\
&= M_u \left\{ 1 - g_a^2(\Lambda_{EW}) \frac{b_a}{8\pi^2} \left[ \ln\left(\frac{\Lambda_{UV} (M_g/M_{PL})^{\alpha/2}}{\Lambda_{EW}}\right) \right] \right\}.
\end{aligned} \tag{5.14}$$

In this parametrization the requirement of universality at the scale  $\Lambda_{UV} = \Lambda_{GUT}$  implies the soft supersymmetry breaking gaugino masses unify at an effective scale given by

$$\Lambda_{mir} = \Lambda_{GUT} \left( \frac{M_g}{M_{PL}} \right)^{\alpha/2}. \tag{5.15}$$

The value of  $\alpha$  can be thought of as the ratio of the anomaly contribution to the universal contribution to gaugino masses. We obtain the gaugino mass ratios (1:2:6) of the minimal supergravity paradigm in the limit of  $\alpha \rightarrow 0$ , while we obtain the gaugino mass ratios (3.3:1:9) of anomaly mediated supersymmetry breaking (AMSB) in the limit of  $\alpha \rightarrow \infty$ .

## 5.2 Setting up the problem

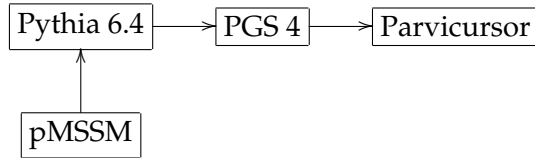
As we mentioned earlier in the beginning of the chapter, our goal is to develop a method to understand if gaugino masses are universal or not, ideally by using the minimum amount of LHC data possible. In terms of the Mirage unification model we used, that translates into determining if  $\alpha$  is zero or not. Our first step is to demonstrate that some set of “targeted observables” [105] (we will call them “signatures” in what follows) is sensitive to small changes in  $\alpha$  when all other SUSY model parameters are kept fixed. Although this is not too realistic, it is a good point of departure and certainly in the spirit of the “slopes” of the Snowmass Points and Slopes [106] and other such benchmark studies. “Slopes” then will correspond to “model lines” in our study in which all parameters are kept fixed but the value of  $\alpha$  is varied in a controlled manner.

To construct a model line we must specify the supersymmetric model in all aspects other

than the gaugino sector. The MSSM has 105 free parameters but it would be impossible to work with all those. Fortunately only a small subset are in any way relevant for the LHC collider phenomenology [107]. We will therefore choose a subset of 19 parameters which is sometimes called the pMSSM or phenomenological MSSM. The parameters <sup>†</sup> of the pMSSM are given as follows:

$$\left\{ \begin{array}{l} \tan\beta, m_{H_u}^2, m_{H_d}^2 \\ A_t, A_b, A_\tau \\ M_1, M_2, M_3 \\ m_{Q_{1,2}}, m_{U_{1,2}}, m_{D_{1,2}}, m_{L_{1,2}}, m_{E_{1,2}} \\ m_{Q_3}, m_{U_3}, m_{D_3}, m_{L_3}, m_{E_3} \end{array} \right\}. \quad (5.16)$$

We specify these parameters in (5.16) at the electroweak scale (specifically  $\Lambda_{EW} = 1$  TeV) so no renormalization group evolution is required. The gluino soft mass  $M_3$  sets the overall mass scale of the gaugino sector and the other two gaugino masses  $M_1$  and  $M_2$  are determined relative to  $M_3$  according to the Mirage mass patterns given in (5.12) as a function of  $\alpha$ . A model line is a collection of model points starting with all the inputs parameters of (5.16) fixed and the parameter  $\alpha$  is varied around  $\alpha = 0$  (the mSUGRA limit).



To simulate each model we use PYTHIA 6.4 [33] for spectrum calculation and event generation. We use PGS4 [34] to simulate the detector response. We then analyze the events in Parvicursor [35]. In the next sections, we will present the method we use to select the optimal set of signatures to distinguish between  $\alpha = 0$  from other points along the model line by using the least amount of integrated luminosity, the signature lists determined with this method, and how they perform on a random set of models.

---

<sup>†</sup>Note that one can also use  $\mu$  and  $M_A$  instead of  $m_{H_u}^2$  and  $m_{H_d}^2$

### 5.3 Signature selection

We would like to combine multiple good signatures to minimize the required integrated luminosity to distinguish two similar models. To accomplish this goal, we need a method to measure the “distance” between two model points in the signature space. This distance definition should take into account the fact that the counting measurements will have uncertainties due to finite statistics. So we define the following distance function similar to a chi-square statistic between any two models  $A$  and  $B$  as the metric on the signature space which is very similar to the one used in [2]:

$$(\Delta S_{AB})^2 = \frac{1}{n} \sum_{i=1}^n \left[ \frac{S_i^A - S_i^B}{\delta S_i^{AB}} \right]^2, \quad (5.17)$$

where  $S_i$  is the  $i^{\text{th}}$  counting signature and  $\delta S_i^{AB}$  is the uncertainty of the numerator, i.e. the difference between the signatures which we will assume to contain only statistical errors. We can identify any signature  $S_i$  with an “effective” cross section  $\bar{\sigma}_i = S_i/L$  which includes the geometric cuts that are performed on the data, the detector efficiencies, etc. At large integrated luminosity this converges to an “exact” cross section  $\sigma_i = \lim_{L \rightarrow \infty} \bar{\sigma}_i$ . Rewriting the metric in terms of these effective cross sections gives us

$$(\Delta S_{AB})^2 = \frac{1}{n} \sum_{i=1}^n \left[ \frac{\bar{\sigma}_i^A - \bar{\sigma}_i^B}{\sqrt{\bar{\sigma}_i^A/L_A + \bar{\sigma}_i^B/L_B}} \right]^2, \quad (5.18)$$

where  $L^A$  and  $L^B$  are the integrated luminosities that are used to compute the effective cross sections.

We can obtain the statistical properties of this metric by replacing each signature (or effective cross section) by a random variable. At a finite integrated luminosity, we can describe the outcome of a counting experiment as a Poisson distribution approximated by a normal distribution (this is a good approximation for approximately 10 counts or more which we require as the minimum to observe a signal). Hence we replace each signature with a random variable following a normal

distribution. After this randomization, the effective cross sections simply become

$$\bar{\sigma}_i = S_i^A/L_A = \sigma_i^A + \sqrt{\sigma_i^A/L_A} Z_A, \quad (5.19)$$

with a similar expression for the model B.

The sum of two normally distributed random variables is again a normally distributed random variable, and we can express the sum as

$$a Z_1(\mu_1, \sigma_1) + b Z_2(\mu_2, \sigma_2) = Z(a \mu_1 + b \mu_2, a^2 \sigma_1^2 + b^2 \sigma_2^2), \quad (5.20)$$

where  $\mu$  is the mean and  $\sigma^2$  is the variance. So we can substitute (5.19) into (5.18) and if we use the addition property of the random variables we get

$$\begin{aligned} (\Delta S_{AB})^2 &= \frac{1}{n} \sum_{i=1}^n \frac{\left[ \sigma_i^A - \sigma_i^B + \sqrt{\frac{\sigma_i^A}{L_A} + \frac{\sigma_i^B}{L_B}} Z_i \right]^2}{\frac{\sigma_i^A}{L_A} + \frac{\sigma_i^B}{L_B} + \sqrt{\frac{1}{L_A^2} \frac{\sigma_i^A}{L_A} + \frac{1}{L_B^2} \frac{\sigma_i^B}{L_B}} Z'_i} \\ &\approx \frac{1}{n} \sum_{i=1}^n \left[ \frac{\sigma_i^A - \sigma_i^B}{\sqrt{\frac{\sigma_i^A}{L_A} + \frac{\sigma_i^B}{L_B}}} + Z''_i \right]^2, \end{aligned} \quad (5.21)$$

where  $Z_i$ ,  $Z'_i$  and  $Z''_i$  are independent normally distributed random variables. We assume all  $Z''_i$  are independent which simply means our  $n$  signatures are independent from each other. The algebraic form of Eqn. 5.21 suggests that  $(\Delta S_{AB})^2$  is itself a random variable following a non central chi-square distribution given as

$$P(\Delta S^2) = n \chi_{n, \lambda}^2(n \Delta S^2), \quad (5.22)$$

where  $\lambda$  is the non-centrality parameter which is given by

$$\lambda = \sum_{i=1}^n \frac{(\sigma_i^A - \sigma_i^B)^2}{\sigma_i^A/L_A + \sigma_i^B/L_B}. \quad (5.23)$$

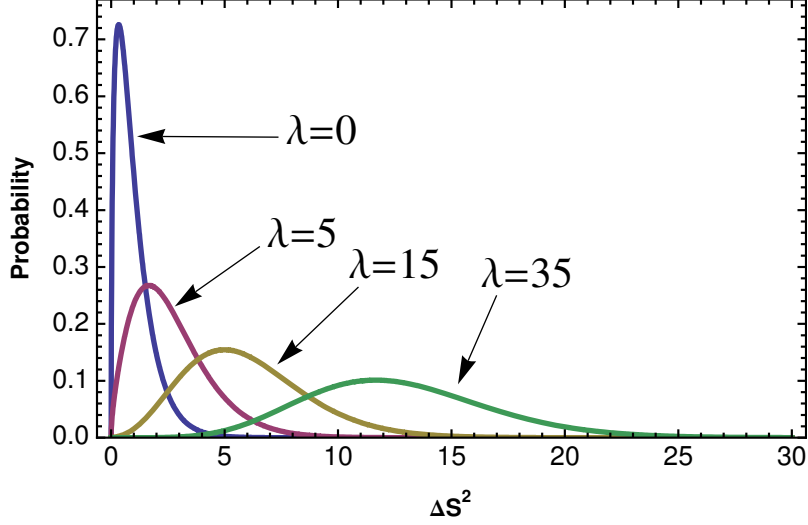


Figure 5.1: Distribution of  $\Delta S^2$  values for 3 signatures ( $n = 3$ ) and various  $\lambda$  values.

Here,  $\lambda = 0$  ( $\neq 0$ ) corresponds to comparing a model to itself (to a different model) by using two sets of independent measurements.

Figure 5.1 shows how the  $(\Delta S)^2$  distribution favors larger values as  $\lambda$  increases. Since our goal is to tell apart two models, we want the possible  $(\Delta S)^2$  values we will get from this comparison to be safely away from the possible values we get by comparing a model to itself, i.e.  $\lambda = 0$  case. If we quantify this safety condition as the requirement that  $(100 \times p)\%$  of the distributions do not overlap, i.e.  $(100 \times p)\%$  of the values we get by comparing the same model to itself are less than  $(100 \times p)\%$  of the values we get by comparing two different models, we obtain the following set of equations

$$p = \int_0^\gamma n \chi_{n,\lambda=0}^2(n\Delta S^2) d(\Delta S^2) \rightarrow \Gamma\left(\frac{n}{2}, \frac{n}{2} \gamma\right) = \Gamma\left(\frac{n}{2}\right)(1-p) \quad (5.24)$$

$$p = \int_\gamma^\infty n \chi_{n,\lambda_{\min}}^2(n\Delta S^2) d(\Delta S^2), \quad (5.25)$$

which can be solved numerically to compute a  $\lambda_{\min}$  value (see Table 5.1) for every number of signatures  $n$  and the non-overlap fraction (or confidence level)  $p$ . We define  $\gamma$  as the  $(\Delta S)^2$  cut-off value for which  $(100 \times p)\%$  of the values we get by comparing a model to itself is less than this cut-off  $\gamma$  and this condition gives us Eqn 5.24 which can be solved numerically to compute  $\gamma$ . Then

Confidence Level $p$				
n	0.95	0.975	0.99	0.999
1	12.99	17.65	24.03	40.71
2	15.44	20.55	27.41	44.99
3	17.17	22.60	29.83	48.10
4	18.57	24.27	31.79	50.66
5	19.78	25.71	33.50	52.88
6	20.86	26.99	35.02	54.88
7	21.84	28.16	36.41	56.71
8	22.74	29.25	37.69	58.40
9	23.59	30.26	38.89	59.99
10	24.39	31.21	40.02	61.48

Table 5.1: List of  $\lambda_{\min}(n, p)$  values for various values of the parameters  $n$  and  $p$ .

this  $\gamma$  value is used as the lower cut-off for Eqn 5.25 which is solved again numerically to compute  $\lambda_{\min}$ .

The condition for two models to be distinguishable is simply  $\lambda > \lambda_{\min}$ . In this inequality,  $\lambda_{\min}$  is just a numerically computed number which is independent of the physics involved in the collider experiment and all the physics is in the quantity  $\lambda$  given in Egn. 5.23 which is a function of cross sections given by each signature.

Let us assume now that “model  $A$ ” is the experimental data, which corresponds to an integrated luminosity of  $L^{\text{exp}}$ , and “model  $B$ ” is the simulation with integrated luminosity  $L^{\text{sim}} = qL^{\text{exp}}$ . We might imagine that  $q$  can be arbitrarily large, limited only by computational resources. Let us make one final notational definition

$$R = \sum_{i=1}^N \frac{(\sigma_i^{\text{exp}} - \sigma_i^{\text{sim}})^2}{\sigma_i^{\text{exp}} + \frac{1}{q} \sigma_i^{\text{sim}}}, \quad (5.26)$$

then we can compute the minimum amount of luminosity required for two models to be distin-

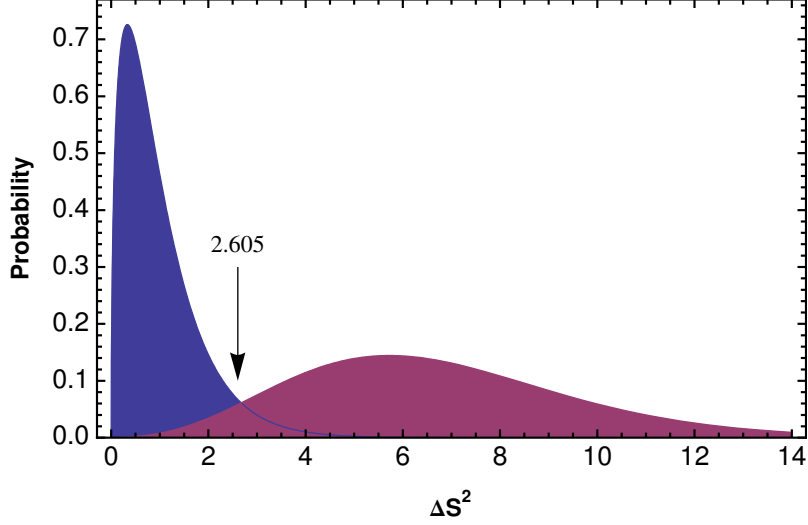


Figure 5.2: The plot shows an example of the distribution of  $\Delta S^2$  for  $n = 3$ . The curve on the left represent  $\lambda = 0$  case, i.e. values we will get when we compare a model to itself. 95% of the possible outcomes of this comparison are below 2.605 which is shown on the plot. The curve on the right has  $\lambda = 17.17$  and 95% of the curve is beyond 2.605. As  $\lambda$  increases, this curve moves further to the right and gets flatter.

guishable which is given by

$$L_{\min} = \frac{\lambda_{\min}(n, p)}{R}. \quad (5.27)$$

If the two models we want to compare are very similar in all the channels (signatures) we consider, then  $R$  will be small and  $L_{\min}$  will be large. On the other hand, if the models are very different  $R$  will be large and  $L_{\min}$  will be small. This is of course what we expect, i.e. similar models require more integrated luminosity to distinguish.

Now the question is how to make  $L_{\min}$  as small as possible. We see from Table 5.1 that  $\lambda_{\min}$  increases as  $n$  increases and since  $R$  is a sum of positive quantities it increases with  $n$  as well. Therefore using more signatures does not necessarily help in distinguishing models and, moreover, the signature space is not big enough (or at least the relevant part of the signature space, see [2]) to allow multiple independent directions. It is easy to see the orthogonality of signatures such as number of events with 1 lepton and 2 leptons, but for more general cases, such as kinematic histograms which we can integrate between limits that are also optimized to increase distinguishability, we need a method to compute correlations between signatures. This can be

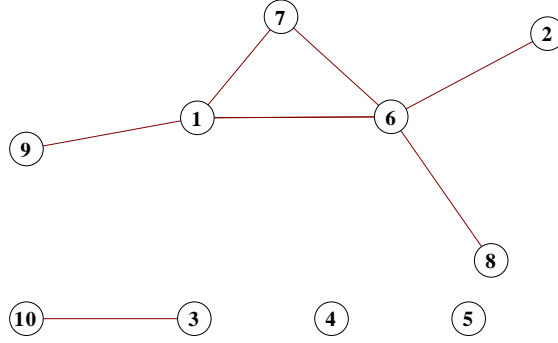


Figure 5.3: A graph generated by a random adjacency matrix. Connections show uncorrelated signatures. For example {1,6,7} can be combined but {1,6,7,9} can not because signature 9 is correlated with signatures 6 and 7.

achieved by simply simulating a model many times, calculating all the signatures and using these statistically independent values to compute the correlation coefficient. The correlation coefficient between different signatures  $a$  and  $b$  is defined as

$$\rho_{ab} = \frac{\text{cov}(a, b)}{\text{var}(a)\text{var}(b)} \approx \frac{\frac{1}{N} \sum_k [\bar{\sigma}_a^k - \sigma_a][\bar{\sigma}_b^k - \sigma_b]}{\sqrt{\frac{1}{N} \sum_k [\bar{\sigma}_a^k - \sigma_a]^2} \sqrt{\frac{1}{N} \sum_k [\bar{\sigma}_b^k - \sigma_b]^2}} \quad \text{for large } N, \quad (5.28)$$

where the  $\bar{\sigma}^k$  represent the individual results obtained from each of the  $N$  cross section measurements, labeled by the index  $k$ . This correlation matrix  $\rho_{ab}$  then can be used to determine the compatible observables, i.e. the ones which are not correlated with each other with more than some fixed threshold  $\epsilon$ . This gives us the adjacency matrix of a graph which we define as

$$C_{ab} = \begin{cases} 1 & \text{if } |\rho_{ab}| \leq \epsilon \\ 0 & \text{if } |\rho_{ab}| > \epsilon. \end{cases} \quad (5.29)$$

Now finding the compatible observables is equivalent to finding all the complete subgraphs (or ‘clique’) of that graph which is a well known problem in graph theory. All these complete subgraphs give us an  $L_{\min}$  value and obviously the one giving the minimum of all these graphs contains the list of the signatures we want to combine together. One might think that the best strategy is to include the largest set of uncorrelated signatures in the analysis but in fact the

optimal strategy is generally to choose a rather small subset of the total signatures. To see this let us first define the individual “resolving power” of a single signature  $S_i$ , or the minimum integrated luminosity required to distinguish between two models  $A$  and  $B$  as

$$(L_{\min})_i = \lambda_{\min}(1, p) \frac{\sigma_i^A + \frac{1}{q} \sigma_i^B}{(\sigma_i^A - \sigma_i^B)^2}. \quad (5.30)$$

then considering  $n$  signatures simultaneously gives the minimum integrated luminosity of

$$L_{\min} = \frac{\lambda_{\min}(n, p)}{\lambda_{\min}(1, p)} \left\{ (L_{\min})_1^{-1} + (L_{\min})_2^{-1} + \dots + (L_{\min})_n^{-1} \right\}^{-1}. \quad (5.31)$$

The identity 5.31 suggests that we can find the optimal set of signatures by sequentially ordering the calculated  $(L_{\min})_i$  values for any particular pair of models in ascending order, then including them one by one to find the global  $L_{\min}$  value. From Table 5.1, we can see that the ratio  $\lambda_{\min}(n, p)/\lambda_{\min}(1, p)$  grows with  $n$  which implies that by adding more signatures we will eventually reach a minimum where the resulting overall  $L_{\min}$  starts to grow again.

This can be seen from Figure 5.4 which represents the outcome of just such an optimization procedure based on an actual pair of models from one of our model lines. In this case the minimum integrated luminosity to distinguish two model points is achieved by using 12 signatures represented by the circled point, which yields  $L_{\min} = 2.4 \text{ fb}^{-1}$ . We typically observed that the optimal signature set usually consisted of  $O(10)$  signatures. If we are willing to settle for a luminosity just 20% higher than this minimal value then we need only  $O(5)$  signatures, typically. It is interesting to compare this to the results of [2] in which the effective dimension of signature space was found to be also  $O(5)$  to  $O(10)$ .

## 5.4 Signatures

To select the best signatures we start with an extremely large initial set of candidate signatures. These include all the counting signatures and most of the kinematic distributions used in [2], all of the signatures of [79], several “classic” observables common in the literature [108] and several

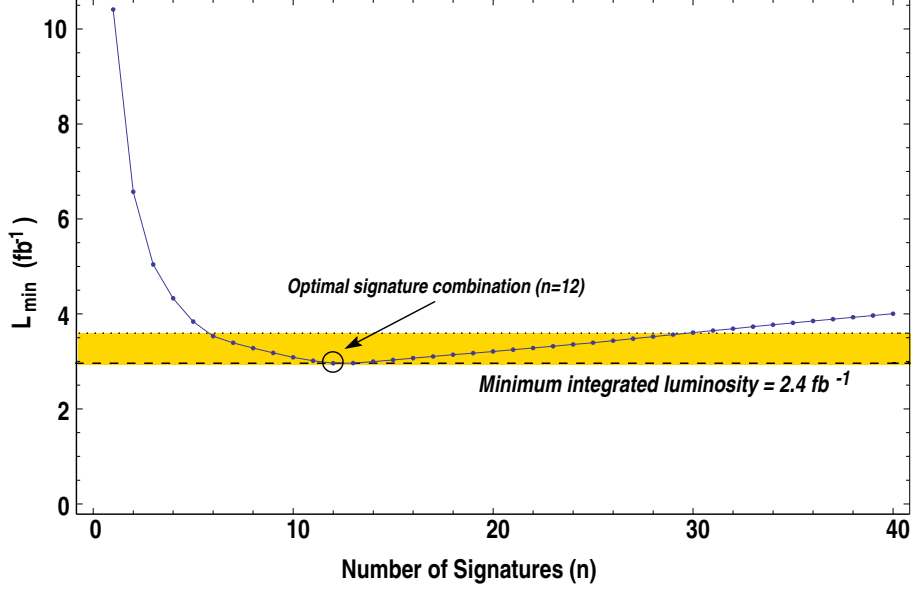


Figure 5.4: In this particular example the minimum value of  $L_{\min}$  is found after combining just the first 12 signatures. After just the best six signatures we are already within 20% of the optimal value, as indicated by the shaded band.

more which we constructed ourselves. Removing redundant instances of the same signature this yielded 46 independent counting signatures and 82 kinematic distributions represented by histograms, adding up to 128 signatures in total.

As the second step, we computed the  $128 \times 128$  correlation matrix (5.28) in the following manner. We took a simple MSSM model specified by a parameter set as in (5.16), with gaugino masses having the unified ratios of mSUGRA. We generated  $N = 2000$  simulations of this model, each containing  $5 \text{ fb}^{-1}$  of events using PYTHIA 6.4, which were then passed to the detector simulation PGS4. After simulating the detector response and object reconstruction the default level-one triggers were applied. We then applied the post-trigger cuts given in Table 5.2. After these object-specific cuts we then applied an event-level cut on the surviving detector objects similar to those used in [2]. Specifically we required all events to have missing transverse energy  $\cancel{E}_T > 150 \text{ GeV}$ , transverse sphericity  $S_T > 0.1$ , and  $H_T > 600 \text{ GeV}$  (400 GeV for events with 2 or more leptons) where  $H_T = \cancel{E}_T + \sum_{\text{jets}} p_T^{\text{jet}}$ . Once all cuts were applied the grand list of 128 signatures was then computed in Parvicursor [35] for each run, and from these signatures the covariance

Object	Minimum $p_T$	Minimum $ \eta $
Photon	20 GeV	2.0
Electron	20 GeV	2.0
Muon	20 GeV	2.0
Tau	20 GeV	2.4
Jet	50 GeV	3.0

Table 5.2: After event reconstruction using the package PGS4 we apply additional cuts to the individual objects in the event record. Detector objects that fail to meet the above criteria are removed from the event record and do not enter our signature analysis. These cuts are applied to all analysis described in this chapter.

matrix in (5.28) was constructed.

The result of the analysis showed that many of the signatures were correlated with one another. For example, the distribution of transverse momenta for the hardest jet in any event was correlated with the overall effective mass of the jets in the events (defined as the scalar sum of all jet  $p_T$  values:  $M_{\text{eff}} = \sum_{\text{Jets}} p_T^{\text{jet}}$ ). Both were correlated with the distribution of  $H_T$  values for the events, and so forth. One way to eliminate correlations is to partition the events into mutually-exclusive subsets through some topological criteria such as the number of jets and/or leptons. One can then apply some other criteria such as the  $H_T$  distribution to further divide the event data into even smaller subsets. Our analysis indicated that this partitioning strategy has its limitations because the resolving power of any given signature tends to diminish as the set it is applied to is made ever more exclusive. This is of course related to the decreasing cross-section associated with the more exclusive final state. We were thus led to consider a very simple two-fold partitioning of the data:

$$\begin{aligned}
N_{\text{jets}} \leq 4 \text{ versus } N_{\text{jets}} \geq 5, \\
N_{\text{leptons}} = 0 \text{ versus } N_{\text{leptons}} \geq 1.
\end{aligned}
\tag{5.32}$$

After constructing the correlation matrix, we then constructed the adjacency matrix 5.29 by allowing small correlations among signatures, i.e. different tolerance levels  $\epsilon$ , which is within the statistical uncertainties given the finite computational time. As we mentioned before, all the

	Description	Min Value	Max Value
1	$M_{\text{eff}}^{\text{any}} = \cancel{E}_T + \sum_{\text{all}} p_T^{\text{all}}$ [All events]	1250 GeV	End

Table 5.3: **Signature List A.** The effective mass formed from the transverse momenta of all objects in the event (including the missing transverse energy) was the single most effective signature of the 128 signatures we investigated. Since this “list” is a single item it was not necessary to partition the data in any way. For this distribution we integrate from the minimum value of 1250 GeV to the end of the distribution.

subgraphs of the graph built from the adjacency matrix give us then the possible combinations of signatures. Each of these signature combinations implies a minimum integrated luminosity and we minimized over these candidate signature lists.

To accomplish this global minimization we constructed a large number of model families in the manner described in (5.16), each involving the range  $-0.5 \leq \alpha \leq 1.0$  for the parameter  $\alpha$  in steps of  $\Delta\alpha = 0.05$ . For each point along these model lines we generated  $10^5$  events using PYTHIA 6.4 and PGS4. We also generated a Standard Model background sample consisting of  $5 \text{ fb}^{-1}$  each of  $t/\bar{t}$  and  $b/\bar{b}$  pair production, high- $p_T$  QCD dijet production, single  $W^\pm$  and Z-boson production, pair production of electroweak gauge bosons ( $W^+ W^-$ ,  $W^\pm Z$  and  $Z Z$ ), and Drell-Yan processes.

Then to compute the best subsets out of our 128 signatures to measure the value of the parameter  $\alpha$ , we fixed “model A” to be the point on each of the model lines with  $\alpha = 0$  and then treated each point along the line with  $\alpha \neq 0$  as a candidate “model B.” The lists we will present in Tables 5.3, 5.4 and 5.5 represent an ensemble average over these model lines, restricted to a maximum correlation amount  $\epsilon$  as described above. Signatures requiring an integration range are also optimized during this process to give better discrimination between different  $\alpha$  values.

The single most effective signature at separating models with different values of the parameter  $\alpha$  is given in Table 5.3. It is simply the effective mass formed from all objects in the event

$$M_{\text{eff}}^{\text{all}} = \cancel{E}_T + \sum_{\text{all objects}} p_T, \quad (5.33)$$

where we form the distribution from all events which pass our initial cuts. It is not surprising for this particular signature to perform well given the way we have set up the problem. It has a

	Description	Min Value	Max Value
1	$M_{\text{eff}}^{\text{jets}}$ [0 leptons, $\geq 5$ jets]	1100 GeV	End
2	$M_{\text{eff}}^{\text{any}}$ [0 leptons, $\leq 4$ jets]	1450 GeV	End
3	$M_{\text{eff}}^{\text{any}}$ [ $\geq 1$ leptons, $\leq 4$ jets]	1550 GeV	End
4	$p_T(\text{Hardest Lepton})$ [ $\geq 1$ lepton, $\geq 5$ jets]	150 GeV	End
5	$M_{\text{inv}}^{\text{jets}}$ [0 leptons, $\leq 4$ jets]	0 GeV	850 GeV

Table 5.4: **Signature List B.** The collection of our most effective observables, restricted to the case where the maximum correlation between any two of these signatures is 10%. Note that the jet-based effective mass variables would normally be highly-correlated if we had not partitioned the data according to (5.32). For these distributions we integrate from “Min Value” to “Max Value”.

large cross section because of its inclusive nature and it is sensitive to the mass differences between the gluino and the lighter electroweak gauginos which is precisely governed by the parameter  $\alpha$ . Although it is the ‘single’ most effective signature it can often fail to be effective at all in certain circumstances as we will see in the next section, resulting in a rather large required  $L_{\text{min}}$  to be able to separate  $\alpha = 0$  from non-vanishing cases. In addition, considering the difficulties in measuring the missing energy and jet transverse momenta, it suffers the most from experimental uncertainties. This suggests a larger and more varied set of signatures would be preferable.

We next allow signatures with up to 10% correlation, i.e.  $\epsilon = 10\%$ . This time we have a larger set consisting of 5 signatures given in Table 5.4. We again see the totally inclusive effective mass variable of (5.33) as well as the more traditional effective mass variable,  $M_{\text{eff}}^{\text{jets}}$ , defined similarly to (5.33) but with the scalar sum of  $p_T$  values now running over the jets only

$$M_{\text{eff}}^{\text{jets}} = \cancel{E}_T + \sum_{\text{jets}} p_T. \quad (5.34)$$

In this second list, we also include the  $p_T$  of the hardest lepton in events with at least one lepton and five or more jets, as well as the invariant mass  $M_{\text{inv}}^{\text{jets}}$  of the jets in events with zero leptons and 4 or less jets, where invariant mass is defined as the norm of the total 4-momenta of objects in consideration. Without the partitioning the data into disjoint sets according to (5.32) the various jet-based effective mass variables would normally be highly correlated with one another. The

reason for favoring jet-based observables to those based on leptons is again largely due to the fact that jet-based signatures have larger effective cross-sections in most of the parameter space given in (5.16) than leptonic signatures. The best performing signatures distinguishing two close  $\alpha$  values are those which track the narrowing gap between the gluino mass and the electroweak gauginos and the narrowing gap between the lightest chargino/second-lightest neutralino mass and the LSP mass. In this case the first leptonic signature to appear, which is the transverse momentum of the leading lepton in events with at least one lepton, is an example of just such a signature.

Finally, we allow as much as 30% correlation between any two signatures in the list and obtain an even larger list with a wider variety of signatures. We display them in Table 5.5 according to the partition of data being considered. As we will see in the next section, it is important to have this wider variety of observables for some of the supersymmetric models that have unusual properties or for the cases where mass hierarchies depend on the  $\alpha$  value.

In this final list in Table 5.5 we have three counting signatures. The first one is the total count of events containing at least 1 lepton and at most 4 jets. The next one is the total count of events with opposite charge dileptons having invariant mass in the Z window (within  $\pm 5$  GeV of Z boson mass), or simply a count of on-shell Z bosons. This is actually related to one of the spoiler modes for the trilepton signal which is one of the well known clean discovery channels of supersymmetry. Unfortunately the cross section for the trilepton channel does not have a strong dependence on  $\alpha$  and that is why it did not make the list. The last counting signature making the list is the total count of events with at least 2 b-jets which is a proxy for counting on-shell Higgs bosons. The effectiveness of these two signatures is more obvious when the mass splitting  $\tilde{\chi}_2^0 - \tilde{\chi}_1^0$  strongly depends on  $\alpha$ .

The remaining signatures are similar to the ones in lists A and B, they all include kinematic variables or combinations of them. For example the effective mass variables from the list B also appear in list C, as well as the new signatures such as  $p_T$  of the 4th hardest jet. There are several signatures in the list C that are ratios of kinematic variables which turned out to be less correlated with other signatures compared to the unnormalized ones. Signature #8, which is one of them, is

	Description	Min Value	Max Value
Counting Signatures			
1	$N_\ell$ [ $\geq 1$ leptons, $\leq 4$ jets]		
2	$N_{\ell^+\ell^-}$ [ $M_{\text{inv}}^{\ell^+\ell^-} = M_Z \pm 5$ GeV]		
3	$N_B$ [ $\geq 2$ B-jets]		
[0 leptons, $\leq 4$ jets]			
4	$M_{\text{eff}}^{\text{any}}$	1000 GeV	End
5	$M_{\text{inv}}^{\text{jets}}$	750 GeV	End
6	$\cancel{E}_T$	500 GeV	End
[0 leptons, $\geq 5$ jets]			
7	$M_{\text{eff}}^{\text{any}}$	1250 GeV	3500 GeV
8	$r_{\text{jet}}$ [3 jets $> 200$ GeV]	0.25	1.0
9	$p_T$ (4th Hardest Jet)	125 GeV	End
10	$\cancel{E}_T/M_{\text{eff}}^{\text{any}}$	0.0	0.25
[ $\geq 1$ leptons, $\geq 5$ jets]			
11	$\cancel{E}_T/M_{\text{eff}}^{\text{any}}$	0.0	0.25
12	$p_T$ (Hardest Lepton)	150 GeV	End
13	$p_T$ (4th Hardest Jet)	125 GeV	End
14	$\cancel{E}_T + M_{\text{eff}}^{\text{jets}}$	1250 GeV	End

Table 5.5: **Signature List C**. In this collection of signatures we have allowed the maximum correlation between any two signatures to be as high as 30%. Note that some of the signatures are normalized signatures, (#8, #10 and #11), while the first three are truly counting signatures. A description of each of these observables is given in the text. For all distributions we integrate from “Min Value” to “Max Value”.

defined as the following ratio

$$r_{\text{jet}} \equiv \frac{p_T^{\text{jet3}} + p_T^{\text{jet4}}}{p_T^{\text{jet1}} + p_T^{\text{jet2}}} \quad (5.35)$$

where we required at least three jets with  $p_T > 200$  GeV. This signature, like the  $p_T$  of the hardest lepton or the  $p_T$  of the 4th hardest jet, was effective at capturing the increasing softness of the products of cascade decays as the value of  $\alpha$  was increased away from  $\alpha = 0$ .

## 5.5 Results

To be able to test the effectiveness of our signature lists, we generated an additional set of 500 pMSSM model lines with parameters given in (5.16). Each line consisted of 6 models with  $\alpha$  value ranging from 0 to 0.5 in steps of 0.1. To capture a broader variety of models we scanned over a wide range of parameters, specifically we allowed slepton and squark masses, the gaugino mass scale determined by  $M_3$  and the  $\mu$  parameter to range between 300 GeV and 1200 GeV, and  $\tan\beta$  to range between 2 and 50. We fixed the pseudoscalar Higgs mass  $m_A$  to be 850 GeV. Finally, all the points on the model lines are required to satisfy experimental mass constraints. We generated  $10^5$  events for each point along the  $\alpha$  lines and computed  $L_{\text{min}}$  for each of our three signature sets.

The results are shown in Figures 5.5 and 5.6. Figure 5.5 shows the ability of our signature lists to separate the case  $\alpha = 0.1$  from  $\alpha = 0$  (top pair of plots) and the case  $\alpha = 0.3$  from  $\alpha = 0$  (bottom pair of plots). On the vertical axis we display the percentages of the models that our signatures are able to distinguish between two  $\alpha$  values. Horizontal axis is the required integrated luminosity. One can see that the signature list C offers a greater efficiency compared to the signature lists A and B. This is due to the very broad range of signatures ranging from effective mass to dileptons.

Figure 5.6 shows the integrated luminosity (or number of supersymmetric events) needed to detect  $\alpha \neq 0$  for 95% of our random models is given as a function of the five non-vanishing  $\alpha$  values simulated.

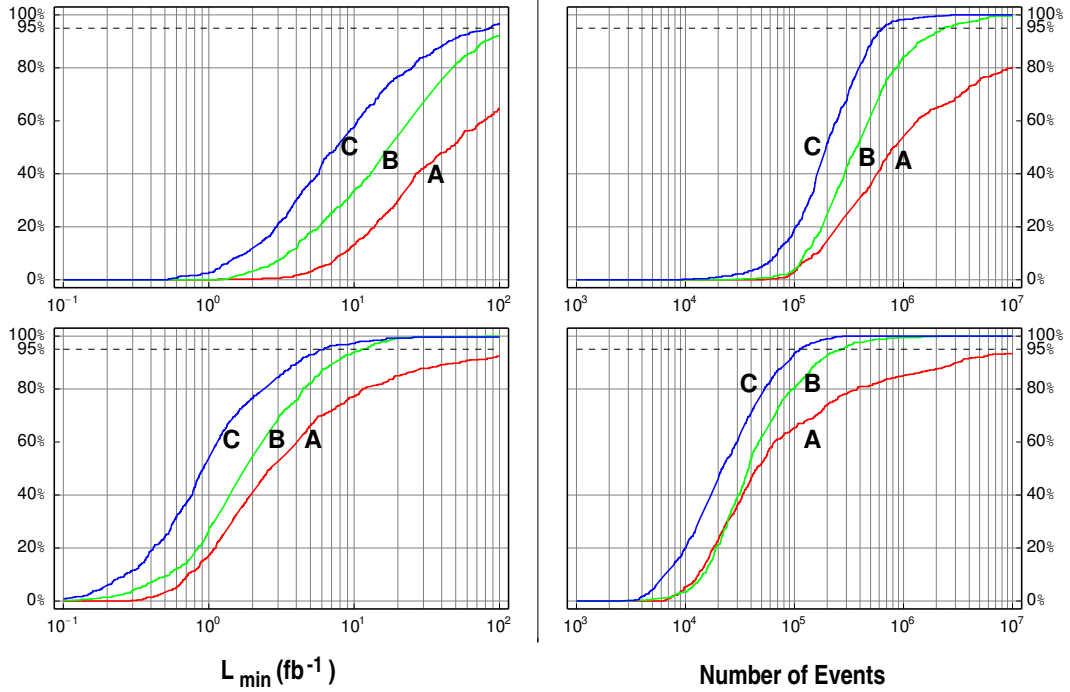


Figure 5.5: A display of the ability of the three signature lists to separate the case  $\alpha = 0.1$  from  $\alpha = 0$  is indicated in the top pair of plots and the simpler case  $\alpha = 0.3$  from  $\alpha = 0$  in the bottom pair of plots. On the left, the percentage of cases that could be distinguished using each of the three signature lists of Tables 5.3, 5.4 and 5.5 is given as a function of integrated luminosity in units of  $\text{fb}^{-1}$ . On the right the same percentage is shown as a function of the number of supersymmetric events. The 95% separability threshold is indicated by the dashed horizontal line.

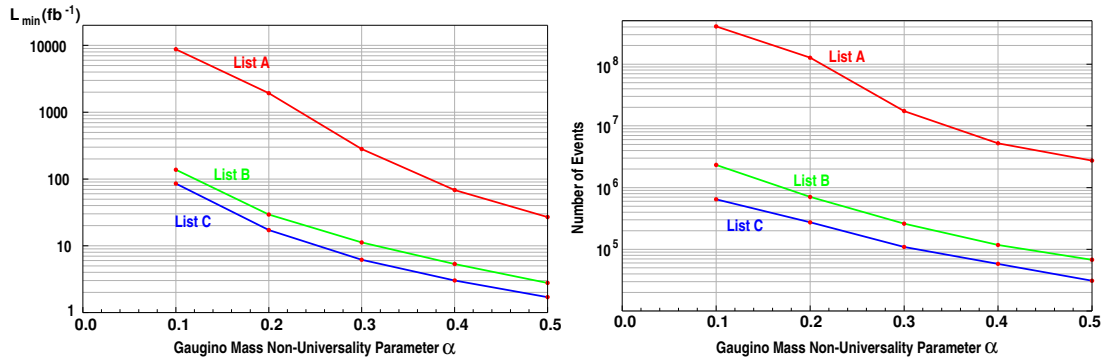


Figure 5.6:  $L_{\min}$  and  $N_{\min}$  required to detect  $\alpha \neq 0$  for 95% of the random models.

## 5.6 Summary

In the work presented in this chapter, we asked ourselves what is the most important information that would be useful to a high energy theorist interested in connecting the supersymmetric physics at the LHC to physics at an even higher energy scale, such as some underlying string theory. We believe the most important information is the question of gaugino mass universality. We developed statistical methods that will let us choose the best signatures to resolve the amount of non-universality in the gaugino sector for a model following the mirage pattern of gaugino masses. Our results concluded that up to a 30% non-universality is resolvable after just one year of LHC data.

## Chapter 6

### Phenomenology of Deflected Mirage Mediation\*

In the next few years, LHC will be able to probe TeV scale softly broken supersymmetry [110, 111]. The breaking of supersymmetry is thought to be realized in a hidden sector and communicated to the observable sector via the interactions of mediator fields. In this scheme, the low energy phenomenology of softly broken supersymmetric models is only governed by the mediation mechanism transmitting supersymmetry breaking to the MSSM fields and is not sensitive to the details of the hidden sector. As the result, the collider phenomenology depends on soft supersymmetry breaking terms only. But large number of these terms (125 in MSSM) makes a general collider study impossible. It is then important to study possible supersymmetry breaking mechanisms instead of the most general parameter set.

The three most popular supersymmetry breaking mechanisms are gravity mediation, gauge mediation and bulk mediation. Gravity mediated terms [22, 112, 113, 114, 115] arise from couplings that vanish as  $M_p \rightarrow \infty$ . Examples are minimal supergravity and modulus mediation models [116, 117, 118], and the anomaly mediation models [119, 120, 103]. Gauge mediated terms arise from loop diagrams involving new messenger fields with Standard Model charges [121, 122, 123, 124, 125, 126, 127, 128, 129, 130]. Bulk-mediated terms arise from bulk mediator fields in braneworld scenarios. Examples include gaugino mediation [131, 132] and  $Z'$  mediation [133, 134]. In most supersymmetric models, one of these mediation mechanisms is assumed to dominate [106].

One can also have models with mixed mediation mechanisms. Such models are motivated within string-theoretic constructions, such as the Kachru-Kalosh-Linde-Trivedi (KKLT) approach to moduli stabilization [135]. As we studied in the previous chapter, Mirage mediation is an example to this in which the gravity mediated terms and the anomaly mediated terms are com-

---

\*This chapter is based on the work that has been published in JHEP [85] and submitted to EPJC [109]

parable in size [136, 137]. As the result of the two supersymmetry breaking mechanisms at work, the phenomenology of Mirage mediation is substantially different than the minimal supergravity models [104, 138, 139, 140, 141, 142, 143] including a relatively squeezed gaugino sector compared to mSUGRA [83] and reduced low energy fine-tuning [144, 145, 146, 147, 148].

Deflected mirage mediation (DMM) is an extension of mirage mediation in which gauge-mediated supersymmetry breaking terms are also present and competitive in size to the gravity-mediated and anomaly-mediated soft terms [149, 150]. Threshold effects due to the gauge mediation messenger fields shifts (or “deflects”) the mirage unification scale. It is a very general framework in the sense that all the single mediation mechanisms are special limits and a broader phenomenology is possible when mixed mediation involving more than one mechanism is turned on by adjusting the dimensionless parameters of the theory.

In this chapter we will study the collider phenomenology of DMM following previous work on the sparticle spectrum [150, 151] and dark matter constraints [86]. We will first focus on the differences between DMM and pure mirage mediation. By adjusting the parameters of the theory one can get a squeezed gaugino sector resulting in gluinos that are typically lighter than other colored superpartners. In this case, the collider phenomenology is dominated by gluino production, with soft decay products due to the compressed chargino and neutralino mass spectrum. We will also look into the possible mass hierarchies of sparticles in the framework of DMM following the work by Feldman, Liu, and Nath (FLN) [69, 78, 79]. We will present the most common hierarchies occurring in deflected mirage mediation models and discuss the phenomenology following this classification.

## 6.1 DMM framework

Here we will briefly review the deflected mirage mediation paradigm and give the soft supersymmetry breaking masses and couplings, as well as the threshold corrections arising due to the gauge mediation messenger fields. DMM is a generalization of pure mirage mediation motivated from the KKLT flux compactification approach within Type IIB string theory [135]. In this framework

gravity and anomaly mediation terms are given by

$$m_{\text{soft}}^{\text{gravity}} \sim \frac{F^T}{T + \bar{T}} \quad , \quad m_{\text{soft}}^{\text{anomaly}} \sim \frac{1}{16\pi^2} \frac{F^C}{C} \quad (6.1)$$

where  $T$  is the Kähler modulus and  $C$  is the compensator of the gravity multiplet. Supersymmetry is broken by an uplifting potential of the form  $(T + \bar{T})^{-2}$  which cancels the otherwise negative cosmological constant and results in the following mirage mediation relation [136, 137]:

$$\frac{F^T}{T + \bar{T}} \sim \frac{1}{\ln(M_P/m_{3/2})} \frac{F^C}{C} \quad (6.2)$$

in which  $M_P = 2.4 \times 10^{18}$  GeV is the reduced Planck mass, and  $m_{3/2}$  is the gravitino mass. As  $m_{3/2}$  is typically  $\sim 100$  TeV in this class of models, the tree-level gravity mediation terms are comparable in magnitude to the anomaly mediation terms.

Deflected mirage mediation also introduces a gauge singlet  $X$  and vectorlike messenger pairs  $\Psi, \bar{\Psi}$  with SM gauge charges which are taken to be  $5, \bar{5}$  representations of  $SU(5)$ , as in many models of gauge mediation. In general,  $X$  can acquire an F term vacuum expectation value, leading to gauge mediated terms of the form

$$m_{\text{soft}}^{\text{gauge}} \sim \frac{1}{16\pi^2} \frac{F^X}{X} \quad (6.3)$$

Depending on the stabilization mechanism for  $X$ , it was shown in [149, 150] that in general,

$$\frac{F^X}{X} \sim \frac{F^C}{C} \quad (6.4)$$

which implies that the gravity, anomaly and gauge mediation terms contribute equally in the framework of DMM.

Without going into details, one can then use supergravity techniques and obtain the observable sector soft supersymmetry breaking Lagrangian, the gaugino and the scalar masses as well as trilinear couplings and threshold corrections. By replacing the F terms with the parametrization

given in [149, 150], as follows:

$$\frac{F^C}{C} = \alpha_m \ln \frac{M_P}{m_{3/2}} \frac{F^T}{T + \bar{T}} = \alpha_m \ln \frac{M_P}{m_{3/2}} M_0 \quad (6.5)$$

$$\frac{F^X}{X} = \alpha_g \frac{F^C}{C} = \alpha_g \alpha_m \ln \frac{M_P}{m_{3/2}} M_0, \quad (6.6)$$

one obtains the soft supersymmetry breaking masses at the GUT scale  $M_G$  as

$$M_a(M_G) = M_0 \left[ 1 + \frac{g_0^2}{16\pi^2} b'_a \alpha_m \ln \frac{M_P}{m_{3/2}} \right], \quad (6.7)$$

$$A_i(M_G) = M_0 \left[ (1 - n_i) - \frac{\gamma_i}{16\pi^2} \alpha_m \ln \frac{M_P}{m_{3/2}} \right], \quad (6.8)$$

$$m_i^2(M_G) = M_0^2 \left[ (1 - n_i) - \frac{\theta'_i}{16\pi^2} \alpha_m \ln \frac{M_P}{m_{3/2}} - \frac{\dot{\gamma}'_i}{(16\pi^2)^2} \left( \alpha_m \ln \frac{M_P}{m_{3/2}} \right)^2 \right], \quad (6.9)$$

and the threshold corrections as

$$\Delta M_a = -M_0 N \frac{g_a^2(M_{\text{mess}})}{16\pi^2} \alpha_m (1 + \alpha_g) \ln \frac{M_P}{m_{3/2}}, \quad (6.10)$$

$$\Delta m_i^2 = M_0^2 \sum_a 2c_a N \frac{g_a^4(M_{\text{mess}})}{(16\pi^2)^2} \left[ \alpha_m (1 + \alpha_g) \ln \frac{M_P}{m_{3/2}} \right]^2. \quad (6.11)$$

where  $g_0 = g_a(M_G)$  is the unified gauge coupling at the GUT scale,  $\gamma$ 's are the anomalous dimensions<sup>†</sup>,  $b_a = (\frac{33}{5}, 1, -3)$  are the MSSM beta function coefficients and  $b'_a$  include contribution from the messenger fields and given as  $b'_a = b_a + N$ .

Let us summarize the model parameters of deflected mirage mediation:

- $M_0$  : Overall scale of the soft terms,
- $M_{\text{mess}}$  : Messenger scale associated with gauge mediation, ranging from 10 – 100 TeV to the GUT scale,
- $\alpha_m$  : Ratio of anomaly mediation to gravity mediation, theoretically-motivated to be in the range  $0 \leq \alpha_m \leq 2$ ,

---

<sup>†</sup>Anomalous dimensions are given in Appendix B in terms of gauge and Yukawa couplings.

- $\alpha_g$  : Ratio of gauge mediation to anomaly mediation, theoretically-motivated to be in the range  $-1 \leq \alpha_g \leq 2$ ,
- $N$  : Number of messenger pairs,
- $\{n_i\}$  : Modular weights of the MSSM multiplets,

and in addition the usual  $\tan\beta$  and sign of  $\mu$  parameters. The modular weights, which describe the couplings of the matter fields to the Kähler modulus, can in principle be flavor and generation-dependent. To avoid this issue, we fix the modular weights to the standard values of  $n_i = 1/2$  for the matter fields and  $n_i = 1$  for the Higgs fields. Hence we end up with 5 continuous parameters, 1 integer parameter and a sign. Despite its small extension of parameters compared to mSUGRA which has 4 continuous parameters and a sign, we will see that DMM provides richer LHC phenomenology.

## 6.2 Comparison with mirage unification

In pure mirage mediation, the soft terms unify not at the unification scale  $M_G \sim 10^{16}$  GeV as in the case of mSUGRA, but rather at a “mirage” scale [136, 137, 104] given by:

$$M_{\text{mir}} = M_G \left( \frac{m_{3/2}}{M_P} \right)^{\alpha_m/2}, \quad (6.12)$$

and in deflected mirage mediation, unification is lost in the scalar sector but gaugino masses still unify [149, 150] at the following (deflected) mirage scale:

$$M_{\text{mir}} = M_G \left( \frac{m_{3/2}}{M_{Pl}} \right)^{\rho \alpha_m/2}, \quad (6.13)$$

where the  $\rho$  parameter is given by

$$\rho = \left( 1 + \frac{2Ng_0^2}{16\pi^2} \ln \frac{M_G}{M_{\text{mess}}} \right) \left( 1 - \frac{\alpha_m \alpha_g N g_0^2}{16\pi^2} \ln \frac{M_P}{m_{3/2}} \right)^{-1}. \quad (6.14)$$

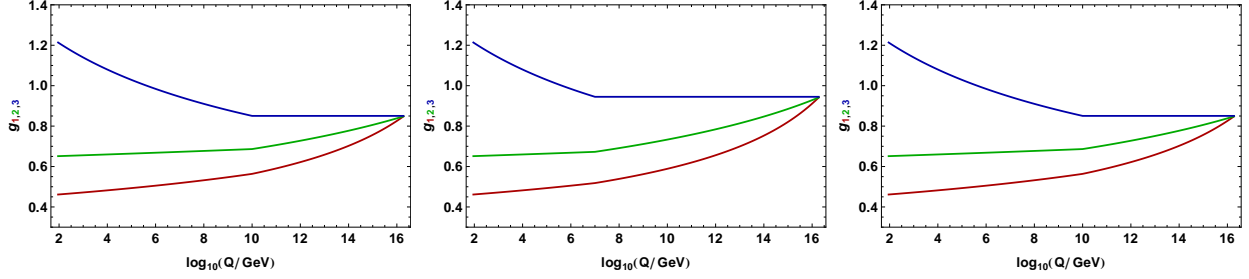


Figure 6.1: Renormalization group evolutions of gauge couplings for our 3 deflected mirage mediation benchmark models given in Table 6.1. Messenger fields turn on at  $10^{10}$  GeV for the first and the third models, and at  $10^7$  GeV for the second model. The beta function coefficients depend on the number of messenger fields and hence result in discontinuities in the energy dependence of the gauge couplings.

In the absence of messenger fields, i.e.  $N = 0$ , we obtain the mirage mediation limit, although in the limit of vanishing gauge mediation contributions, i.e.  $\alpha_g = 0$ , the messenger fields still contribute to anomaly mediation. In the presence of the messenger fields, i.e.  $N > 0$ , we obtain  $\rho > 1$  when  $\alpha_g = 0$ , such that the mirage unification scale is lowered compared to that of the pure mirage mediation case. If  $\alpha_m$ ,  $N$ , and  $M_{\text{mess}}$  are fixed; for  $\alpha_g > 0$ ,  $\rho$  increases and  $M_{\text{mir}}$  is lowered, while for  $\alpha_g < 0$ ,  $\rho$  decreases and  $M_{\text{mir}}$  is correspondingly increased.

To see the difference more clearly between pure mirage mediation and deflected mirage mediation, we will consider a set of benchmark points. We display the high scale input parameters of these benchmark points in Table 6.1. The models are grouped into  $\mathcal{D}$ M (pure mirage mediation) and DMM (deflected mirage mediation) pairs. All the DMM models are chosen in such a way that they satisfy LEP sparticle mass bounds and dark matter relic density constraints.

In Figure 6.1 we display the running of gauge couplings of our deflected mirage mediation benchmark points given in Table 6.1. In the presence of the messenger fields, the values of the beta function coefficients increase by the number of messenger fields, i.e.,  $b'_a = b_a + N$ . With the messengers, gauge couplings are still unified but at a higher value depending on the number of messenger fields. In Fig. (6.2) we display a comparison of the renormalization group evolution of the gaugino masses for our 3 pairs of benchmark models.

For the first pair of models  $\alpha_m$  and  $\alpha_g$  are chosen to obtain similar mirage unification scales of

approximately a TeV. The unification is not exact due to two-loop effects: for the DMM model of the pair, the three gaugino soft masses at the electroweak scale are  $M_1 = 500$  GeV,  $M_2 = 494$  GeV, and  $M_3 = 574$  GeV, while for the pure mirage mediation model they are  $M_1 = 929$  GeV,  $M_2 = 929$  GeV, and  $M_3 = 1062$  GeV. For the pure mirage mediation model, the electroweak symmetry breaking conditions constrain the  $\mu$ -parameter to a relatively small value of  $\mu = 239$  GeV. The approximate unification at the electroweak scale is then between the gluino and the heavier pair of neutralinos and heavier chargino. The lighter pair of neutralinos are mostly Higgsino-like, as indicated by the LSP composition given in Table 6.1. For the deflected mirage mediation model, however, the gaugino spectrum is compressed and the gluino approximately unifies with the entire ensemble of neutral and charged gauginos.

In the remaining two pairs of models, we keep  $\alpha_m$  fixed and add nonvanishing gauge mediation contributions by including messenger fields and a nonvanishing  $\alpha_g$ . The second pair is designed to show the impact of adding the effects of gauge mediation on the resulting gaugino masses. Both points have  $M_0 = 1$  TeV and  $\alpha_m = 0.6$ , yet the two cases have very different phenomenology. The spectrum for the pure mirage mediation point is similar to typical mSUGRA models, with a bino-like LSP, large mass gap between the lightest and second lightest neutralinos, gluinos and squarks of roughly comparable size, and relatively light sleptons. In contrast, the deflected mirage mediation point has a mixed bino/wino-like LSP, a degenerate trio of  $\tilde{\chi}_1^0$ ,  $\tilde{\chi}_2^0$  and  $\tilde{\chi}_1^\pm$ , and a very light gluino relative to the squarks and sleptons. The third pair have again the same values of  $\alpha_m = 1$  and  $M_0 = 800$  GeV. These models have very similar spectra for the light superpartners, but very different values for the gluino and squark masses and the  $\mu$ -parameter. The pure mirage mediation point has a mostly bino-like LSP, the deflected mirage mediation point has a neutralino LSP which is a mixed bino-wino-Higgsino state.

We also studied the LHC collider signatures of these benchmark points given in Table 6.1. We generated  $5 \times 10^4$  events for each model at  $\sqrt{s} = 14$  TeV using PYTHIA 6.4 [33] and used PGS 4 [34] to simulate the detector response. We imposed the PGS4 level one triggers, designed to mimic the CMS trigger tables [152] and object-level post-trigger cuts. We require all photons, electrons, muons and taus to have transverse momentum  $p_T \geq 10$  GeV and  $|\eta| < 2.4$  and we require hadronic

	Pair #1		Pair #2		Pair #3	
	∅MM Point 1	DMM Point 2	∅MM Point 3	DMM Point 4	∅MM Point 5	DMM Point 6
$\alpha_m$	1.9	1.0	0.6	0.6	1.0	1.0
$\alpha_g$	0	0.5	0	1.0	0	0.2
$M_0$	1000	1000	1000	1000	800	800
$M_{\text{mess}}$	-	$10^{10}$	-	$10^7$	-	$10^{10}$
$N$	0	3	0	3	0	3
$m_{\tilde{\chi}_1^0}$	236	493	602	322	562	424
$m_{\tilde{\chi}_2^0}$	247	516	848	329	660	452
$m_{\tilde{\chi}_3^0}$	936	698	1114	943	725	569
$m_{\tilde{\chi}_4^0}$	954	718	1127	946	779	601
$m_{\tilde{\chi}_1^\pm}$	243	498	848	328	658	441
$m_{\tilde{\chi}_2^\pm}$	937	718	1133	952	779	599
$m_{\tilde{\tau}_1}$	676	700	763	717	594	556
$m_{\tilde{\tau}_2}$	687	760	892	808	672	605
$m_{\tilde{\mu}_R}, m_{\tilde{e}_R}$	679	706	773	726	600	562
$m_{\tilde{\mu}_L}, m_{\tilde{e}_L}$	685	761	894	810	672	605
$m_{\tilde{t}_1}$	620	687	1278	803	875	560
$m_{\tilde{t}_2}$	829	913	1579	1091	1115	777
$m_{\tilde{b}_1}$	716	865	1542	1055	1062	713
$m_{\tilde{b}_2}$	751	936	1624	1153	1115	773
$m_{\tilde{c}_R}, m_{\tilde{u}_R}$	733	933	1639	1160	1121	769
$m_{\tilde{c}_L}, m_{\tilde{u}_L}$	713	962	1695	1204	1155	788
$m_{\tilde{s}_R}, m_{\tilde{d}_R}$	751	940	1633	1162	1119	777
$m_{\tilde{s}_L}, m_{\tilde{d}_L}$	721	968	1702	1210	1162	794
$m_{\tilde{g}}$	979	603	1816	431	1266	646
LSP Bino %	0.2%	19.1%	99.5%	82.0%	93.1%	52.5%
LSP Wino %	0.8%	70.0%	0.0%	17.0%	0.9%	30.1%
LSP Higgsino %	99.0%	10.9%	0.5%	1.0%	6.0%	17.4%

Table 6.1: Input parameters, physical masses, and LSP composition of the benchmark models. The first model in each pair is a mirage mediation model and the second is a deflected mirage mediation model with  $N = 3$ . All masses are given in GeV. Low energy physical masses are given at the scale 1 TeV.

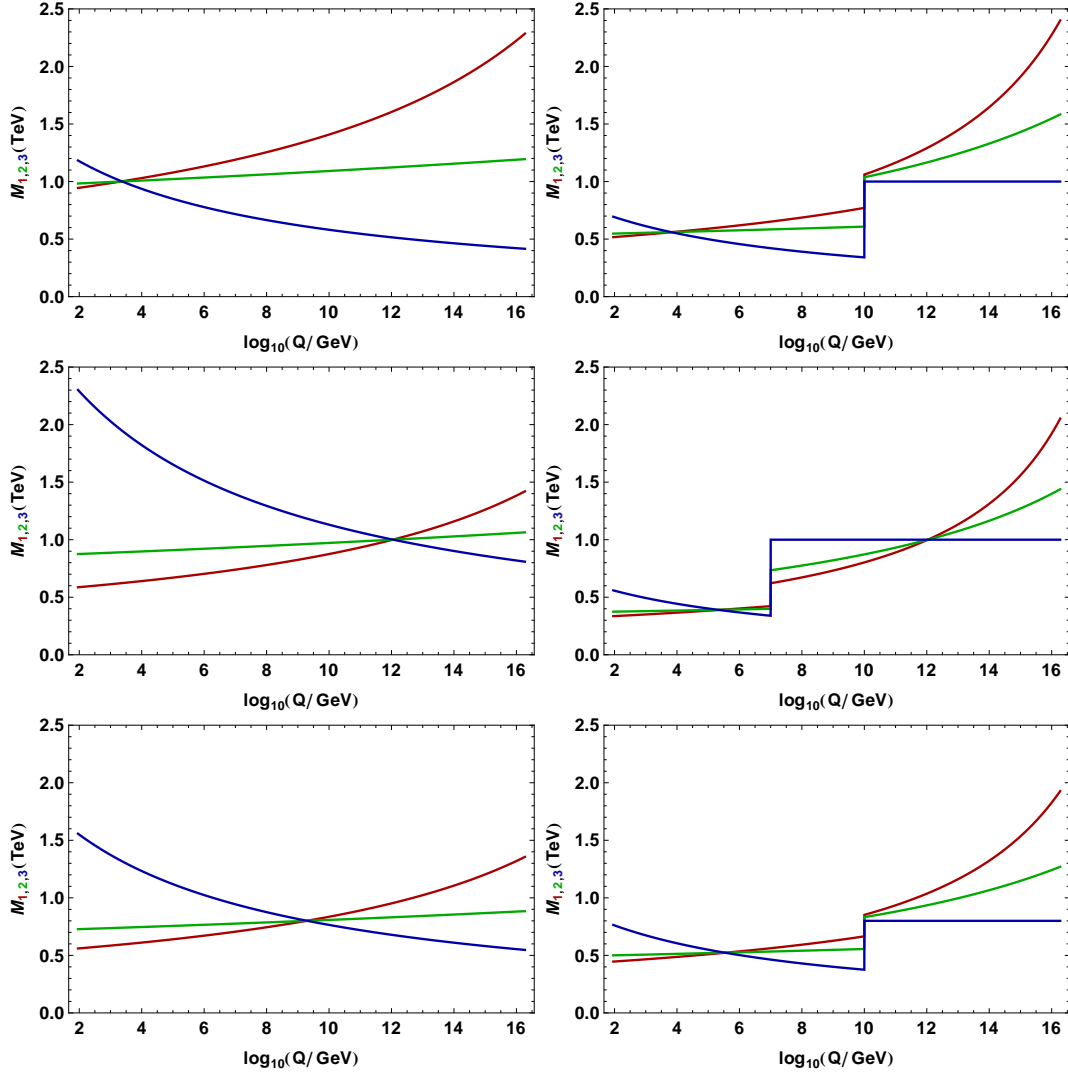


Figure 6.2: Renormalization group evolutions of gaugino masses for our benchmark pairs given in Table 6.1. First row: on the left, pure mirage mediation model and on the right corresponding deflected mirage mediation model designed to have the same gaugino mass unification scale. Second row: On the left, pure mirage mediation model and on the right corresponding deflected mirage mediation model with same high scale input parameters and  $\alpha_g = 1$ . Third row: On the left, pure mirage mediation model and on the right corresponding deflected mirage mediation model with same high scale input parameters and  $\alpha_g = 0.2$ .

	Point 1	Point 2	Point 3	Point 4	Point 5	Point 6
$\sigma_{\text{SUSY}}$ (pb)	5.86	10.86	0.045	44.71	0.58	13.26
Trigger Efficiency	84.8%	78.9%	99.3%	59.4%	98.4%	87.1%
Counts per 50,000 Events						
Multijet	5064	1250	10113	579	4645	1246
1 Lepton	694	69	3861	19	4266	445
OS Dilepton	28	0	370	0	1623	9
SS Dilepton	3	0	124	0	201	3
Trilepton	0	0	70	0	388	1

Table 6.2: **Gross LHC Features for Benchmark Points.** The trigger efficiency is here computed using the level one trigger table of PGS4. The number of events passing our selection criteria in the multijet, single lepton plus jets, opposite-sign dilepton plus jets, same-sign dilepton plus jets, and trilepton plus jets channels are given for 50,000 generated events.

	Point 1	Point 2	Point 3	Point 4	Point 5	Point 6
Multijet	0.17	0.37	70.30	0.20	1.90	0.30
1 Lepton	2.18	64.20	–	49.90	5.87	1.04
OS Dilepton	68.80	–	–	–	2.08	–
SS Dilepton	–	–	–	–	11.91	–
Trilepton	–	–	–	–	2.94	–

Table 6.3: **Necessary Integrated Luminosity for  $5\sigma$  Discovery in Selected Channels.** The integrated luminosity (in  $\text{fb}^{-1}$ ) at  $\sqrt{s} = 14$  TeV to produce a  $5\sigma$  excess over Standard Model backgrounds is given for all cases in which  $\mathcal{L}_{\text{int}} \leq 100 \text{fb}^{-1}$ . We require a minimum of 100 signal events in the no-lepton and single lepton channels, and a minimum of ten signal events in the multi-lepton channels.

jets to satisfy  $|\eta| < 3$ . We display the result of this analysis in Tables (6.2, 6.3). To study the discovery potential we also generated a sample of  $5 \text{fb}^{-1}$  Standard Model background events, consisting of Drell-Yan, QCD dijet,  $t\bar{t}$ ,  $b\bar{b}$ ,  $W/Z$ +jets and diboson production.

We display the total SUSY cross section for each benchmark model in Table 6.2 which depends, to a first approximation, only on the gluino mass. Thus deflected mirage mediation models offer the prospect of larger LHC signals relative to comparable pure mirage mediation models. The trigger efficiency is estimated using the level one trigger table of PGS4 and represents the fraction of the  $5 \times 10^4$  generated events that passed the trigger criteria. As we see in Table 6.2, however, the actual number of events that pass post-trigger cuts will often be much smaller.

The most striking effects of a non zero gauge mediation contribution to soft terms can be seen in Points 3 and 4. The total SUSY cross section increases by 3 orders of magnitude with increasing

$\alpha_g$ . Actually, Point 3 will require an integrated luminosity of  $1000 \text{ fb}^{-1}$  to produce 50K events, while for Point 4,  $1 \text{ fb}^{-1}$  will be enough. For smaller values of  $N$ , the gluino mass would be larger and hence the expected signal size would diminish.

Table (6.2) shows that triggering efficiencies are generally slightly better for models with a less compressed gaugino mass spectrum. This results in slightly harder leptonic decay products at the final stages of cascade decays of gluinos and squarks. The PGS4 default level one trigger criteria requires leptons ( $e^\pm$  and  $\mu^\pm$ ) to have  $p_T \geq 10 \text{ GeV}$  in the dilepton channel,  $p_T \geq 15 \text{ GeV}$  for an isolated lepton produced with a tau, and  $p_T \geq 20 \text{ GeV}$  for a single isolated lepton produced in association with hard jets. In addition to this trigger requirement, standard supersymmetry search algorithms involving jets, leptons and missing transverse energy generally also demand minimum  $p_T$  values for leptonic objects.

To demonstrate the differences between deflected mirage mediation models and their pure mirage mediation model analogs, we study traditional discovery channels of supersymmetry [108]. These signatures shown in Table (6.2) are defined as follows. All five require transverse sphericity  $S_T \geq 0.2$  and missing energy  $\cancel{E}_T \geq 250 \text{ GeV}$  except for the trilepton signature, where only  $\cancel{E}_T \geq 200 \text{ GeV}$  is required. Multijets here refers to events with at least four jets with the transverse momenta of the four leading jets satisfying  $p_T \geq (200, 150, 50, 50) \text{ GeV}$ , respectively. For this signature we impose a veto on isolated leptons. For the single lepton, opposite-sign dilepton, same-sign dilepton and trilepton signatures we include only electron and muon final states and demand at least two jets with the leading jets satisfying  $p_T \geq (100, 50) \text{ GeV}$ , respectively. The drastic reduction in the multijet and the leptonic signatures for the deflected mirage mediation models seen in Table 6.2 is caused by the small mass gap between the LSP and either the gluino or the lightest chargino/second neutralino. This is also true of the TeV-scale mirage unification model of Point 1.

Since the total cross sections vary significantly between the benchmark models, we display the amount of integrated luminosity necessary to observe a 5 sigma excess over the Standard Model background. The results are given in Table 6.3. Note that we only extrapolate the value of  $S/\sqrt{B}$  for cases where  $\mathcal{L}_{\text{int}} \leq 100 \text{ fb}^{-1}$  and we require at least 100 signal events for the multijet and single-

	Parameter Set			$\alpha_g$ Value				
	$\alpha_m$	$M_0$	$M_{\text{mess}}$	-1.0	-0.5	0	0.5	1.0
Line A	1	2 TeV	$10^{12}$ GeV	$\tilde{\tau}$ LSP	✓	✓	✓	✓✓
Line B	1	1 TeV	$10^8$ GeV	✓	✓✓	✓	$\tilde{g}$ LSP	$\tilde{g}$ LSP
Line C	0.771	0.8 TeV	$10^{12}$ GeV	✓	✓	✓	✓	✓
Line D	0.755	0.4 TeV	$10^{12}$ GeV	✓	✓	✓	✓	✓

Table 6.4: **Input Parameters for Benchmark Lines.** For each model line we begin with the input parameter set indicated in the initial three columns. Five values of the parameter  $\alpha_g$  were studied, keeping other parameters fixed. Points marked with a check-mark had acceptable low-energy phenomenology. Points marked with the double check-mark were studied in Ref. [149].

lepton channels and at least 10 signal events for the multi-lepton channels. Except Point 3, all of these benchmark points will be discoverable in the multijet channel early at the LHC running at 14 TeV center of mass energy. Leptonic discovery channels will generally take longer to observe. Point 5, despite its modest production cross-section of 0.6 picobarns, gives sizable signals in all leptonic channels within the first  $10 \text{ fb}^{-1}$ . This is largely due to the mass ordering  $m_{\tilde{\chi}_1^0} < m_{\tilde{\tau}_1} < m_{\tilde{\chi}_2^0}$ , which does not appear in any of the deflected mirage mediation models considered here.

### 6.3 Influence of $\alpha_g$ on LHC Phenomenology

In this section, we study the effect of the gauge mediated contribution to the expected collider signatures. To do so we construct four model “lines” in which we vary only the parameter  $\alpha_g$  while keeping the other parameters determining the soft supersymmetry breaking masses constant. We summarize the relevant input parameters in Table 6.4. For each case, we have chosen to fix  $N = 3$ ,  $n_i = 1/2$  for the matter representations and  $n_i = 1$  for the Higgs fields, and  $\tan \beta = 10$ . Each line involves five discrete points with  $\alpha_g = \{-1.0, -0.5, 0.0, 0.5, 1.0\}$ .

From Eqn. (6.11), we see that all three soft gaugino mass parameters decrease as  $\alpha_g$  is varied from  $\mathcal{O}(1)$  negative values to  $\mathcal{O}(1)$  positive values. Since the threshold correction of  $M_3$  is proportional to  $g_3^2(M_{\text{mess}})$ , the effect is strongest for the gluino. Therefore we expect some value of  $\alpha_g$  to exist above which the gluino will become the LSP, which happens for  $\alpha_g = 0.5$  and  $1.0$  in model line B as shown in Table 6.4. However, states which are charged only under  $U(1)_Y$ , such as the right-handed sleptons, are largely unaffected by the variation in  $\alpha_g$  since the threshold correction to their soft

Model	$m_{\tilde{g}}$	$m_{\tilde{q}_1}$	$m_{\tilde{t}_1}$	$m_{\text{LSP}}$	$\Delta^0$	$\Delta^\pm$	$m_{\tilde{\ell}_1}$	B%	W%	H%
Line A										
A2	2828	2492	2027	1400	175	179	1445	96.4%	0.1%	3.5%
A3	2260	2144	1710	1265	132	132	1429	94.9%	0.4%	4.8%
A4	1677	1895	1479	1133	70	69	1427	94.1%	1.6%	4.3%
A5	1045	1814	1380	977	30	1.6	1441	3.6%	92.5%	3.9%
Line B										
B1	1347	1197	942	663	84	80	686	88.7%	1.6%	9.6%
B2	1038	1038	785	595	54	49	679	85.7%	4.5%	9.7%
B3	711	952	707	525	20	11	677	51.4%	37.8%	13.4%
Line C										
C1	1440	1277	999	530	167	167	596	98.4%	0.1%	1.4%
C2	1244	1133	868	487	132	132	587	98.0%	0.2%	1.8%
C3	1048	1003	747	444	99	98	582	97.4%	0.4%	2.2%
C4	847	894	647	402	66	65	580	96.4%	1.0%	2.6%
C5	640	818	578	359	34	32	583	93.3%	3.7%	3.1%
Line D										
D1	752	672	496	254	75	73	297	94.3%	1.1%	4.5%
D2	647	594	423	232	58	56	292	91.6%	2.3%	5.8%
D3	542	521	357	209	43	39	289	86.3%	5.0%	8.7%
D4	436	460	304	186	30	24	289	75.3%	12.5%	12.2%
D5	325	415	273	161	22	12	290	51.6%	32.6%	15.8%

Table 6.5: **Some Key Masses for Model Lines.** Low-lying superpartner masses are given in units of GeV as well as the wavefunction composition of the LSP neutralino. Here  $m_{\tilde{q}_1}$  is the lightest first generation squark,  $m_{\tilde{t}_1}$  is the lighter stop, and we have defined the two mass differences  $\Delta^\pm \equiv m_{\tilde{\chi}_1^\pm} - m_{\tilde{\chi}_1^0}$  and  $\Delta^0 \equiv m_{\tilde{\chi}_2^0} - m_{\tilde{\chi}_1^0}$ .

masses scales as  $g_1^4(M_{\text{mess}})$ . As a result the lightest stau will have a roughly constant mass across the entire model line. For  $\alpha_g < 0$ , there can be points for which the lightest stau is the LSP which occurred for  $\alpha_g = -1.0$  in model line A.

The collider phenomenology of these models depends mostly on the overall mass scale of the superpartners which carry  $SU(3)$  quantum numbers. This scale varies dramatically with  $\alpha_g$ . As has been pointed out recently [79], once event rates are normalized to the overall mass scale of the colored superpartners, the next most important factor determining the inclusive signatures for a model at the LHC is the hierarchy of low-lying superpartner masses. This is particularly true for leptonic signatures produced through the production and decay of light neutralino and chargino states. We will study the possible hierarchy patterns in deflected mirage mediation and compare them to the mSUGRA hierarchy patterns in the next section.

Table (6.5) shows the lightest neutralino mass, the lightest slepton mass (generally a scalar tau), the gluino and lightest stop mass, and the two mass differences that we define as

$$\Delta^0 \equiv m_{\tilde{\chi}_2^0} - m_{\tilde{\chi}_1^0}, \quad (6.15)$$

$$\Delta^\pm \equiv m_{\tilde{\chi}_2^\pm} - m_{\tilde{\chi}_1^0}. \quad (6.16)$$

These mass differences decrease monotonically with increasing  $\alpha_g$  values because the gaugino spectrum becomes more squeezed. As a result, the leptonic decay products of cascade decays involving  $\tilde{\chi}_2^\pm$  and  $\tilde{\chi}_2^0$  become softer and one typically encounters a point at which the on-shell decays of the chargino (or second-lightest neutralino) to a slepton become kinematically forbidden which further suppresses leptonic final state signatures. These properties are common to many models in which anomaly-mediated supersymmetry breaking dominates [153]. To illustrate this we give the bino, wino and Higgsino composition of the lightest neutralino in Table 6.5.

## 6.4 Comparison with mSUGRA and sparticle landscape

In this section we will compare the sparticle landscape of deflected mirage mediation models to mSUGRA models following the analysis first proposed by Feldman, Liu and Nath (FLN) [69].

Model Point	$\sigma_{\text{SUSY}}$ (pb)	Trigger Eff.	Multijet	1 Lepton	OS Dilepton	Trilepton
Line A						
A2	$1 \times 10^{-3}$	98.8%	7794	3846	687	213
A3	$5 \times 10^{-3}$	99.1%	8238	3741	360	105
A4	0.02	98.4%	6171	5976	823	252
A5	0.21	73.8%	1447	31	3	2
Line B						
B1	0.38	98.4%	4339	4031	1486	447
B2	1.54	96.8%	3155	3441	379	75
B3	5.56	88.0%	2409	182	0	0
Line C						
C1	0.25	98.9%	8798	3784	398	90
C2	0.59	98.6%	7932	3588	310	68
C3	1.45	98.0%	5591	3718	499	102
C4	3.80	96.1%	2931	3577	353	76
C5	11.71	90.2%	2785	871	12	2
Line D						
D1	12.7	95.9%	2680	2728	654	145
D2	27.0	94.0%	2274	2195	309	48
D3	61.1	91.0%	1328	1278	132	16
D4	152.0	84.6%	759	660	34	2
D5	459.7	67.2%	365	109	4	1

Table 6.6: **Gross LHC Features for Model Lines of Table 4.** The total cross section for production of superpartners and PGS4 level one trigger efficiency are given in the first two columns. The following four columns give the number of events in each channel per 50,000 generated events. The definitions of these signatures are modified slightly from those of Section 4.1.

To be able perform this analysis precisely, we have generated a large set of model parameters and corresponding low energy spectra, then studied how the patterns of the lightest four non-SM particles (superpartners and non-SM Higgs fields) vary as we impose a series of phenomenological constraints.

For mSUGRA, we followed the procedure of FLN [69] and generated 2 million mSUGRA models by randomly selecting input parameters from the following ranges with flat priors:

$$\left\{ \begin{array}{l} 0 \leq m_0 \leq 4 \text{ TeV} \\ 0 \leq m_{1/2} \leq 2 \text{ TeV} \\ \left| \frac{A_0}{m_0} \right| \leq 10 \\ 1 \leq \tan \beta \leq 60 \end{array} \right\}. \quad (6.17)$$

To be able to compare our results, these ranges and flat priors are chosen to be identical to those studied by FLN. The ranges of the input parameters are limited by what will be observable at the LHC after many years of integrated luminosity. The choice of priors is also important for these kind of statistical studies, since the result might depend on how the parameters are chosen. Without a more general theory that predicts infinitely many universes with different sets of physics parameters, nature is limited by a single choice of a set of parameters. It is not obvious in this case how those parameters acquire the observed values,<sup>‡</sup> unless there is a dynamical mechanism that determine those values or a more general theory, i.e. string theory, that predicts those values based on geometrical arguments.<sup>§</sup> We argue that doing a statistical analysis with flat priors (or any priors) is interesting and important to understand the phenomenology of the theory better even if the percentages may or may not imply the realizability of the theory in nature with the most common sparticle spectrum. Hence we follow the FLN analysis and scan the input parameters with flat priors<sup>¶</sup>.

For the case of DMM models, which involve a larger parameter space and have not been

---

<sup>‡</sup>To be observed in this case, since supersymmetry has not been observed yet.

<sup>§</sup>Although the premise of string theory is to calculate those “free” parameters, different ways of compactifying extra dimensions result in a very large number of possible vacua (in the orders of  $10^{500}$ ) which creates another uniqueness problem.

<sup>¶</sup>Note that because of the large number of models we considered ( $\sim 26$  million), repeating the computation with different set of priors was not computationally possible given the finite CPU time we had access to.

studied in this way in previous literature, we generated a much larger model set consisting of 24.75 million models. The models in this set were obtained by randomly scanning over the DMM parameter ranges given below once again with flat priors:

$$\left\{ \begin{array}{l} 1 \leq N \leq 5 \\ 4 \leq \log(M_{\text{mess}}/\text{GeV}) \leq 16 \\ 50 \text{ GeV} \leq M_0 \leq 2000 \text{ GeV} \\ 0 \leq \alpha_m \leq 2 \\ -1 \leq \alpha_g \leq 2 \\ 1 \leq \tan \beta \leq 60 \end{array} \right\}, \quad (6.18)$$

where the ranges chosen for the dimensionless ratio parameters  $\alpha_m$  and  $\alpha_g$  are the theoretically-motivated ranges studied in [150, 136, 137].

After generating our model sets for both mSUGRA and DMM, the parameters are then evolved to the electroweak symmetry-breaking scale using a modified version of `SoftSUSY 3.0.7` to handle the threshold effects in DMM models. After obtaining the soft supersymmetry breaking parameters, the spectrum is determined again in `SoftSUSY 3.0.7` which is then fed into `MicrOmegas 2.2` CPC to determine the physical mass spectrum as well as collider and cosmological observables. We then study the effect of applying a sequence of phenomenological requirements on the models. These requirements are explained in detail in the following and summarized in Tables (6.7, 6.8, 6.9).

1. **Radiative EWSB:** Our first requirement is the presence of radiative electroweak symmetry-breaking, which in both model sets reduces the sample size by a large fraction as we will see in Table 6.10 where we show the results of the progressive cuts.
2. **Neutralino LSP:** Our second requirement is that the lightest R-parity odd state is a neutralino, which we denote as the lightest supersymmetric particle (LSP). We emphasize that the acronym “LSP” refers to this state because, as we will see, quite often the lightest particle beyond those of the Standard Model is one of the heavier Higgs states.

3. **Direct Search Limits:** Our third requirement is a set of bounds that we call the “direct” bounds, in that they reflect conservative direct search limits for new states beyond the Standard Model. We summarize these constraints in Table 6.7. Many of these constraints are similar to FLN analysis [69] and a similar scan by Djouadi *et al.* [154]. However, We have augmented the Higgs bounds by including direct limits on the pseudoscalar and charged Higgs masses. In addition, to analyze the effects of tightening the light Higgs mass bound, we use two separate limits on the Higgs boson mass: the 100 GeV bound of FLN, and the direct limit on the SM Higgs mass of  $m_h > 114.4$  GeV. Next, we have added a rather conservative gluino mass bound of  $m_{\tilde{g}} \geq 309$  GeV [155]. This bound is automatically satisfied once the chargino bound is imposed in mSUGRA models; however, this is not necessarily the case in DMM models. For the case of squeezed spectrum, it is also necessary to modify not only this bound but also the chargino bound which can easily occur in DMM models. The chargino bound essentially vanishes in the case in which the lightest chargino and the LSP are almost degenerate ( $m_{\tilde{\chi}_1^\pm} - m_{\tilde{\chi}_1^0} < 3$  GeV) [82]. Similarly, the gluino bound is degraded when the gauginos are squeezed [156, 157]. To model this effect, we used another conservative constraint that the gluino bound degrades to 125 GeV when  $m_{\tilde{g}}/m_{\tilde{\chi}_1^0} < 5$ .
4. **Indirect Limits:** Our fourth requirement is a set of constraints on the rare decays  $b \rightarrow s\gamma$  and  $B_s \rightarrow \mu^+\mu^-$ , as well as the new physics contributions to the anomalous magnetic moment of the muon. For the inclusive  $b \rightarrow s\gamma$  rate, we consider the average value as derived by the Heavy Flavor Averaging Group [158]:

$$\text{Br}(b \rightarrow s\gamma) = (355 \pm 24_{-10}^{+9} \pm 3) \times 10^{-6}, \quad (6.19)$$

and use a  $3.5\sigma$  range about the best fit value which was also used in the FLN analysis [79]. We note that the first FLN paper used the slightly tighter range of  $283 \times 10^{-6} < \text{Br}(b \rightarrow s\gamma) < 463 \times 10^{-6}$ . For the rare decay  $B_s \rightarrow \mu^+\mu^-$ , we use the recent 95% confidence level upper

bound determined by CDF [53]:

$$\text{Br}(B_s \rightarrow \mu^+ \mu^-) < 5.8 \times 10^{-8}. \quad (6.20)$$

This bound is significantly more stringent than the one employed in the original papers of FLN, which was  $\text{Br}(B_s \rightarrow \mu^+ \mu^-) < 9 \times 10^{-6}$  <sup>||</sup>. Finally, for the anomalous magnetic moment of the muon, we use the conservative range of FLN and Djouadi *et al.*:

$$-11.4 \times 10^{-10} \leq (g_\mu - 2)_{\text{SUSY}} \leq 9.4 \times 10^{-9}. \quad (6.21)$$

5. **Relic Density Constraints:** Our fifth requirement is on the relic density of dark matter in the universe which is inferred from the measured cosmic microwave background. The standard approach is to assume that the LSP neutralinos make up the entirety of the dark matter. The resulting relic abundance, which is determined by standard cosmology, is then compared to the current constraints from the WMAP satellite to obtain bounds on the SUSY parameter space. The FLN papers used a  $2\sigma$  bound from WMAP3 ( $0.0855 < \Omega_{\tilde{\chi}} h^2 < 0.1189$ ). WMAP has now reported  $1\sigma$  results of the five years [160] and seven years [161] as:

$$\Omega_{\tilde{\chi}} h^2|_{5\text{yr}} = 0.1099 \pm 0.0062, \quad (6.22)$$

$$\Omega_{\tilde{\chi}} h^2|_{7\text{yr}} = 0.1109 \pm 0.0056. \quad (6.23)$$

We can imagine that since these values have been measured really precisely by WMAP, this will put strong bounds on supersymmetric theories. But the LSP might not be the only dark matter particle. There may be also effects from non-standard cosmology that alter the relic abundance (such as in kination-dominated quintessence theories [162, 163]). The theoretical and computational tools are not precise enough to match the precision of the WMAP results, the most important being the uncertainties in the halo models. For our computation we use the package `MicrOmegas 2.2 CPC`, but results from `DarkSUSY` often give values that differ

---

<sup>||</sup>Note that D0 collaboration has recently updated this bound to  $\text{Br}(B_s \rightarrow \mu^+ \mu^-) < 5.1 \times 10^{-8}$  [159]

by more than the quoted errors in the WMAP measurements. For these reasons, we will consider three options for the dark matter constraints, which are summarized in Table 6.9. The first is the  $2\sigma$  range from WMAP7 [161]:

$$0.0997 < \Omega_{\tilde{\chi}} h^2 < 0.1221. \quad (6.24)$$

The second option is to consider a broader range that we call “WMAP Preferred”:

$$0.07 \leq \Omega_{\tilde{\chi}} h^2 \leq 0.14, \quad (6.25)$$

which is slightly more expansive than the WMAP3  $2\sigma$  range utilized by FLN of  $0.0855 \leq \Omega_{\tilde{\chi}} h^2 \leq 0.121$ . The third option, which is even less restrictive, is to follow the procedure of [82], and only impose an upper limit on the relic abundance obtained from WMAP5:

$$\Omega_{\tilde{\chi}} h^2 \leq 0.121. \quad (6.26)$$

Before we show our results, we would like to note the differences between SoftSUSY, which we used, and SuSpect, which was used by FLN. The radiative corrections to the mass matrices of neutralinos and charginos are interpreted differently in both software which results in sometimes different hierarchies. In SuSpect, the lightest chargino is always lighter than the second-lightest neutralino (for  $\mu > 0$ ), but in SoftSUSY either mass ordering between these two states is possible, and the ordering can indicate whether the states are primarily wino-like, or whether they have a significant Higgsino component. To be able to compare our results, we repeat the analysis of FLN using SoftSUSY. Therefore we will present the results of updated FLN analysis as well as our very large analysis of deflected mirage mediation models in the following sections.

## 6.5 Impact of Progressive Cuts

In this section we will discuss the hierarchy patterns of the lightest four states we observe in minimal supergravity and deflected mirage mediation models. We begin our analysis with a

Condition	Bound
Higgs	$m_h > 100 \text{ GeV}$ or $m_h > 114.4 \text{ GeV}$
Chargino**	$m_{\tilde{\chi}_1^\pm} > 104.5 \text{ GeV}$
Stop	$m_{\tilde{t}_1} > 101.5 \text{ GeV}$
Stau	$m_{\tilde{\tau}_1} > 98.8 \text{ GeV}$
Gluino**	$m_{\tilde{g}} > 309 \text{ GeV}$ ( $m_{\tilde{g}} > 125 \text{ GeV}$ )
Pseudoscalar Higgs	$m_A > 85 \text{ GeV}$
Charged Higgs	$m_{H^\pm} > 79.3 \text{ GeV}$

Table 6.7: **Direct (collider) mass bounds:** Our direct limits follow those of FLN [69], with the following additions. In addition to the FLN Higgs mass limit of 100 GeV, we also consider the SM Higgs mass limit of 114.4 GeV, and include limits on the pseudoscalar and charged Higgs masses. The asterisks indicate that the chargino limit is applied only when the mass difference between the lightest chargino and the LSP exceeds 3 GeV, and the 309 GeV gluino bound is degraded to 125 GeV if the ratio of the gluino mass to the LSP is less than 5, as discussed in the text. For a more detailed analysis of gluino bounds, see [156, 157].

Condition	Bound
$b \rightarrow s\gamma$	$229 \times 10^{-6} \leq \text{Br}(b \rightarrow s\gamma) \leq 481 \times 10^{-6}$
$B_s \rightarrow \mu^+\mu^-$	$\text{Br}(B_s \rightarrow \mu^+\mu^-) < 5.8 \times 10^{-8}$
$(g_\mu - 2)_{\text{SUSY}}$	$-11.4 \times 10^{-10} \leq (g_\mu - 2)_{\text{SUSY}} \leq 9.4 \times 10^{-9}$

Table 6.8: **Indirect bounds:** Our indirect limits include the update to  $\text{Br}(B_s \rightarrow \mu^+\mu^-)$  rate [53]. We use the HFAG range for  $b \rightarrow s\gamma$  [158], and the FLN and Djouadi range for  $(g_\mu - 2)_{\text{SUSY}}$ .

Condition	Bound
WMAP7	$0.0997 < \Omega_{\tilde{\chi}} h^2 < 0.1221$
WMAP Preferred	$0.07 < \Omega_{\tilde{\chi}} h^2 < 0.14$
WMAP Upper	$\Omega_{\tilde{\chi}} h^2 < 0.121$

Table 6.9: **Dark matter bounds:** We consider three options for the dark matter constraints: the WMAP7  $2\sigma$  range [161], a broader “WMAP Preferred” range, and the WMAP5 upper bound, as used in [82].

general discussion of the effect of each set of phenomenological requirements on the data sample set for each model. In Table 6.10, we show the impact of the five progressive cuts described in the previous section, starting with the full data sample of 2 million model points for mSUGRA and 24.75 million model points for DMM. More precisely, we give the number of model points which survive the requirement, beginning with the demand for proper electroweak symmetry breaking. We provide the number of distinct hierarchy patterns which survive, as defined by the absolute ordering of the four lightest new particles. Here we have taken  $m_h > 100$  GeV and chosen the WMAP Preferred range of Eqn. (6.25).

Table 6.10 shows that the combination of gravity, gauge and anomaly mediation in DMM provides a much richer set of possible mass hierarchies than mSUGRA. The requirement of radiative electroweak symmetry breaking eliminates approximately 66% of the mSUGRA parameter space but only 29% of the DMM parameter space we considered. Once this requirement is satisfied the impact of the remaining progressive cuts is similar for the two cases.

The indirect limits are slightly more stringent for the DMM models than for mSUGRA models, with  $b \rightarrow s\gamma$  and  $B_s \rightarrow \mu^+\mu^-$  providing the strongest limits. The  $b \rightarrow s\gamma$  bound constrains in particular models with light charginos, which often occur in deflected mirage mediation since the gaugino spectrum is generically squeezed in comparison to that of minimal supergravity. The  $B_s \rightarrow \mu^+\mu^-$  constraint tends to reduce the number of scenarios in which the additional Higgs bosons  $H$ ,  $A$ , and  $H^\pm$  are light. As we will see, these patterns often occur in DMM, so these limits have a significant effect on the associated model space.

For both mSUGRA and DMM models, the relic density constraint has a dramatic impact on the allowed parameter space and on the number of the hierarchy patterns that survive but they are much easier to satisfy in the DMM parameter space than in the mSUGRA parameter space. It is well known that most of the viable parameter space in mSUGRA results in a bino-like LSP, which typically results in a thermal relic abundance well in excess of the upper bounds in Eq. (6.26) with the exception of the hyperbolic branch/focus point region, in which the LSP has a nontrivial Higgsino component. Co-annihilation channels or resonance effects are thus needed in the early universe to reduce the resulting abundance at freeze-out to acceptable levels,

Requirement	mSUGRA Sample			DMM Sample		
	Points	%	Patterns	Points	%	Patterns
Radiative EWSB	686,204	–	195	17,580,869	–	1338
Neutralino LSP	528,140	77.0%	105	13,639,985	77.6%	380
Direct Search Limits	491,262	71.6%	64	12,332,788	70.1%	226
Indirect Limits	477,608	69.6%	52	9,948,427	56.6%	194
WMAP Preferred Range	3,829	0.6%	35	657,624	3.7%	96

Table 6.10: **Progressive Cuts and Impact on Final Data Sample Size:** The number of surviving mSUGRA and DMM models is given as a series of progressive cuts is imposed. The second column of each of the model categories is the percentage of surviving models with respect to the number of models that survives the radiative electroweak symmetry breaking constraint. The light Higgs mass bound is 100 GeV.

NLSP	Proper EWSB		Neutralino LSP		Exper. Bounds		WMAP Preferred	
	# Models	%	# Models	%	# Models	%	# Models	%
$\chi_2^0$	348,859	50.8%	348,849	66.1%	323,167	67.7%	981	25.6%
$\chi_1^\pm$	20,614	3.0%	20,614	3.9%	8,312	1.7%	648	16.9%
$\tilde{\tau}_1$	131,809	19.2%	131,809	25.0%	125,492	26.3%	1,870	48.8%
$\tilde{g}$	70	0.0%	70	0.0%	0	–	0	–
$\tilde{t}_1$	16,039	2.3%	16,039	3.0%	12,899	2.7%	227	5.9%
$H$ or $A$	8,338	1.2%	8,338	1.6%	6,720	1.4%	98	2.6%
$\tilde{\nu}$	63	0.0%	63	0.0%	0	–	0	–
Higgs LSP	2,790	0.4%	2,358	0.4%	1018	0.2%	5	0.1%
$\tilde{\nu}$ LSP	15	0.0%	0	–	0	–	0	–
Other LSP	157,607	23.0%	0	–	0	–	0	–

Table 6.11: **Progressive cuts in mSUGRA:** We list the NLSPs of minimal supergravity models as a series of progressive cuts is imposed. The experimental bounds include the direct and indirect bounds with  $m_h > 100$  GeV.

NLSP	Proper EWSB		Neutralino LSP		Exper. Bounds		WMAP Preferred	
	# Models	%	# Models	%	# Models	%	# Models	%
$\chi_2^0$	3,494,589	19.9%	3,494,589	25.6%	3,184,847	32.0%	104,672	15.9%
$\chi_1^\pm$	4,604,411	26.2%	4,604,411	33.8%	2,777,966	27.9%	222,095	33.8%
$\tilde{\tau}_1$	3,271,607	18.6%	3,271,607	24.0%	2,774,387	27.9%	105,472	16.0%
$\tilde{g}$	16,731	0.1%	16,731	0.1%	7,185	0.1%	0	–
$\tilde{t}_1$	2,871	0.0%	2,871	0.0%	149	0.0%	7	0.0%
$\tilde{e}_R$	37,921	0.2%	37,921	0.3%	33,701	0.3%	282	0.0%
$H$ or $A$	242,500	1.4%	242,500	1.8%	148,322	1.5%	14,676	2.2%
$\tilde{\nu}$	5,653	0.0%	5,653	0.0%	0	–	0	–
Higgs LSP	3,106,146	17.7%	1,963,702	14.4%	1,021,870	10.3%	210,420	32.0%
$\tilde{\nu}$ LSP	4,310	0.0%	0	–	0	–	0	–
Other LSP	2,794,130	15.9%	0	–	0	–	0	–

Table 6.12: **Progressive cuts in DMM:** The NLSPs in deflected mirage mediation models are given with the same set of progressive cuts used in the previous table.

which disproportionately favors models with light staus or stops [110, 111]. In deflected mirage mediation, we will see that the LSP can be bino-like as in mSUGRA models, but it can also be purely Higgsino with an LSP mass in the TeV range, or it can be a mixture of gauginos and Higgsinos, *i.e.*, a “well-tempered” neutralino [164].

In Tables (6.11, 6.12) we show the impact of the cuts on the distributions of NLSP’s for mSUGRA and DMM models. For this analysis, we group the direct search bounds with the indirect constraints and denote them as experimental bounds. We first note that there is a sizable set of patterns in which the second lightest neutralino is the NLSP; as mentioned previously, this is a result from running SoftSUSY as opposed to SuSpect, as done in FLN. We see from Table 6.11 that in mSUGRA the direct and indirect constraints affect all NLSP categories more or less equally, but the dark matter requirement heavily favors co-annihilation with staus or stops or (to a lesser extent) charginos. In contrast, we see from Table 6.12 that in DMM the preferred patterns from the dark matter constraints are the chargino NLSP and Higgs LSP patterns. The stau NLSP patterns are no longer particularly favored, although a significant number of them remain. As we mentioned

previously, this shows that there are additional ways to satisfy relic density constraint in DMM.

Another reason for these features is that the overall mass scale for the scalars and gauginos are controlled by the same mass scale  $M_0$  in DMM models and it is the gauginos that can be more easily deflected by threshold corrections to lower values. Furthermore, in DMM models the trilinear couplings ( $A$  terms) are not separately adjustable, which also affects the low energy spectrum. This is clearly a different situation than the mSUGRA case, where the masses of the scalars and the gauginos are governed by two separately adjustable parameters ( $m_0$  and  $m_{1/2}$ ), and the left-right scalar mixing terms also have contributions from the independent parameter  $A_0$ . For this reason, patterns in which sfermions are the NLSP are relatively disfavored in DMM models. We see the biggest impact of this on the number of stop NLSP patterns. Even before any experimental cuts, the percentage of stop NLSP patterns in the full data set is significantly smaller than it is in mSUGRA, and with the experimental cuts and the dark matter cuts imposed the stop NLSP patterns are completely eliminated. The selectron NLSP patterns, while numerically insignificant, also result from these features. In these patterns, the selectron NLSP is highly degenerate with the stau, and the patterns share similar features with stau NLSP models.

We see from Table 6.12 that the gluino NLSP patterns are also absent in DMM models once the dark matter cuts are imposed. Although spectra with relatively light gluinos occur naturally in deflected mirage mediation [85], pushing the gluino below the lightest chargino requires fine-tuning of the mirage unification scale to be at a very particular low scale region. This is not generic in DMM, but it can happen and in fact, prior to the dark matter cuts, it is relatively easier to have a gluino NLSP than a stop NLSP. However, such points in parameter space are severely constrained by the dark matter bounds. As we will see, gluino NLSP patterns typically predict too low of a relic abundance because the LSP is generically a mixed-composition state with a relatively low mass, and hence such patterns are completely eliminated by the WMAP preferred constraint.

We now show the impact of the different dark matter cuts and the light Higgs bounds on the NLSPs in both sets of models after the direct and indirect bounds are imposed, with  $m_{h_1} > 100$  GeV in Table 6.13 and  $m_{h_1} > 114.4$  GeV in Table 6.14. The WMAP Preferred and WMAP7 bounds show similar results for both models and both Higgs bounds, with the WMAP7 limits showing

a stronger preference for  $\tilde{\tau}$  NLSPs than the WMAP Preferred bound, and a weaker preference for Higgs LSP patterns in the DMM case. By comparing Tables 6.13 and 6.14, one sees that the effect of the stronger Higgs limit is to decrease the number of stop and stau NLSP cases in minimal supergravity models, and to decrease the number of chargino NLSP cases and increase the number of Higgs LSP cases in deflected mirage mediation models. However, the situation is different when only the WMAP upper bound is imposed. As expected, for both model sets the number of chargino NLSPs drastically increases and the number of stau NLSPs decreases as compared to what is found with the WMAP Preferred and WMAP7 cuts.

NLSP	WMAP Preferred		WMAP 7-Year		Upper Bound Only	
	mSUGRA	DMM	mSUGRA	DMM	mSUGRA	DMM
$\chi_2^0$	25.6	15.9	26.3	18.3	23.8	5.3
$\chi_1^\pm$	16.9	33.8	15.2	33.9	35.4	62.0
$\tilde{\tau}_1$	48.8	16.0	51.1	18.8	31.7	6.4
$\tilde{g}$	–	–	–	–	–	0.2
$\tilde{t}_1$	5.9	–	5.2	–	7.5	–
$H$ or $A$	2.6	2.2	2.2	2.1	1.6	1.9
Higgs LSP	0.1	32.0	–	26.8	0.1	24.2

Total Models	3,829	657,624	1,256	179,834	9,213	3,637,491
Number of Patterns	35	96	29	80	40	175

Table 6.13: **NLSPs and Number of Models/Patterns for Different Dark Matter Assumptions:** The numbers in the upper table are percentages of the total datasets. The Higgs bound is  $m_h > 100$  GeV.

## 6.6 Hierarchy Patterns in mSUGRA and DMM

We now present a detailed analysis of the hierarchy patterns of the lightest four non-Standard Model states obtained in minimal supergravity and deflected mirage mediation models. The results are summarized in Table 6.15 and shown in detail for the original FLN cuts in Table 6.16 and with the updated cuts in Tables (6.17, 6.18). Let us emphasize again that since we used SoftSUSY as opposed to SuSpect (used by FLN and Berger *et al.*), the details of the hierarchies

NLSP	WMAP Preferred		WMAP 7-Year		Upper Bound Only	
	mSUGRA	DMM	mSUGRA	DMM	mSUGRA	DMM
$\chi_2^0$	29.5	17.8	29.9	20.7	25.7	7.7
$\chi_1^\pm$	21.2	27.7	19.5	27.9	43.7	52.3
$\tilde{\tau}_1$	44.1	14.1	46.1	16.9	26.7	6.9
$\tilde{g}$	–	–	–	–	–	0.1
$\tilde{t}_1$	2.0	–	1.9	–	2.2	–
$H$ or $A$	3.1	2.6	2.6	2.5	1.6	1.8
Higgs LSP	0.2	37.7	–	32.0	0.1	31.2

Total Models	2,908	555,631	959	150,392	7,351	2,355,932
Number of Patterns	27	90	24	76	33	137

Table 6.14: **NLSPs and Number of Models/Patterns for Different Dark Matter Assumptions:** The numbers in the upper table are percentages of the total datasets. The Higgs bound is  $m_h > 114.4$  GeV.

differ from the FLN results because of the differences of the two codes in handling the chargino and neutralino sectors when the lightest chargino and second-lightest neutralino are nearly degenerate. As mentioned earlier, in this limit, it is found that for minimal supergravity models, the lightest chargino is almost always lighter than the second-lightest neutralino when SuSpect is used, while either outcome can occur when SoftSUSY is used, depending on whether these two states are wino-dominated or whether they include a nontrivial Higgsino component.

To see this more explicitly, we reproduce the mSUGRA analysis of the first FLN paper [69]. The FLN cuts include a 100 GeV Higgs mass bound and direct limits as given in Table 6.7, the branching ratios  $283 \times 10^{-6} < \text{Br}(b \rightarrow s\gamma) < 463 \times 10^{-6}$  and  $\text{Br}(B_s \rightarrow \mu^+\mu^-) < 9 \times 10^{-6}$  as well as the muon anomalous magnetic moment limit of Table 6.8, and the WMAP3  $2\sigma$  limits,  $0.0855 < \Omega_\chi h^2 < 0.1189$ . The results are presented in Table 6.16. We follow the FLN notation in labeling the patterns as mSP1, mSP2, etc., but use primes when the ordering of the lightest chargino and second-lightest neutralino is reversed from that of FLN. We also note that in the FLN papers, the Higgs LSP and Higgs NLSP patterns were grouped together in a single pattern, but here we will not do so presenting the DMM results.

**FLN Analysis**

Stau NLSP	$\chi_1^0 < \tilde{\tau}_1 < \tilde{\ell}_R < \tilde{\nu}_3$ (mSP5), $\chi_1^0 < \tilde{\tau}_1 < \chi_2^0 < \chi_1^\pm$ (mSP6')
Chargino NLSP	$\chi_1^0 < \chi_1^\pm < \chi_2^0 < \chi_3^0$ (mSP1)
Neutralino NLSP	$\chi_1^0 < \chi_2^0 < \chi_1^\pm < H, A$ (mSP2'), $\chi_1^0 < \chi_2^0 < \chi_1^\pm < \chi_3^0$ (mSP1')

**Updated FLN Analysis**

Stau NLSP	$\chi_1^0 < \tilde{\tau}_1 < \chi_2^0 < \chi_1^\pm$ (mSP6')
Chargino NLSP	$\chi_1^0 < \chi_1^\pm < \chi_2^0 < \chi_3^0$ (mSP1)
Stau NLSP	$\chi_1^0 < \tilde{\tau}_1 < \tilde{\ell}_R < \tilde{\nu}_3$ (mSP5)
Neutralino NLSP	$\chi_1^0 < \chi_2^0 < \chi_1^\pm < H, A$ (mSP2'), $\chi_1^0 < \chi_2^0 < \chi_1^\pm < \chi_3^0$ (mSP1')

**DMM Hierarchies: Weak Higgs Bound**

Higgs LSP	$H, A < H^\pm < \chi_1^0$
Chargino NLSP	$\chi_1^0 < \chi_1^\pm < \chi_2^0 < \tilde{\tau}_1$ (mSP3), $\chi_1^0 < \chi_1^\pm < \chi_2^0 < H, A$ (mSP2)
Neutralino NLSP	$\chi_1^0 < \chi_2^0 < \chi_1^\pm < \tilde{\tau}_1$ (mSP3'), $\chi_1^0 < \chi_2^0 < \chi_1^\pm < H, A$ (mSP2')
Stau NLSP	$\chi_1^0 < \tilde{\tau}_1 < \chi_2^0 < \chi_1^\pm$ (mSP6')

**DMM Hierarchies: Strict Higgs Bound**

Higgs LSP	$H, A < H^\pm < \chi_1^0$
Chargino NLSP	$\chi_1^0 < \chi_1^\pm < \chi_2^0 < H, A$ (mSP2)
Neutralino NLSP	$\chi_1^0 < \chi_2^0 < \chi_1^\pm < \tilde{\tau}_1$ (mSP3'), $\chi_1^0 < \chi_2^0 < \chi_1^\pm < H, A$ (mSP2')
Chargino / Stau NLSP	$\chi_1^0 < \chi_1^\pm < \chi_2^0 < \tilde{\tau}_1$ (mSP3), $\chi_1^0 < \tilde{\tau}_1 < \chi_2^0 < \chi_1^\pm$ (mSP6')

Table 6.15: **Summary of the most dominant hierarchy patterns:** The hierarchies of the most dominant mSUGRA patterns we observed by using the original FLN cuts and updated FLN cuts as well as the most dominant DMM hierarchy patterns we observed with the weak Higgs bound of  $m_h > 100$  GeV and the strict Higgs bound of  $m_h > 114.4$  GeV.

As the result of using SoftSUSY to determine the spectrum, we obtain several patterns in which the NLSP is the second-lightest neutralino rather than the lightest chargino. The dominant neutralino NLSP patterns always have the chargino as the third-lightest state, which indicates that the lightest chargino and second-lightest neutralino are wino-like. These kinds of patterns with a bino-like LSP are very common in mSUGRA. In fact, the only surviving chargino NLSP pattern is the mSP1 pattern of FLN, where the second-lightest neutralino is the third-lightest new state. This pattern corresponds to the focus point/hyperbolic branch region of mSUGRA, for which the LSP has a nontrivial Higgsino component.

In general, the overall percentages obtained from summing the original pattern and the primed pattern (when needed) are in agreement with the FLN results. As found in FLN, there are also a number of subdominant hierarchy patterns in which the stop is the NLSP, with the most popular one being the  $\chi_1^0 < \tilde{t}_1 < \chi_2^0 < \chi_1^\pm$  (mSP11') pattern, and patterns in which the heavy Higgses are the NLSP, with the most popular one being  $\chi_1^0 < H, A < H^\pm$  (mSP14).

We now use our updated sets of cuts and show the hierarchy patterns for both mSUGRA and DMM in Table 6.17 for  $m_h > 100$  GeV, and Table 6.18 for  $m_h > 114.4$  GeV and for all three sets of dark matter bounds. The favored patterns by the dark matter constraints are very different for the two models. While in mSUGRA the dominant patterns tend to be stau NLSP patterns, in DMM the favored pattern is always the Higgs LSP pattern, with  $H, A < H^\pm < \chi_1^0$ . The Higgs LSP pattern found in DMM models is quite different from typical mSUGRA mass patterns, with a relatively squeezed spectrum, an LSP with a mixed composition of bino, wino, and Higgsino states, and a high degree of degeneracy between the lightest chargino and the lightest two neutralinos, as we will discuss in greater detail in the next section. The other favored patterns in DMM models have light charginos and neutralinos compared to the scalar masses, which is expected since the gaugino mass ratios at low energies are adjustable depending on the size of the mirage unification scale and the threshold effects from integrating out the messenger fields from gauge mediation.

In addition, we see from Tables (6.17,6.18) that for both mSUGRA and DMM models the WMAP Preferred and WMAP7 bounds result in similar orderings of the most common patterns for a given light Higgs mass limit, but the pattern ordering is quite different for the WMAP upper bound. This cut preferentially selects patterns with light charginos, which include the Higgs LSP pattern and the chargino NLSP patterns. This result is expected since such patterns typically have LSPs with a significant fraction of wino and/or Higgsino components. For all dark matter cuts, increasing the bound on the lightest Higgs boson disfavors models with lighter scalars, which is also expected since the Higgs limit tends to require an increase in the third generation scalar masses.

For mSUGRA models with the 100 GeV Higgs bound, the WMAP Preferred and WMAP7 bounds lead to the same dominant patterns as the FLN cuts. Increasing the light Higgs mass bound to 114.4 GeV favors patterns with light charginos, neutralinos, and additional Higgs bosons, and

	Hierarchy				FLN Cuts
	1	2	3	4	mSUGRA
mSP					
mSP2'	$\lambda_1^0$	$\lambda_2^0$	$\chi_1^\pm$	$H, A$	10.9
mSP1'	$\lambda_1^0$	$\lambda_2^0$	$\chi_1^\pm$	$\chi_3^0$	9.3
mSP3'	$\lambda_1^0$	$\lambda_2^0$	$\chi_1^\pm$	$\tilde{\tau}_1$	2.8
mSP4' (mSP22)	$\lambda_1^0$	$\lambda_2^0$	$\chi_1^\pm$	$\tilde{g}$	1.4
	$\lambda_1^0$	$\lambda_2^0$	$\chi_3^0$	$\chi_1^\pm$	0.6
	$\lambda_1^0$	$\lambda_2^0$	$H, A$	$\chi_1^\pm$	0.1
	$\lambda_1^0$	$\lambda_2^0$	$\tilde{\tau}_1$	$\chi_1^\pm$	0.1
	$\lambda_1^0$	$\lambda_2^0$	$\chi_1^\pm$	$\tilde{t}_1$	0.1
mSP1	$\lambda_1^0$	$\chi_1^\pm$	$\chi_2^0$	$\chi_3^0$	17.0
mSP5	$\lambda_1^0$	$\tilde{\tau}_1$	$\tilde{\ell}_R$	$\tilde{\nu}_3$	20.1
mSP6'	$\lambda_1^0$	$\tilde{\tau}_1$	$\chi_2^0$	$\chi_1^\pm$	19.2
mSP7'	$\lambda_1^0$	$\tilde{\tau}_1$	$\tilde{\ell}_R$	$\chi_2^0$	3.8
mSP8	$\lambda_1^0$	$\tilde{\tau}_1$	$H, A$		2.9
mSP7	$\lambda_1^0$	$\tilde{\tau}_1$	$\tilde{\ell}_R$	$\chi_1^\pm$	0.4
mSP9	$\lambda_1^0$	$\tilde{\tau}_1$	$\tilde{\ell}_R$	$H, A$	0.3
mSP6	$\lambda_1^0$	$\tilde{\tau}_1$	$\chi_1^\pm$	$\chi_2^0$	0.1
	$\lambda_1^0$	$\tilde{\tau}_1$	$\tilde{t}_1$	$\chi_2^0$	0.1
	$\lambda_1^0$	$\tilde{\tau}_1$	$H, A$	$\chi_2^0$	0.1
mSP10	$\lambda_1^0$	$\tilde{\tau}_1$	$\tilde{t}_1$	$\tilde{\ell}_R$	0.1
mSP14	$\lambda_1^0$	$H, A$		$H^\pm$	3.7
mSP15'	$\lambda_1^0$	$H, A$		$\chi_2^0$	0.3
	$\lambda_1^0$	$H$	$\chi_2^0$	$A$	0.2
mSP16	$\lambda_1^0$	$H, A$		$\tilde{\tau}_1$	0.2
mSP11'	$\lambda_1^0$	$\tilde{t}_1$	$\chi_2^0$	$\chi_1^\pm$	4.5
mSP12'	$\lambda_1^0$	$\tilde{t}_1$	$\tilde{\tau}_1$	$\chi_2^0$	1.0
mSP13	$\lambda_1^0$	$\tilde{t}_1$	$\tilde{\tau}_1$	$\tilde{\ell}_R$	0.4
	$H, A$		$H^\pm$	$\chi_1^0$	0.1
	$H, A$		$\chi_1^0$	$H^\pm$	0.1

Table 6.16: **Hierarchy Patterns and Relative Percentages: FLN cuts.** The hierarchies of the four lightest non-SM states for mSUGRA models with cuts given in FLN [69].

slightly disfavors those with light sneutrinos, first/second generation sleptons, and stops. For the 114.4 GeV Higgs bound, the preferred patterns for the WMAP preferred and WMAP7 bounds are the same as in FLN, but with a different ordering in which models with light sleptons tend to be less dominant.

As seen in Table 6.17, when the weak Higgs bound is imposed the dominant hierarchy patterns are different from the FLN set. The Higgs LSP pattern, which is essentially negligible in mSUGRA models, is the most popular pattern in DMM models. This is also true for the WMAP upper bound as well as for an increased light Higgs mass bound. Table 6.18 shows that for the 114.4 GeV Higgs bound, the dominant patterns for the WMAP Preferred and WMAP7 bounds are identical but with a change in order.

The increased Higgs mass bound has a negligible effect on the Higgs LSP pattern, but it does reduce the number of allowed models for the other patterns. The most significant effect is for the mSP3 pattern, for which 55% of the model points that satisfy the 100 GeV Higgs mass bound are lost. The bound predominantly affects patterns in which the heavy CP odd Higgs boson  $A$  is in the lightest four non-SM particles, with 26% of the mSP2 patterns and 17% of the mSP2' patterns with  $A$  as the fourth-lightest state lost, as opposed to the mSP2 and mSP2' cases with  $H$  as the fourth-lightest state, for which 2.6% and 0.03% of the points are lost, respectively.

In summary, the most dominant DMM hierarchy patterns have minimal overlap with their mSUGRA counterparts. The dominant DMM pattern is the Higgs LSP pattern, for which the heavy Higgs particles are lighter than the LSP. For two other sets of dominant DMM patterns, the only difference in the lightest four non-SM particles is the ordering of the lightest chargino and the second-lightest neutralino as either the NLSP or the third-lightest particle. There are also DMM patterns in which the stau is the NLSP, which more closely resemble similar mSUGRA patterns. In the next section, we will study the typical DMM mass spectra within several of these dominant patterns, and when relevant, compare the outcome to analogous mSUGRA patterns.

Hierarchy					WMAP Preferred		WMAP 7-year		Upper Bound Only	
mSP	1	2	3	4	mSUGRA	DMM	mSUGRA	DMM	mSUGRA	DMM
mSP3'	$\chi_1^0$	$\chi_2^0$	$\chi_1^\pm$	$\tilde{\tau}_1$	3.1	7.1	3.0	8.4	2.1	3.1
mSP2'	$\chi_1^0$	$\chi_2^0$	$\chi_1^\pm$	$H,A$	10.3	6.8	11.0	7.5	11.4	1.6
mSP4'	$\chi_1^0$	$\chi_2^0$	$\chi_1^\pm$	$\tilde{g}$	1.8	1.7	1.8	2.0	1.2	0.5
	$\chi_1^0$	$\chi_2^0$	$\chi_1^\pm$	$\tilde{t}_1$	0.1	0.1	0.1	0.1	0.1	–
	$\chi_1^0$	$\chi_2^0$	$\chi_1^\pm$	$\tilde{\ell}_R$	–	0.1	–	0.1	–	–
mSP1'	$\chi_1^0$	$\chi_2^0$	$\chi_1^\pm$	$\chi_3^0$	9.7	–	9.9	–	8.4	–
	$\chi_1^0$	$\chi_2^0$	$\chi_3^0$	$\chi_1^\pm$	0.6	–	0.3	–	0.6	–
mSP3	$\chi_1^0$	$\chi_1^\pm$	$\chi_2^0$	$\tilde{\tau}_1$	0.3	12.6	0.1	14.2	–	22.9
mSP2	$\chi_1^0$	$\chi_1^\pm$	$\chi_2^0$	$H,A$	0.1	10.8	–	9.3	0.1	9.8
mSP4	$\chi_1^0$	$\chi_1^\pm$	$\chi_2^0$	$\tilde{g}$	–	3.8	–	3.6	–	12.9
	$\chi_1^0$	$\chi_1^\pm$	$\tilde{g}$	$\chi_2^0$	–	–	–	–	–	4.9
	$\chi_1^0$	$\chi_1^\pm$	$H,A$		–	0.8	–	0.6	–	3.4
	$\chi_1^0$	$\chi_1^\pm$	$\chi_2^0$	$\tilde{\ell}_R$	–	–	–	–	–	1.8
mSP1	$\chi_1^0$	$\chi_1^\pm$	$\chi_2^0$	$\chi_3^0$	16.5	3.7	15.0	4	35.2	2.3
	$\chi_1^0$	$\chi_1^\pm$	$\tilde{\ell}_R$	$\tilde{\tau}_1$	–	–	–	–	–	0.6
	$\chi_1^0$	$\chi_1^\pm$	$\tilde{g}$	$H,A$	–	–	–	–	–	0.5
	$\chi_1^0$	$\chi_1^\pm$	$\tilde{\tau}_1$	$\chi_2^0$	0.1	0.7	0.1	0.8	–	0.5
	$\chi_1^0$	$\chi_1^\pm$	$\tilde{\tau}_1$	$\tilde{\ell}_R$	–	0.5	–	0.5	–	0.9
	$\chi_1^0$	$\chi_1^\pm$	$\tilde{\ell}_R$	$\chi_2^0$	–	–	–	–	–	0.1
	$\chi_1^0$	$\chi_1^\pm$	$\chi_2^0$	$\tilde{t}_1$	–	0.8	–	0.9	–	1.0
	$\chi_1^0$	$\chi_1^\pm$	$\tilde{\tau}_1$	$H,A$	–	0.1	–	0.1	–	0.1
	$\chi_1^0$	$\chi_1^\pm$	$H,A$	$\chi_2^0$	–	0.1	–	0.1	–	0.2
mSP6'	$\chi_1^0$	$\tilde{\tau}_1$	$\chi_2^0$	$\chi_1^\pm$	19.7	5.8	21.0	6.7	15.4	2.7
mSP7'	$\chi_1^0$	$\tilde{\tau}_1$	$\tilde{\ell}_R$	$\chi_2^0$	4.8	2.7	4.4	3.2	3.7	1.3
mSP8	$\chi_1^0$	$\tilde{\tau}_1$	$H,A$		1.7	1.6	1.8	1.9	0.8	0.3
mSP7	$\chi_1^0$	$\tilde{\tau}_1$	$\tilde{\ell}_R$	$\chi_1^\pm$	1.3	2.8	1.5	3.3	0.2	1.0
mSP6	$\chi_1^0$	$\tilde{\tau}_1$	$\chi_1^\pm$	$\chi_2^0$	0.5	1.8	0.6	2.2	0.1	0.6
	$\chi_1^0$	$\tilde{\tau}_1$	$\chi_1^\pm$	$\tilde{\ell}_R$	–	0.7	–	0.7	–	0.4
mSP5	$\chi_1^0$	$\tilde{\tau}_1$	$\tilde{\ell}_R$	$\tilde{\nu}$	20.2	0.5	21.0	0.5	11.0	0.1
mSP9	$\chi_1^0$	$\tilde{\tau}_1$	$\chi_1^\pm$	$H,A$	–	0.1	–	0.2	–	0.1
	$\chi_1^0$	$\tilde{\tau}_1$	$\tilde{\ell}_R$	$H,A$	0.2	0.1	0.3	0.1	0.1	–
mSP14	$\chi_1^0$	$H,A$		$H^\pm$	1.9	1.5	1.8	1.5	1	0.7
	$\chi_1^0$	$H,A$		$\chi_1^\pm$	–	0.4	–	0.3	0.1	1.0
mSP15'	$\chi_1^0$	$H,A$		$\chi_2^0$	0.3	0.2	0.2	0.2	0.4	0.1
mSP16	$\chi_1^0$	$H,A$		$\tilde{\tau}_1$	0.1	0.1	–	0.1	–	–
	$\chi_1^0$	$\tilde{g}$	$\chi_1^\pm$	$\chi_2^0$	–	–	–	–	–	0.2
mSP11'	$\chi_1^0$	$\tilde{t}_1$	$\chi_2^0$	$\chi_1^\pm$	4.5	–	4.0	–	5.6	–
mSP12'	$\chi_1^0$	$\tilde{t}_1$	$\tilde{\tau}_1$	$\chi_2^0$	0.9	–	0.7	–	1.2	–
mSP13	$\chi_1^0$	$\tilde{t}_1$	$\tilde{\tau}_1$	$\tilde{\ell}_R$	0.5	–	0.5	–	0.7	–
	$H,A$		$H^\pm$	$\chi_1^0$	0.1	31.3	–	26.2	–	23.0
	$H,A$		$\chi_1^0$	$H^\pm$	–	0.6	–	0.5	–	1.0
	TOTAL				99.3	99.9	99.1	99.8	99.4	99.6

Table 6.17: **Hierarchy Patterns and Relative Percentages.** The hierarchies of the four lightest non-SM states, with some grouping of cases. The Higgs mass bound is  $m_h > 100$  GeV.

Hierarchy					WMAP Preferred		WMAP 7-year		Upper Bound Only	
mSP	1	2	3	4	mSUGRA	DMM	mSUGRA	DMM	mSUGRA	DMM
mSP3'	$\chi_1^0$	$\chi_2^0$	$\chi_1^\pm$	$\tilde{\tau}_1$	2.8	7.9	2.2	9.3	1.8	4.5
mSP2'	$\chi_1^0$	$\chi_2^0$	$\chi_1^\pm$	$H,A$	12.0	7.6	13.0	8.7	12.1	2.2
mSP4'	$\chi_1^0$	$\chi_2^0$	$\chi_1^\pm$	$\tilde{g}$	1.6	2.0	1.8	2.3	0.9	0.8
	$\chi_1^0$	$\chi_2^0$	$\chi_1^\pm$	$\tilde{t}_1$	0.2	0.1	0.1	0.1	–	–
mSP1'	$\chi_1^0$	$\chi_2^0$	$\chi_1^\pm$	$\tilde{\ell}_R$	–	0.1	–	0.1	–	–
	$\chi_1^0$	$\chi_2^0$	$\chi_1^\pm$	$\chi_3^0$	12.0	–	12.0	–	10.1	–
	$\chi_1^0$	$\chi_2^0$	$\chi_3^0$	$\chi_1^\pm$	0.8	–	0.4	–	0.7	–
mSP3	$\chi_1^0$	$\chi_1^\pm$	$\chi_2^0$	$\tilde{\tau}_1$	–	6.7	–	7.8	–	19.3
mSP2	$\chi_1^0$	$\chi_1^\pm$	$\chi_2^0$	$H,A$	–	11.7	–	10.5	0.1	10.4
mSP4	$\chi_1^0$	$\chi_1^\pm$	$\chi_2^0$	$\tilde{g}$	–	3.5	–	3.3	–	10.2
	$\chi_1^0$	$\chi_1^\pm$	$\tilde{g}$	$\chi_2^0$	–	–	–	–	–	3.0
mSP1	$\chi_1^0$	$\chi_1^\pm$	$H,A$	$\tilde{g}$	–	0.9	–	0.7	–	2.6
	$\chi_1^0$	$\chi_1^\pm$	$\chi_2^0$	$\tilde{\ell}_R$	–	–	–	–	–	2.5
	$\chi_1^0$	$\chi_1^\pm$	$\chi_2^0$	$\chi_3^0$	21.0	3.8	20.0	4.3	43.7	2.4
	$\chi_1^0$	$\chi_1^\pm$	$\tilde{\ell}_R$	$\tilde{\tau}_1$	–	–	–	–	–	0.7
	$\chi_1^0$	$\chi_1^\pm$	$\tilde{g}$	$H,A$	–	–	–	–	–	0.3
	$\chi_1^0$	$\chi_1^\pm$	$\tilde{\tau}_1$	$\chi_2^0$	–	0.6	–	0.7	–	0.3
	$\chi_1^0$	$\chi_1^\pm$	$\tilde{\tau}_1$	$\tilde{\ell}_R$	–	0.3	–	0.3	–	0.2
	$\chi_1^0$	$\chi_1^\pm$	$\tilde{\ell}_R$	$\chi_2^0$	–	–	–	–	–	0.1
	$\chi_1^0$	$\chi_1^\pm$	$\chi_2^0$	$\tilde{t}_1$	–	0.1	–	0.2	–	0.1
	$\chi_1^0$	$\chi_1^\pm$	$\tilde{\tau}_1$	$H,A$	–	0.1	–	–	–	0.1
$\chi_1^0$	$\chi_1^\pm$	$H,A$	$\chi_2^0$	–	0.1	–	–	–	0.1	
mSP6'	$\chi_1^0$	$\tilde{\tau}_1$	$\chi_2^0$	$\chi_1^\pm$	23.0	6.7	23.0	7.8	16.0	3.9
mSP7'	$\chi_1^0$	$\tilde{\tau}_1$	$\tilde{\ell}_R$	$\chi_2^0$	5.3	3.0	4.8	3.5	3.9	1.8
mSP8	$\chi_1^0$	$\tilde{\tau}_1$	$H,A$	$\chi_1^\pm$	1.9	1.8	2.2	2.4	0.8	0.4
mSP7	$\chi_1^0$	$\tilde{\tau}_1$	$\tilde{\ell}_R$	$\chi_1^\pm$	–	0.9	–	1.2	–	0.2
mSP6	$\chi_1^0$	$\tilde{\tau}_1$	$\chi_1^\pm$	$\chi_2^0$	–	0.6	–	0.8	–	0.2
	$\chi_1^0$	$\tilde{\tau}_1$	$\chi_1^\pm$	$\tilde{\ell}_R$	–	0.6	–	0.6	–	0.2
mSP5	$\chi_1^0$	$\tilde{\tau}_1$	$\tilde{\ell}_R$	$\tilde{\nu}$	14.0	0.3	15.0	0.3	5.7	0.1
	$\chi_1^0$	$\tilde{\tau}_1$	$\chi_1^\pm$	$H,A$	–	0.2	–	0.2	–	0.1
mSP9	$\chi_1^0$	$\tilde{\tau}_1$	$\tilde{\ell}_R$	$H,A$	0.3	0.1	0.4	0.1	0.1	–
mSP14	$\chi_1^0$	$H,A$	$H^\pm$	$\chi_1^\pm$	2.2	1.8	2.1	1.7	1.0	1.0
	$\chi_1^0$	$H,A$	$\chi_1^\pm$	$\chi_2^0$	–	0.4	0.2	0.3	–	0.7
mSP15'	$\chi_1^0$	$H,A$	$\chi_2^0$	$\chi_1^\pm$	0.4	0.2	0.2	0.2	0.5	0.1
mSP16	$\chi_1^0$	$H,A$	$\tilde{\tau}_1$	$\chi_1^\pm$	–	0.1	0.1	0.1	–	–
mSP11'	$\chi_1^0$	$\tilde{t}_1$	$\chi_2^0$	$\chi_1^\pm$	1.7	–	1.8	–	2.0	–
mSP12'	$\chi_1^0$	$\tilde{t}_1$	$\tilde{\tau}_1$	$\chi_2^0$	0.2	–	0.1	–	0.2	–
mSP13	$\chi_1^0$	$\tilde{t}_1$	$\tilde{\tau}_1$	$\tilde{\ell}_R$	–	–	–	–	–	–
	$H,A$	$H^\pm$	$\chi_1^0$	$H^\pm$	0.2	36.9	–	31.3	0.1	30.3
	$H,A$	$\chi_1^0$	$H^\pm$	$H^\pm$	–	0.7	–	0.6	–	0.8
	TOTAL				99.6	99.8	99.4	99.4	99.7	99.7

Table 6.18: **Hierarchy Patterns and Relative Percentages.** The hierarchies of the four lightest non-SM states, with some grouping of cases. The Higgs mass bound is  $m_h > 114.4$  GeV.

## 6.7 Focusing on DMM Hierarchy Patterns

In this section, we investigate the characteristic mass spectra of several of the most common DMM hierarchy patterns discussed in the previous section. Throughout, we will use the WMAP Preferred dark matter bounds and the stronger Higgs mass bound of  $m_h > 114.4$  GeV. We will first briefly discuss more generic features of several classes of hierarchy patterns and point out the similarities in their underlying DMM parameter space.

We start with the dependence on the gaugino mirage unification scale as given in Eqn. (6.13), where the gaugino mass parameters unify at one-loop. Although no new physics enters at the mirage unification scale, it has a strong impact on the gaugino mass ratios at low energies. In mSUGRA models, the unification of the gaugino masses arises at the GUT scale, leading to a very specific set of splittings between the gauginos at the TeV scale. However, the “deflected” mirage unification scale in DMM models can lead to very different mass splittings, which in turn has a strong impact on both dark matter and collider signatures.

To see this explicitly, in Fig. (6.3) we show the distribution of the mirage unification scale for four of the most common DMM hierarchy patterns discussed in the previous section: the Higgs LSP ( $H, A < H^\pm < \chi_1^0$ ), mSP6' ( $\chi_1^0 < \tilde{\tau}_1 < \chi_2^0 < \chi_1^\pm$ ), mSP2 ( $\chi_1^0 < \chi_1^\pm < \chi_2^0 < H, A$ ), and mSP3' ( $\chi_1^0 < \chi_2^0 < \chi_1^\pm < \tilde{\tau}_1$ ).<sup>\*\*</sup> The distribution of the mirage unification scale peaks at lower values and has a sharp cutoff at  $10^8$  GeV for the Higgs LSP and mSP2 patterns, as well as for the narrower peak of the mSP3' pattern. We will see that the relatively low typical value of the mirage unification scale for these patterns indicates a mass spectrum characterized by Higgsino-dominated and/or mixed-composition LSP's. The similar structure of the distributions also suggests that these patterns share similar phenomenological features that we will explore below in more detail. In contrast, the peak of the mSP6' distribution and the right peak of the mSP3' distribution have much higher values of the mirage unification scale, with the peak for the mSP6' pattern approaching the mSUGRA limit of  $M_G \sim 10^{16}$  GeV. Hence, in these cases the gaugino mass splittings are more similar to those

---

<sup>\*\*</sup>Although mSP2' is one of the common patterns we do not display the distributions for it, because it strongly resembles that of mSP2, and mSP3, which resembles mSP3' except that the large peak at higher values of the mirage unification scale is dramatically reduced.

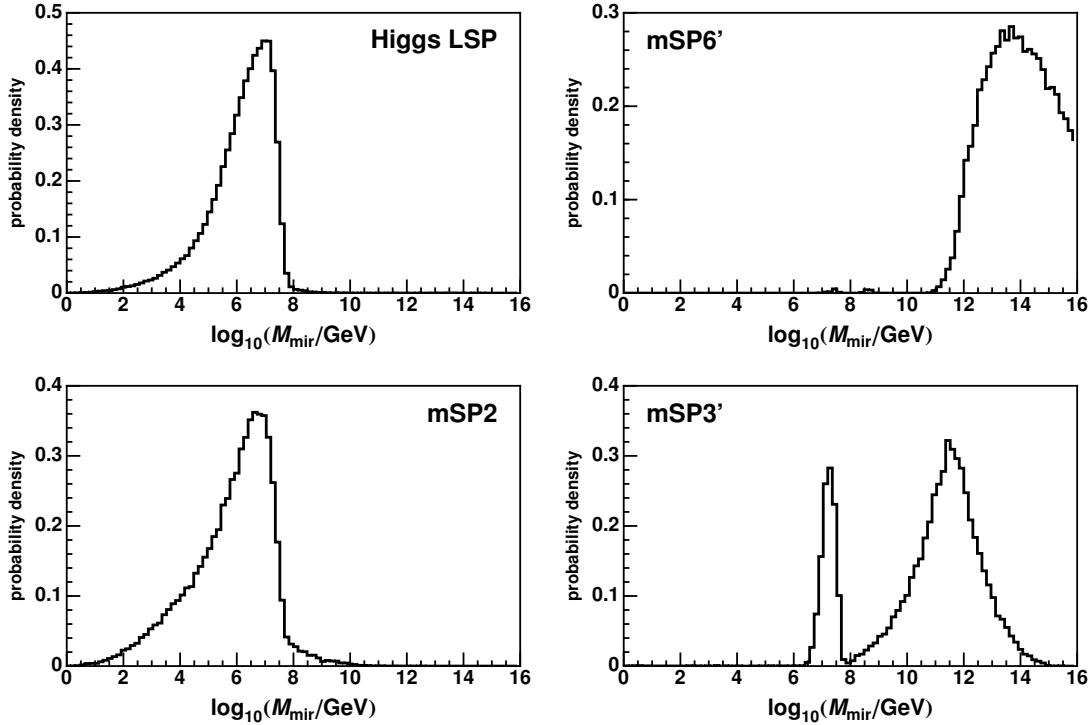


Figure 6.3: **Mirage unification scale.** Histograms of the gaugino sector mirage unification scale (in GeV) for the Higgs LSP (upper left panel), mSP6' (upper right panel), mSP2 (lower left panel) and mSP3' (lower right panel) patterns, with the WMAP Preferred dark matter constraints and  $m_h > 114.4$  GeV.

found in mSUGRA models, resulting in bino-dominated neutralino LSP's.

We will consider several patterns sequentially according to their mirage unification scales. With a rough grouping of patterns we also give less weight to the specific rankings of the hierarchy patterns obtained in our analysis which depend, for example, on the choice of priors. Rough grouping is also useful for the cases where lightest states are almost degenerate which makes classifying the LHC phenomenology difficult by just using the lightest four sparticles.

We will begin our analysis with the Higgs LSP pattern, then compare it to the mSP2 pattern, which also has a low mirage unification scale. We will then study the mSP3' pattern, which is a mixed pattern with both features. Finally, we will study the mSP6' pattern, and compare it to the mSUGRA expectations.

## 6.8 DMM Higgsino/mixed LSP patterns: Higgs LSP

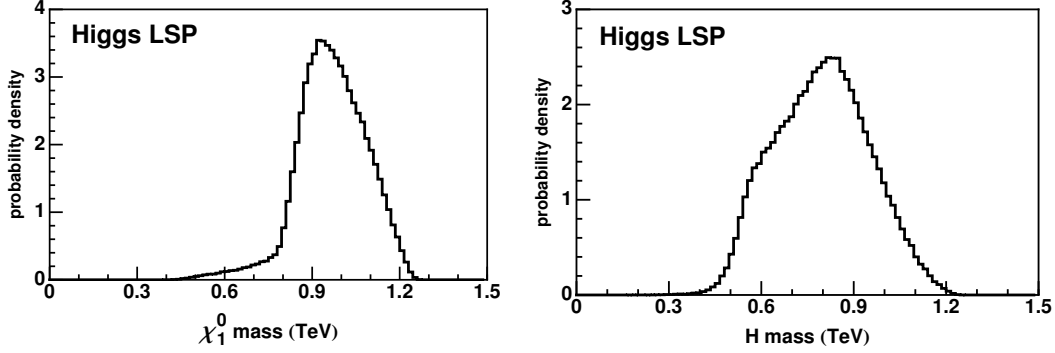


Figure 6.4: **Higgs LSP pattern:  $\chi_1^0$  mass and  $H$  mass.** Histograms of the mass of the neutralino LSP  $\chi_1^0$  (left panel) and the mass of the heavy Higgs  $H$  (right panel) for the Higgs LSP pattern, with the WMAP Preferred dark matter constraints and  $m_{h_1} > 114.4$  GeV.

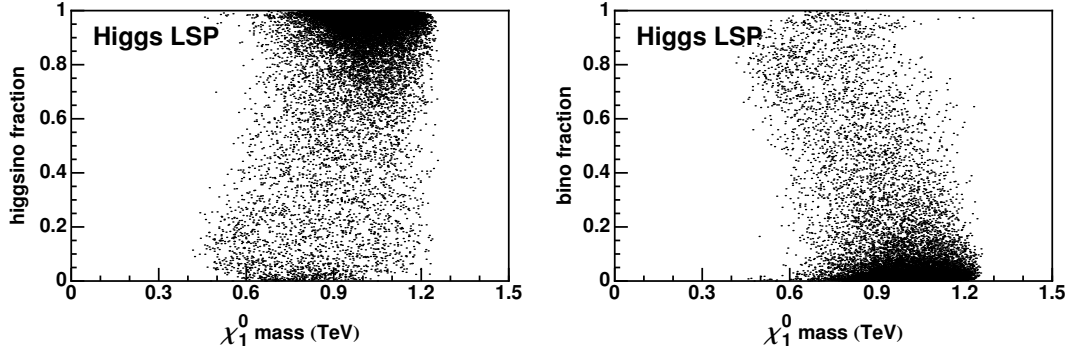


Figure 6.5: **Higgs LSP pattern: Higgsino and bino fraction.** Two-dimensional histograms of the Higgsino fraction (left panel) and bino fraction (right panel)  $\chi_1^0$  as a function of the  $\chi_1^0$  mass for the Higgs LSP pattern, with the WMAP Preferred dark matter constraints and  $m_{h_1} > 114.4$  GeV.

We begin with the Higgs LSP pattern ( $H, A < H^\pm < \chi_1^0$ ), since this pattern is the most dominant one once the dark matter constraints are taken into account, and because of the rarity of this pattern in mSUGRA. In Fig.(6.4), we show the distribution of the mass of the lightest neutralino  $\tilde{\chi}_1^0$  (the true LSP) and the heavy Higgs  $H$ . The heavy Higgses  $H, A$ , and  $H^\pm$  are strongly degenerate, with typical masses in the order of 800 GeV. We see that the heavy Higgs particles are not particularly light in the Higgs LSP pattern; these particles are lighter than the lightest neutralino simply because

$\tilde{\chi}_1^0$  is forced to be in the order of the TeV scale to satisfy the dark matter constraints.

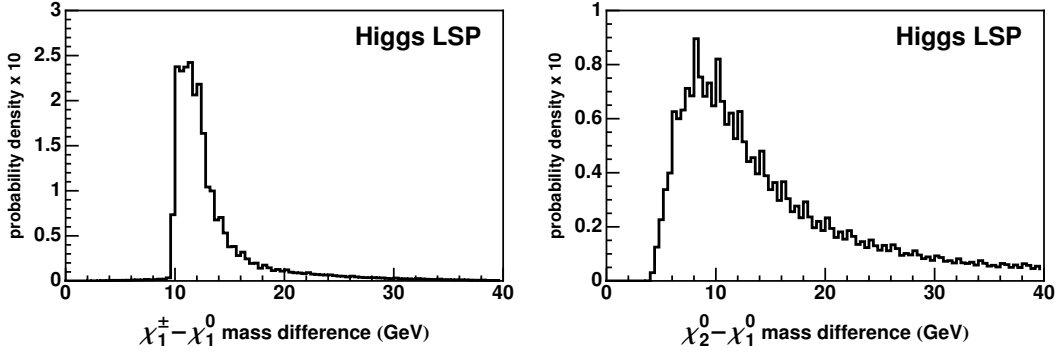


Figure 6.6: **Higgs LSP pattern:  $\chi_1^\pm - \chi_1^0$  and  $\chi_2^0 - \chi_1^0$  mass differences.** Histograms of the mass difference between  $\chi_1^\pm$  and  $\chi_1^0$  (left panel) and the mass difference between  $\chi_2^0$  and  $\chi_1^0$  (right panel) for the Higgs LSP pattern, with the WMAP Preferred dark matter constraints and  $m_h > 114.4$  GeV.

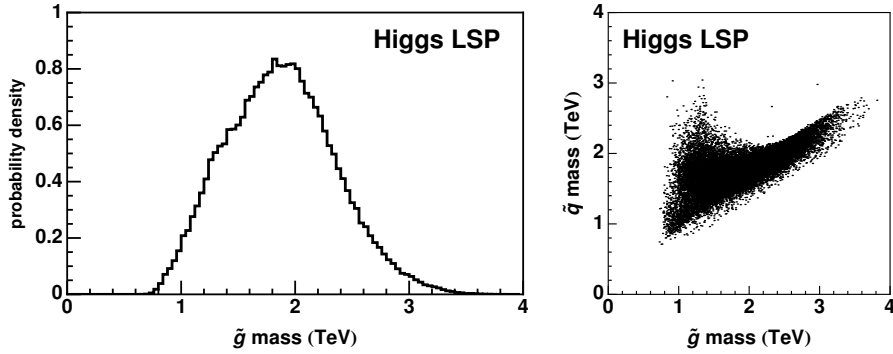


Figure 6.7: **Higgs LSP pattern: gluino and squark masses.** Histograms of the mass of the gluino (left panel) and the first generation squark versus gluino masses for the Higgs LSP pattern, with the WMAP Preferred dark matter constraints and  $m_h > 114.4$  GeV.

The Higgsino and bino fraction of  $\tilde{\chi}_1^0$  as a function of the mass of  $\tilde{\chi}_1^0$  is shown in Fig. (6.5). Clearly, this is a very common pattern in Higgsino-dominated LSP's with masses in the order of the TeV scale. As we will see, this type of neutralino LSP will be characteristic of all DMM patterns with mirage unification scales less than  $10^8$  GeV. In addition, the lightest chargino  $\tilde{\chi}_1^\pm$  and second-lightest neutralino  $\tilde{\chi}_2^0$  are very close in mass to  $\tilde{\chi}_1^0$ , with  $(m_{\tilde{\chi}_1^\pm} - m_{\tilde{\chi}_1^0})/m_{\tilde{\chi}_1^0} \sim 0.01$  and  $(m_{\tilde{\chi}_2^0} - m_{\tilde{\chi}_1^0})/m_{\tilde{\chi}_1^0} \sim 0.02$  on the average, as shown in Fig. (6.6).

We show the distribution of the gluino mass and the gluino versus lightest up-type squark

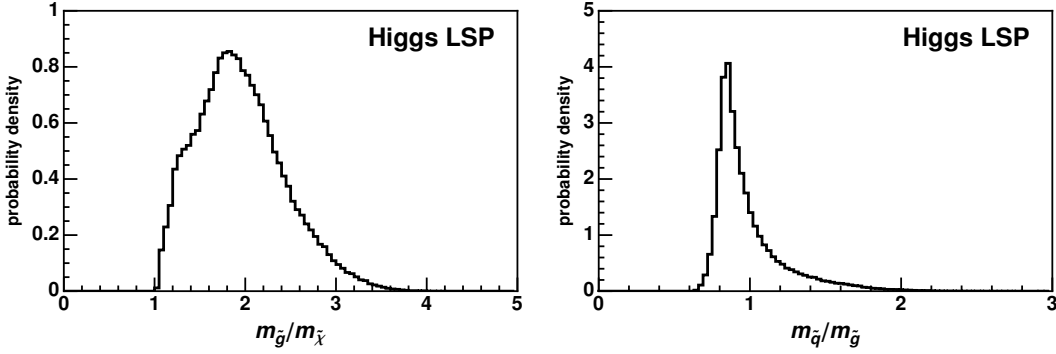


Figure 6.8: **Higgs LSP pattern: gluino/neutralino mass ratio and squark/gluino mass ratio.** One-dimensional histogram of the ratio of the gluino mass to the mass of the lightest neutralino (left panel) and the ratio of the first generation up-type squark mass to the gluino mass (right panel) for the Higgs LSP pattern, with the WMAP Preferred dark matter constraints and  $m_{H_t} > 114.4$  GeV.

masses in Fig. (6.7). We see that the gluino and the lighter generation squarks have masses in the order of 1-3 TeV. In Fig. (6.8), we show the ratio of the gluino mass to the mass of the lightest superpartner in the left panel, and the ratio of the first generation up-type squark mass to the gluino mass in the right panel. Note that the peak value of the gluino to neutralino mass ratio is about 2, as opposed to the much higher values found in mSUGRA because of the characteristic splitting of the low energy values of the three gaugino masses in minimal supergravity ( $M_1 : M_2 : M_3 \sim 1 : 2 : 6$ ). The first generation squark to gluino mass ratio distribution shown in Fig. (6.8) implies that the gluino and squarks are typically comparable in size. Overall, the spectrum is relatively heavy due to the need for a TeV-scale  $\tilde{\chi}_1^0$  in order to satisfy the relic density constraints, but quite compressed. This makes the light Higgs mass heavy enough to be above the 114.4 GeV mass bound. Relaxing the bound to 100 GeV does not change the number of viable models with this pattern, so it is quite robust with respect to this constraint.

## 6.9 DMM patterns: mSP2 and mSP3'

The mSP2 pattern has low peak values of the mirage unification scale, and hence it shares many common features with the Higgs LSP pattern. In Fig. (6.9), we show the masses of the neutralino LSP and the heavy Higgs boson  $H$  for the mSP2 pattern. We see that the LSP is again of order the

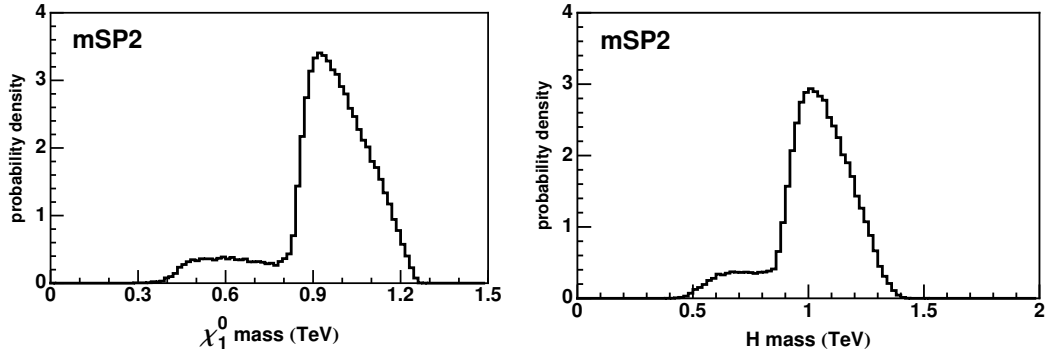


Figure 6.9: **mSP2 pattern:  $\chi_1^0$  mass and  $H$  mass.** Histograms of the mass of the neutralino LSP  $\tilde{\chi}_1^0$  (left panel) and the mass of the  $H$  boson (right panel) for the mSP2 pattern, with the WMAP Preferred dark matter constraints and  $m_h > 114.4$  GeV.

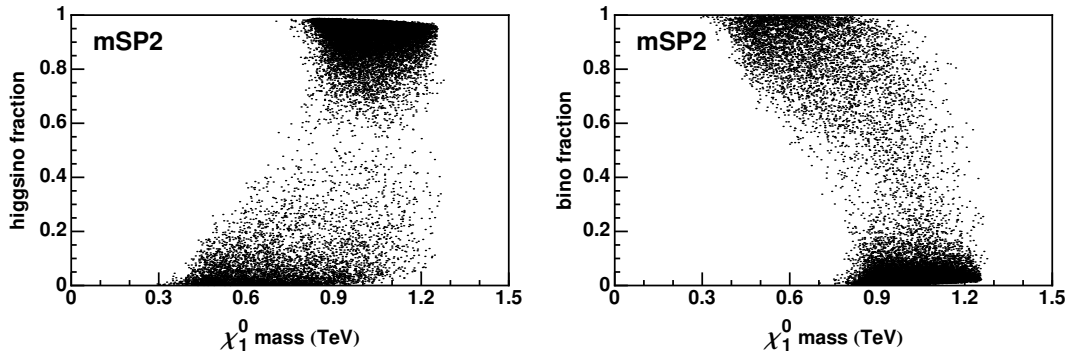


Figure 6.10: **mSP2 pattern: Higgsino and bino fraction.** Two-dimensional histograms of the Higgsino fraction (left panel) and bino fraction (right panel)  $\chi_1^0$  as a function of the  $\chi_1^0$  mass for the mSP2 pattern, with the WMAP Preferred dark matter constraints and  $m_h > 114.4$  GeV.

TeV scale, and that the heavy Higgses tend to be very close in mass to  $\tilde{\chi}_1^0$ . As shown in Fig. (6.10), the LSP is most typically Higgsino-dominated, with masses peaked at the TeV scale, though in this pattern there is a subset of models with a bino-dominated LSP that is correspondingly lighter. The spectrum is relatively heavy but compressed, similar to the Higgs LSP pattern. The lightest chargino and second-lightest neutralino are both highly degenerate with  $\chi_1^0$ , with  $(m_{\chi_1^\pm} - m_{\chi_1^0})/m_{\chi_1^0} \sim 0.02$  and  $(m_{\chi_2^0} - m_{\chi_1^0})/m_{\chi_1^0} \sim 0.03$ . Fig. (6.11) (which should be compared to Fig. (6.7)) shows that the gluino mass distribution tends to peak at higher values but has a sharp cutoff around 2.5 TeV. As seen in Fig. (6.12), the ratio of the gluino mass to the LSP mass and the

ratio of the first generation squark masses to the gluino mass are similar to that of the Higgs LSP pattern, as expected.

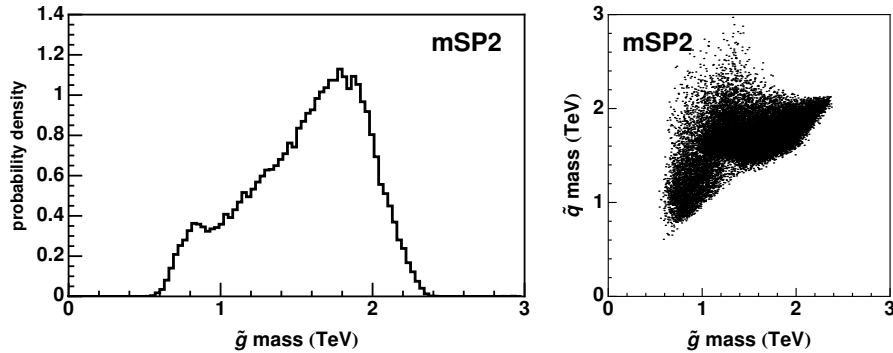


Figure 6.11: **mSP2 pattern: gluino and squark masses.** Histograms of the mass of the gluino (left panel) and the squark versus gluino masses (right panel) for the mSP2 pattern, with the WMAP Preferred dark matter constraints and  $m_h > 114.4$  GeV.

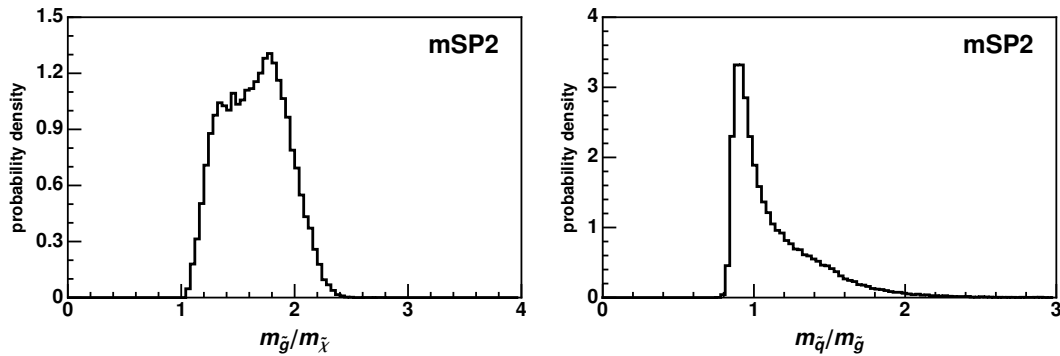


Figure 6.12: **mSP2 pattern: gluino/neutralino mass ratio and squark/gluino mass ratio.** Histograms of the ratio of the gluino mass to the mass of the lightest neutralino (left panel) and the ratio of the first generation up-type squark mass to the gluino mass (right panel) for the mSP2 pattern, with the WMAP Preferred dark matter constraints and  $m_h > 114.4$  GeV.

For the mSP3' pattern ( $\chi_1^0 < \chi_2^0 < \chi_1^\pm < \tilde{\tau}$ ), we see significant differences from the Higgs LSP and mSP2 patterns, which can also be expected from the peak values of the mirage scale as shown in Fig. (6.3). Recall that this pattern was dominated by higher values of the mirage unification scale, indicating that typical models in this category would more closely resemble mSUGRA models. We see from Fig. (6.13) that the LSP tends to be lighter than in the Higgs LSP and mSP2 patterns,

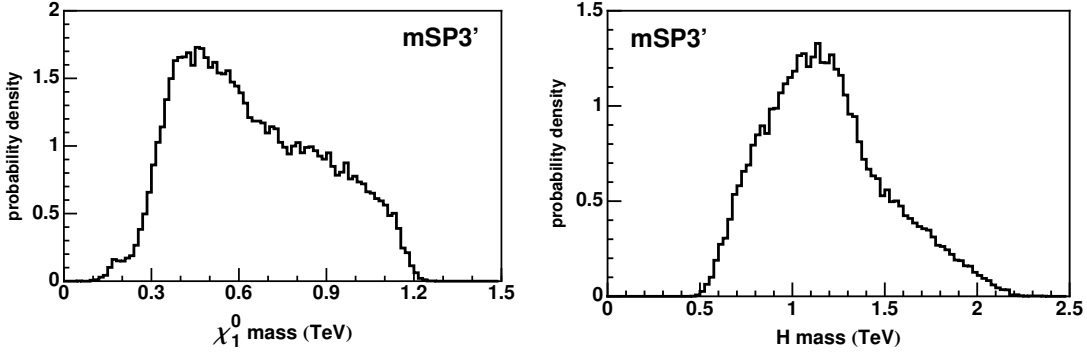


Figure 6.13: **mSP3' pattern:  $\chi_1^0$  mass and heavy Higgs mass.** Histograms of the mass of the neutralino LSP  $\chi_1^0$  (left panel) and the heavy Higgs boson mass (right panel) for the mSP3' pattern, with the WMAP Preferred dark matter constraints and  $m_h > 114.4$  GeV.

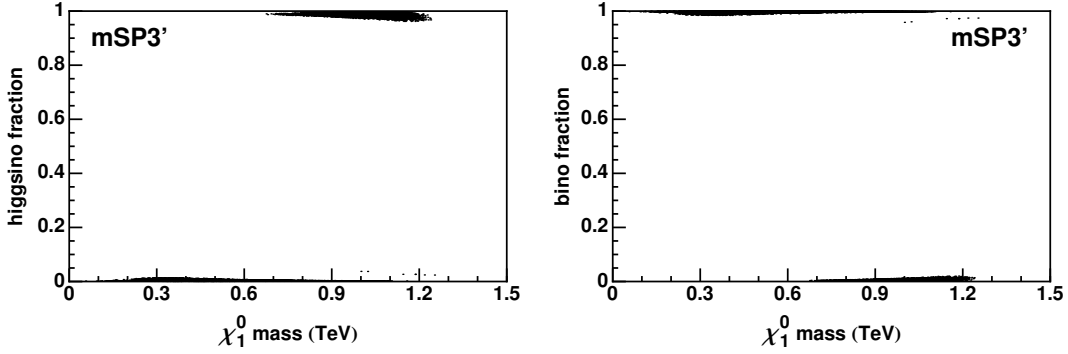


Figure 6.14: **mSP3' pattern: Higgsino and bino fraction.** Histograms of the Higgsino (left panel) and bino (right panel) fractions of  $\chi_1^0$  as a function of the  $\chi_1^0$  mass for the mSP3' pattern, with the WMAP Preferred dark matter constraints and  $m_h > 114.4$  GeV.

while the peak value of the heavy Higgs mass has shifted to higher values.

Fig. (6.14) demonstrates that the LSP is most often bino-dominated, with a subset of models with heavier LSP's that are Higgsino dominated. For this pattern,  $(m_{\chi_1^\pm} - m_{\chi_1^0})/m_{\chi_1^0}$  and  $(m_{\chi_2^0} - m_{\chi_1^0})/m_{\chi_1^0} \sim 0.26$  on average. The lightest chargino and the second-lightest neutralino are typically quite degenerate, since for the majority of models there is a bino-like  $\chi_1^0$  and a nearly degenerate wino-like pair  $\chi_1^\pm, \chi_2^0$ , as is often the case in mSUGRA models.

The distributions of the gluino and squark masses are shown in Fig. (6.15), and the  $m_{\tilde{g}}/m_{\chi_1^0}$ , and  $m_{\tilde{q}}/m_{\tilde{g}}$  distributions are shown in Fig. (6.16). Both distributions feature two peaks, with the

dominant peak of the gluino mass distribution being at lower values than that of mSP2. The squark to gluino mass ratio has two peaks at  $\sim 1$  while the ratio of the gluino to LSP masses peaks at  $\sim 3$ , representing a shift toward mSUGRA-like features. The one sharp peak at  $m_{\tilde{q}}/m_{\tilde{g}} < 1$  corresponds to the low mirage scale behavior found also in the mSP2 case, but there is also a much larger peak at higher values that corresponds to models with a high mirage unification scale.

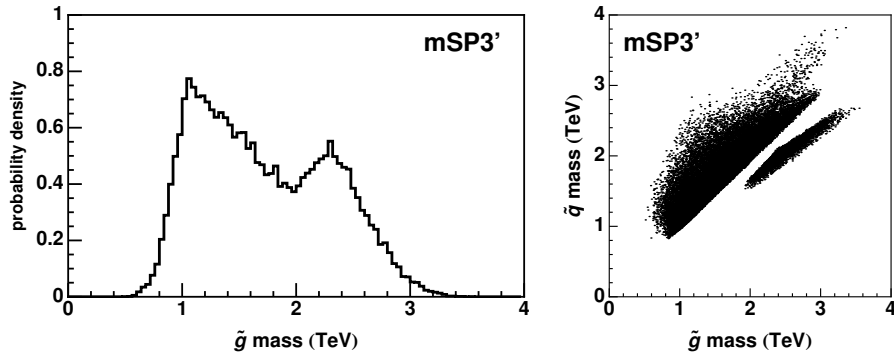


Figure 6.15: **mSP3' pattern: gluino and squark mass distributions.** Histograms of the gluino mass (left panel) and the squark versus gluino (right panel) for the mSP3' pattern, with the WMAP Preferred dark matter constraints and  $m_h > 114.4$  GeV.

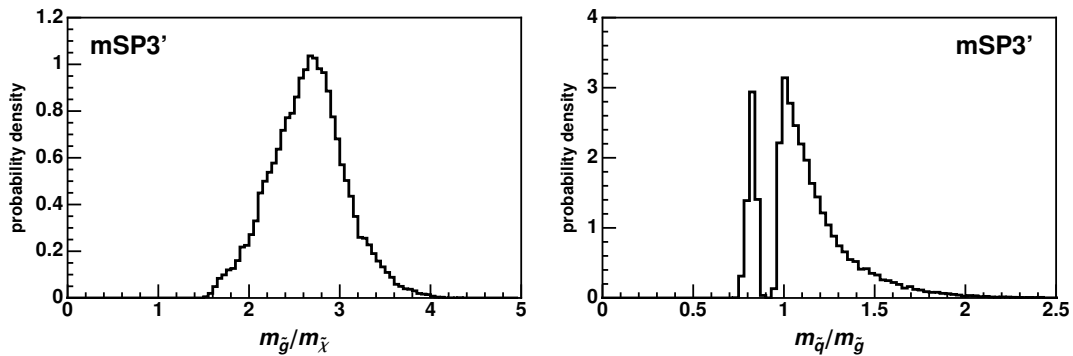


Figure 6.16: **mSP3' pattern: gluino/LSP mass ratio and squark/gluino mass ratio.** Histograms of the ratio of the mass of the gluino to the LSP mass (left panel) and the ratio of the first generation up-type squark mass to the gluino mass (right panel) for the mSP3' pattern, with the WMAP Preferred dark matter constraints and  $m_h > 114.4$  GeV.

## 6.10 mSUGRA-like DMM patterns: mSP6'

The final DMM hierarchy pattern we will consider is the mSP6' pattern, in which the NLSP is the lightest stau. As we will see, this pattern is similar to the typical hierarchy patterns found in mSUGRA models (significantly more so than the DMM mSP3' pattern described in the previous section), though the spectrum will once again exhibit the compressed features that are characteristic of DMM models.

We begin by showing the distribution of the LSP mass and the bino fraction of the LSP as a function of its mass, which are given in Fig. (6.17). This pattern is characterized by a bino-dominated LSP that is correspondingly much lighter than the Higgsino-dominated neutralino LSP's found in the Higgs LSP pattern and the mSP2 pattern. In fact, the mass pattern of the charginos and neutralinos very much resembles that of standard minimal supergravity, with the lowest mass state given by bino-like LSP and the next lightest states in the electroweak chargino/neutralino sector consisting of degenerate wino-like pair consisting of  $\chi_2^0$  and  $\chi_1^\pm$ . The splitting of the  $\chi_1^0$  mass compared to the  $\chi_1^\pm$  and  $\chi_2^0$  is more substantial for this pattern, with both  $(m_{\chi_1^\pm} - m_{\chi_1^0})/m_{\chi_1^0}$  and  $(m_{\chi_2^0} - m_{\chi_1^0})/m_{\chi_1^0} \sim 0.6$  on average.

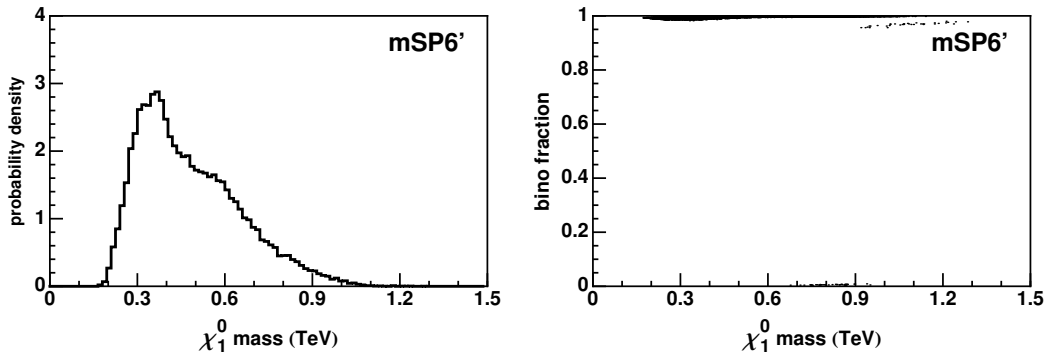


Figure 6.17: **mSP6' pattern:  $\chi_1^0$  mass and bino fraction.** Histograms of the mass of the neutralino LSP  $\chi_1^0$  (left panel) and the bino fraction of  $\chi_1^0$  as a function of the LSP mass (right panel) for the mSP6' pattern, with the WMAP Preferred dark matter constraints and  $m_h > 114.4$  GeV.

The spectrum of the mSP6' pattern is less compressed on the average than the other DMM pattern considered. In Figs. (6.18 and 6.19), we plot histograms of the gluino mass (upper left

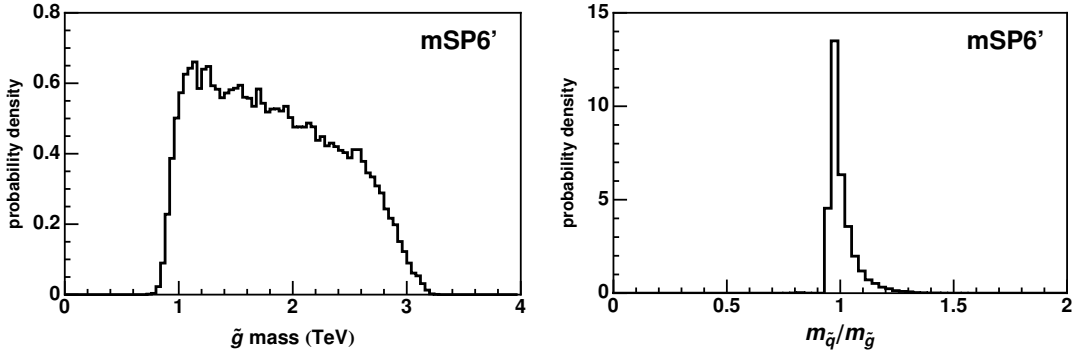


Figure 6.18: **mSP6' pattern: gluino mass and  $m_{\tilde{q}}/m_{\tilde{g}}$  distributions.** Histograms for the mSP6' of the gluino mass (left panel) and the ratio of the first generation squark mass to the gluino mass (right panel), with the WMAP Preferred bounds and  $m_h > 114.4$  GeV.

panel) and the ratio of the gluino mass to the LSP mass as well as the ratio of the typical first generation squark mass to the gluino mass. The  $m_{\tilde{g}}/m_{\chi_1^0}$  distribution is peaked at significantly larger values than the other DMM patterns, which is as expected since the mSP6' pattern favors high values of the mirage unification scale. For the purposes of comparison, the gluino to LSP mass ratio for the analogous mSP6' pattern in mSUGRA models is also shown in Fig. (6.19), which indicates that this ratio is peaked at still higher values in minimal supergravity. The ratio of the squark to gluino masses in the DMM mSP6' pattern, in contrast, is very sharply peaked at  $m_{\tilde{q}}/m_{\tilde{g}} \sim 1$ , indicating that on average the first generation squark and gluino masses tend to be clustered and significantly heavier than the LSP.

## 6.11 Summary

In this chapter we studied the phenomenology of deflected mirage mediation, a string-motivated scenario involving comparable contributions to supersymmetry breaking from gravity, anomaly and gauge mediation. We first focused on the implications for LHC physics between deflected mirage mediation and pure mirage mediation, which includes gravity and anomaly mediation, but not gauge mediation. We generated benchmark points with similar gaugino mass unification scale in both frameworks. We also studied the effects of turning on the gauge mediation starting

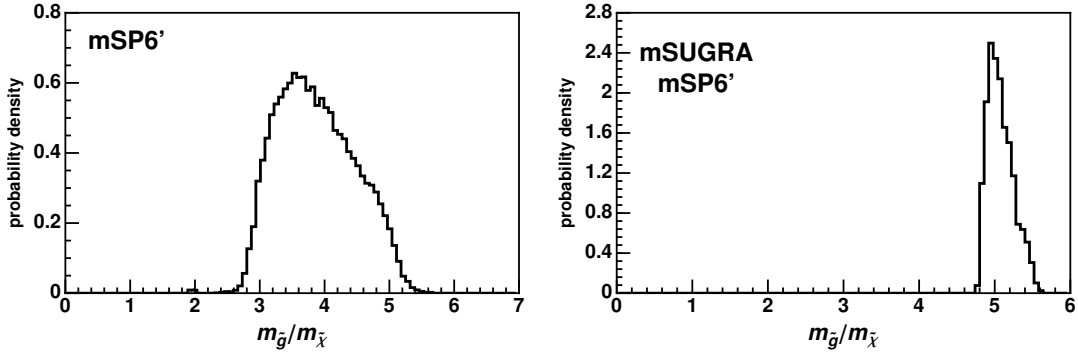


Figure 6.19: **mSP6' pattern:  $m_{\tilde{g}}/m_{\chi_1^0}$  and comparisons with mSUGRA.** Histograms for the mSP6' of the the ratio of the gluino mass to the LSP mass in DMM (left panel) and in mSUGRA (right panel), with the WMAP Preferred bounds and  $m_h > 114.4$  GeV.

from pure mirage mediation scenarios.

The results show that there is a broad variety of phenomenological outcomes within deflected mirage mediation, depending on the messenger scale and the size of the threshold effects from gauge mediation. One interesting class of examples have a deflected gaugino mirage unification scale at TeV energies, leading to a squeezed spectrum in which the gluino can be the lightest colored superpartner, which in turn results in LHC signals with softer jets and leptons than in standard MSSM models. The effects of gauge mediation can also have a large impact on the total superpartner production cross section, in some cases by several orders of magnitude. We see that for the deflected mirage mediation examples studied here, the most robust discovery mode will be the multijet channel.

Next we have used the hierarchy of mass eigenstates for the superpartners as an organizing principle, and investigated the landscape of these hierarchies for both the mSUGRA and DMM frameworks. We generate a very large data set of mSUGRA and DMM models, and apply progressive cuts motivated by phenomenology: radiative electroweak symmetry breaking, a neutral lightest superpartner that can be a dark matter candidate, direct search limits on superpartner masses and indirect limits from rare processes. We show that if we impose a strict dark matter constraint, there is no overlap between the five most populated hierarchies in mSUGRA with the six most populated hierarchies in deflected mirage mediation. These hierarchies account for 77.5%

of all DMM models when the WMAP Preferred constraint of (6.25) is imposed.

We also studied the distributions of various masses relevant to the collider phenomenology within the top 6 hierarchy patterns, namely Higgs LSP, mSP2, mSP2', mSP3, mSP3' and mSP6'. One interesting observation is that the Higgs LSP pattern appears to dominate the parameter space of DMM, in contrast it appears very rarely in the mSUGRA framework.

## Chapter 7

### Conclusions

In this thesis, we focused on the collider phenomenology of supersymmetry, one of the best motivated candidate for beyond the Standard Model physics. The analyses presented were carried out in the framework of mSUGRA, mirage mediation and deflected mirage mediation. We summarize the main conclusions below.

- In Chapter 4, we studied the SUSY discovery potential of the early LHC run at 7 GeV center of mass energy with up to  $2 \text{ fb}^{-1}$  of data. As a first step we worked on generating a good representation of the Standard Model background at the LHC which is generally consistent with a previous study [31]. We then looked into mSUGRA and nonuniversal mSUGRA frameworks with a nonuniversality in the gaugino sector. Specifically we analyzed the LHC reach in the mSUGRA framework and showed a reach of  $m_{1/2} \approx 400 \text{ GeV}$  (for low  $m_0$ ) and  $m_0 \approx 2000 \text{ GeV}$  (for low  $m_{1/2}$ ) is possible within the first inverse femtobarn of data. We then studied nonuniversal mSUGRA and generated the benchmark models given in Table (4.4) satisfying both the theoretical and the experimental constraints. These benchmark models are grouped according to their next to lightest sparticles and represent different phenomenological properties which can be studied further for the early detection of supersymmetry at the LHC as well as in direct detection experiments of dark matter.
- In Chapter 5, we asked ourself what is the most important information that would be useful to a high energy theorist interested in connecting the supersymmetric physics at the LHC to physics at an even higher energy scale, such as some underlying string theory. We believe the most important information is the question of gaugino mass universality. We developed statistical methods that will let us choose the best signatures to resolve the amount of non-universality in the gaugino sector for a model following the mirage pattern of gaugino

masses. Our results concluded that up to a 30% non-universality is resolvable after just one year of LHC data.

- In Chapter 6 we studied the phenomenology of deflected mirage mediation, a string-motivated scenario involving comparable contributions to supersymmetry breaking from gravity, anomaly and gauge mediation. We first focused on the implications for LHC physics between deflected mirage mediation and pure mirage mediation, which includes gravity and anomaly mediation, but not gauge mediation. We generated benchmark points with similar gaugino mass unification scale in both frameworks. We also studied the effects of turning on the gauge mediation starting from pure mirage mediation scenarios.

The results show that there is a broad variety of phenomenological outcomes within deflected mirage mediation, depending on the messenger scale and the size of the threshold effects from gauge mediation. One interesting class of examples have a deflected gaugino mirage unification scale at TeV energies, leading to a squeezed spectrum in which the gluino can be the lightest colored superpartner, which in turn results in LHC signals with softer jets and leptons than in standard MSSM models. The effects of gauge mediation can also have a large impact on the total superpartner production cross section, in some cases by several orders of magnitude. We see that for the deflected mirage mediation examples studied here, the most robust discovery mode will be the multijet channel.

Next we have used the hierarchy of mass eigenstates for the superpartners as an organizing principle, and investigated the landscape of these hierarchies for both the mSUGRA and DMM frameworks. We generate a very large data set of mSUGRA and DMM models, and apply progressive cuts motivated by phenomenology: radiative electroweak symmetry breaking, a neutral lightest superpartner that can be a dark matter candidate, direct search limits on superpartner masses and indirect limits from rare processes. We show that if we impose a strict dark matter constraint, there is no overlap between the five most populated hierarchies in mSUGRA with the six most populated hierarchies in deflected mirage mediation. These hierarchies account for 77.5% of all DMM models when the WMAP Preferred constraint of (6.25) is imposed.

We also studied the distributions of various masses relevant to the collider phenomenology within the top 6 hierarchy patterns, namely Higgs LSP, mSP2, mSP2', mSP3, mSP3' and mSP6'. One interesting observation is that the Higgs LSP pattern appears to dominate the parameter space of DMM, in contrast it appears very rarely in the mSUGRA framework.

## Appendix A

### Benchmark models for early discovery of SUSY at the LHC

Here we display the spectra of the selected benchmark models.

Label	C1	C2	C3	C4	C5	G1	G2	G3	G4	G5	G6
NLSP	$\chi_1^\pm$	$\chi_1^\pm$	$\chi_1^\pm$	$\chi_1^\pm$	$\chi_1^\pm$	$\tilde{g}$	$\tilde{g}$	$\tilde{g}$	$\tilde{g}$	$\tilde{g}$	$\tilde{g}$
$\sigma_{\text{SUSY}}$ (pb)	24.3	2.4	14.8	11.3	3.5	2.2	24.2	3.1	5.8	19.4	3.7
$\mu$	145	345	239	231	489	480	314	523	434	324	539
$m_{\tilde{N}_1}$	103	130	140	171	123	327	256	270	283	275	328
$m_{\tilde{N}_2}$	157	151	189	240	146	485	324	522	439	333	541
$m_{\tilde{C}_1^\pm}$	141	150	183	229	145	480	316	520	435	326	539
$m_{\tilde{\tau}_1}$	1463	441	1318	1170	260	1079	2155	1542	1475	1719	1311
$m_{\tilde{t}_1}$	922	560	828	621	402	612	1145	1115	1048	1054	863
$m_{\tilde{g}}$	316	698	341	354	680	452	314	432	393	325	421

Label	H1	S1	S2	S3	S4	S5	S6	S7	T1	T2
NLSP	$A^0$	$\tilde{\tau}_1$	$\tilde{t}_1$	$\tilde{t}_1$						
$\sigma_{\text{SUSY}}$ (pb)	0.3	1.4	0.4	0.5	0.6	0.4	2.0	0.2	2.3	3.8
$\mu$	630	425	426	301	393	443	388	432	1213	691
$m_{\tilde{N}_1}$	297	157	181	188	241	280	159	211	232	324
$m_{\tilde{N}_2}$	630	198	408	303	395	415	189	408	508	689
$m_{\tilde{C}_1^\pm}$	629	198	405	295	390	409	187	406	508	687
$m_{\tilde{\tau}_1}$	1456	167	194	192	248	289	176	221	1546	1436
$m_{\tilde{t}_1}$	1032	541	504	529	329	506	497	615	258	357
$m_{\tilde{g}}$	594	771	835	817	834	817	709	913	532	422

Table A.1: An exhibition of the light sparticles for the benchmarks given. These benchmarks are listed in Table (4.4). All masses are given in GeV.

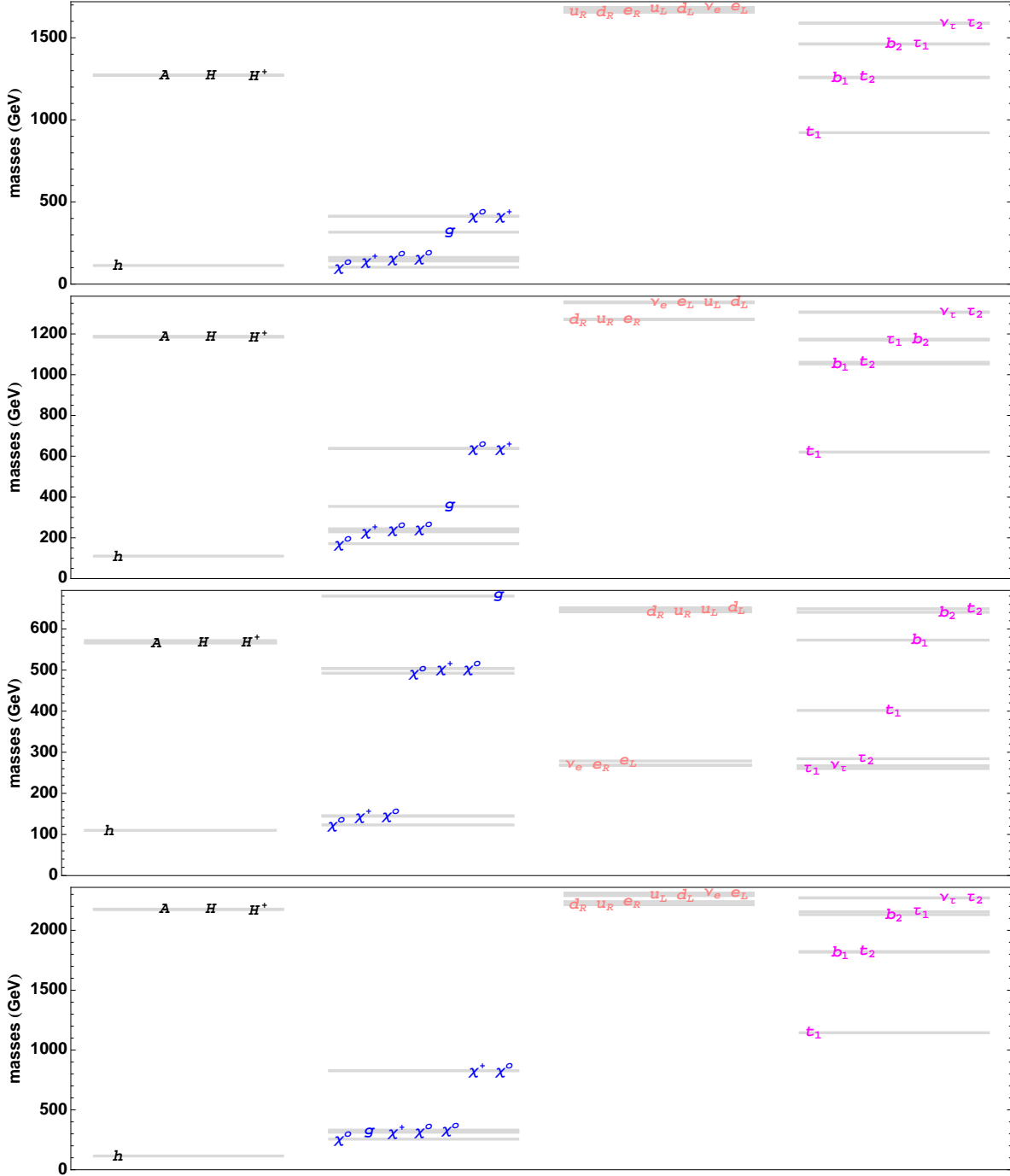


Figure A.1: Spectrum of the benchmark models C1, C4, C5, G2. In each column masses increase from left to right.

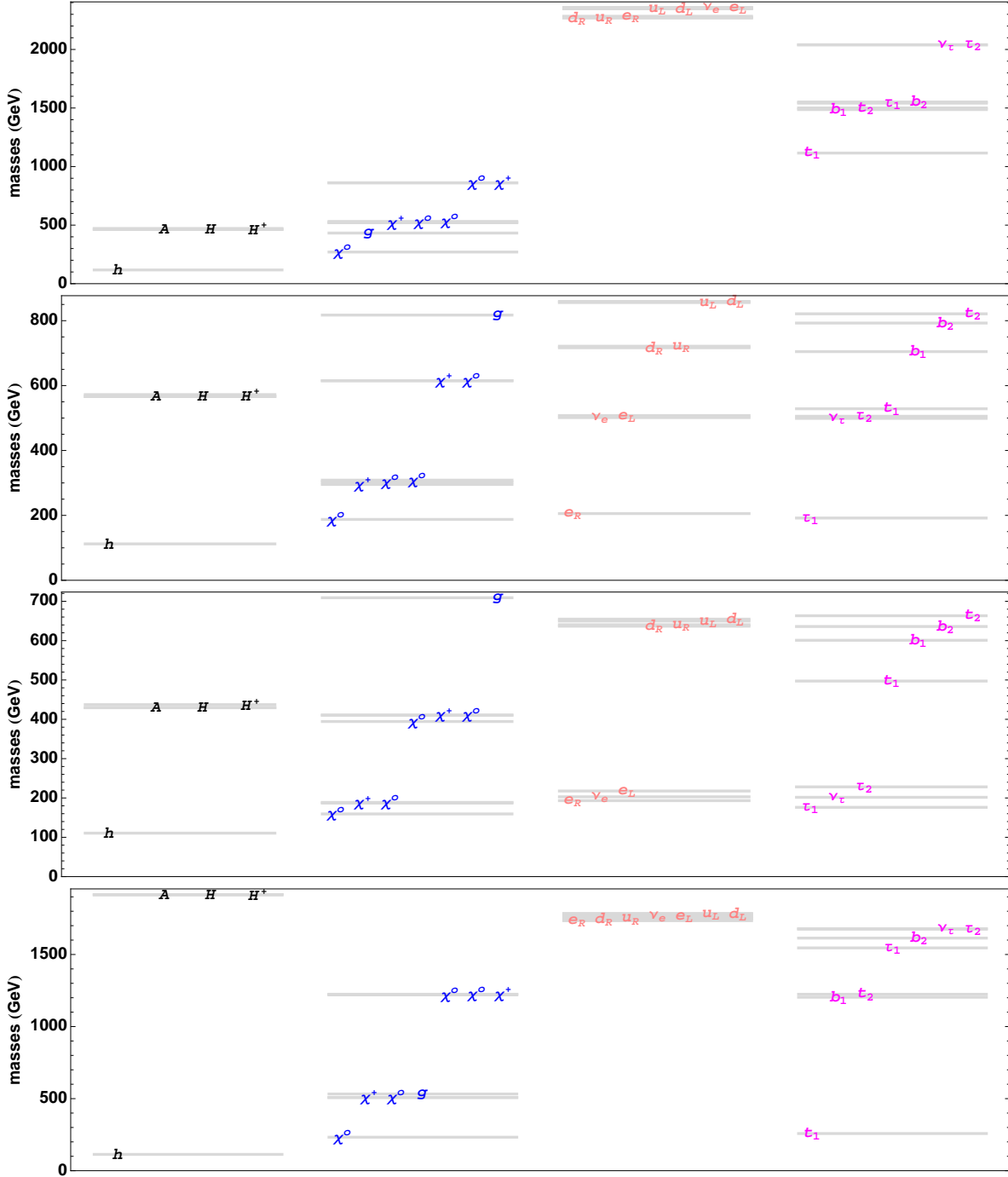


Figure A.2: Spectrum of the benchmark models: G3, S3, S6, T1. In each column masses increase from left to right.

## Appendix B

### Anomalous dimensions in the DMM framework

At one loop, the anomalous dimensions are given by

$$\gamma_i = 2 \sum_a g_a^2 c_a(\Phi_i) - \frac{1}{2} \sum_{lm} |y_{ilm}|^2, \quad (\text{B.1})$$

in which  $c_a$  is the quadratic Casimir, and  $y_{ilm}$  are the normalized Yukawa couplings. Here we will consider only the Yukawa couplings of the third generation  $y_t$ ,  $y_b$ , and  $y_\tau$ . For the MSSM fields  $Q$ ,  $U^c$ ,  $D^c$ ,  $L$ ,  $E^c$ ,  $H_u$  and  $H_d$ , the anomalous dimensions are

$$\begin{aligned} \gamma_{Q,i} &= \frac{8}{3}g_3^2 + \frac{3}{2}g_2^2 + \frac{1}{30}g_1^2 - (y_t^2 + y_b^2)\delta_{i3} \\ \gamma_{U,i} &= \frac{8}{3}g_3^2 + \frac{8}{15}g_1^2 - 2y_t^2\delta_{i3}, \quad \gamma_{D,i} = \frac{8}{3}g_3^2 + \frac{2}{15}g_1^2 - 2y_b^2\delta_{i3}, \\ \gamma_{L,i} &= \frac{3}{2}g_2^2 + \frac{3}{10}g_1^2 - y_\tau^2\delta_{i3}, \quad \gamma_{E,i} = \frac{6}{5}g_1^2 - 2y_\tau^2\delta_{i3}, \\ \gamma_{H_u} &= \frac{3}{2}g_2^2 + \frac{3}{10}g_1^2 - 3y_t^2, \quad \gamma_{H_d} = \frac{3}{2}g_2^2 + \frac{3}{10}g_1^2 - 3y_b^2 - y_\tau^2, \end{aligned} \quad (\text{B.2})$$

respectively. Above  $M_{\text{mess}}$ , the beta function of the gauge couplings changes because of the messenger fields. However,  $\gamma_i$  does not change according to Eq. (B.1), and hence  $\gamma'_i = \gamma_i$ . The  $\gamma'_i$ 's are given by the expression

$$\gamma'_i = 2 \sum_a g_a^4 b_a c_a(\Phi_i) - \sum_{lm} |y_{ilm}|^2 b_{y_{ilm}}, \quad (\text{B.3})$$

in which  $b_{y_{ilm}}$  is the beta function for the Yukawa coupling  $y_{ilm}$ . The  $\gamma_i$ 's are given by

$$\begin{aligned}
\dot{\gamma}_{Q,i} &= \frac{8}{3}b_3g_3^4 + \frac{3}{2}b_2g_2^4 + \frac{1}{30}b_1g_1^4 - (y_t^2b_t + y_b^2b_b)\delta_{i3} \\
\dot{\gamma}_{U,i} &= \frac{8}{3}b_3g_3^4 + \frac{8}{15}b_1g_1^4 - 2y_t^2b_t\delta_{i3}, \quad \dot{\gamma}_{D,i} = \frac{8}{3}b_3g_3^4 + \frac{2}{15}b_1g_1^4 - 2y_b^2b_b\delta_{i3} \\
\dot{\gamma}_{L,i} &= \frac{3}{2}b_2g_2^4 + \frac{3}{10}b_1g_1^4 - y_\tau^2b_\tau\delta_{i3}, \quad \dot{\gamma}_{E,i} = \frac{6}{5}b_1g_1^4 - 2y_\tau^2b_\tau\delta_{i3} \\
\dot{\gamma}_{H_u} &= \frac{3}{2}b_2g_2^4 + \frac{3}{10}b_1g_1^4 - 3y_t^2b_t, \quad \dot{\gamma}_{H_d} = \frac{3}{2}b_2g_2^4 + \frac{3}{10}b_1g_1^4 - 3y_b^2b_b - y_\tau^2b_\tau,
\end{aligned} \tag{B.4}$$

where  $b_t = 6y_t^2 + y_b^2 - \frac{16}{3}g_3^2 - 3g_2^2 - \frac{13}{15}g_1^2$ ,  $b_b = y_t^2 + 6y_b^2 + y_\tau^2 - \frac{16}{3}g_3^2 - 3g_2^2 - \frac{7}{15}g_1^2$  and  $b_\tau = 3y_b^2 + 4y_\tau^2 - 3g_2^2 - \frac{9}{5}g_1^2$ .  $\dot{\gamma}'_i$  is obtained by replacing  $b_a$  with  $b'_a = b_a + N$  in Eq. (B.4).

Finally,  $\theta_i$ , which appears in the mixed modulus-anomaly term in the soft scalar mass-squared parameters, is given by

$$\theta_i = 4 \sum_a g_a^2 c_a(Q_i) - \sum_{i,j,k} |y_{ijk}|^2 (3 - n_i - n_j - n_k). \tag{B.5}$$

For the MSSM fields, they take the form

$$\begin{aligned}
\theta_{Q,i} &= \frac{16}{3}g_3^2 + 3g_2^2 + \frac{1}{15}g_1^2 - 2(y_t^2(3 - n_{H_u} - n_Q - n_U) + y_b^2(3 - n_{H_d} - n_Q - n_D))\delta_{i3}, \\
\theta_{U,i} &= \frac{16}{3}g_3^2 + \frac{16}{15}g_1^2 - 4y_t^2(3 - n_{H_u} - n_Q - n_U)\delta_{i3} \\
\theta_{D,i} &= \frac{16}{3}g_3^2 + \frac{4}{15}g_1^2 - 4y_b^2(3 - n_{H_d} - n_Q - n_D)\delta_{i3}, \\
\theta_{L,i} &= 3g_2^2 + \frac{3}{5}g_1^2 - 2y_\tau^2(3 - n_{H_d} - n_L - n_E)\delta_{i3} \\
\theta_{E,i} &= \frac{12}{5}g_1^2 - 4y_\tau^2(3 - n_{H_d} - n_L - n_E)\delta_{i3}, \\
\theta_{H_u} &= 3g_2^2 + \frac{3}{5}g_1^2 - 6y_t^2(3 - n_{H_u} - n_Q - n_U) \\
\theta_{H_d} &= 3g_2^2 + \frac{3}{5}g_1^2 - 6y_b^2(3 - n_{H_d} - n_Q - n_D) - 2y_\tau^2(3 - n_{H_d} - n_L - n_E).
\end{aligned} \tag{B.6}$$

As in the case of  $\gamma_i$ ,  $\theta'_i$  is the same as  $\theta_i$ .

## Bibliography

- [1] B. Altunkaynak, M. Holmes, B. D. Nelson, "Solving the LHC Inverse Problem with Dark Matter Observations," JHEP **0810**, 013 (2008). [arXiv:0804.2899 [hep-ph]].
- [2] N. Arkani-Hamed, G. L. Kane, J. Thaler *et al.*, "Supersymmetry and the LHC inverse problem," JHEP **0608**, 070 (2006). [hep-ph/0512190].
- [3] P. Binetruy, G. L. Kane, J. D. Lykken *et al.*, "Twenty-five questions for string theorists," J. Phys. G **G32**, 129-150 (2006). [hep-th/0509157].
- [4] S. L. Glashow, "Partial Symmetries of Weak Interactions," Nucl. Phys. **22**, 579-588 (1961).
- [5] S. Weinberg, "A Model of Leptons," Phys. Rev. Lett. **19**, 1264-1266 (1967).
- [6] A. Salam, "Weak and Electromagnetic Interactions," Originally printed in Svartholm: Elementary Particle Theory, Proceedings Of The Nobel Symposium Held 1968 At Lerum, Sweden, Stockholm 1968, 367-377.
- [7] H. Fritzsch, M. Gell-Mann, "Current algebra: Quarks and what else?," [hep-ph/0208010].
- [8] D. J. Gross, F. Wilczek, "Ultraviolet Behavior of Nonabelian Gauge Theories," Phys. Rev. Lett. **30**, 1343-1346 (1973).
- [9] D. J. Gross, F. Wilczek, "Asymptotically Free Gauge Theories. 1," Phys. Rev. **D8**, 3633-3652 (1973).
- [10] D. J. Gross, F. Wilczek, "Asymptotically Free Gauge Theories. 2.," Phys. Rev. **D9**, 980-993 (1974).
- [11] H. D. Politzer, "Reliable Perturbative Results for Strong Interactions?," Phys. Rev. Lett. **30**, 1346-1349 (1973).
- [12] H. D. Politzer, "Asymptotic Freedom: An Approach to Strong Interactions," Phys. Rept. **14**, 129-180 (1974).
- [13] S. R. Coleman, J. Mandula, "All Possible Symmetries Of The S Matrix," Phys. Rev. **159**, 1251-1256 (1967).
- [14] R. Haag, J. T. Lopuszanski, M. Sohnius, "All Possible Generators of Supersymmetries of the s Matrix," Nucl. Phys. **B88**, 257 (1975).
- [15] J. Wess, B. Zumino, "Supergauge Transformations in Four-Dimensions," Nucl. Phys. **B70**, 39-50 (1974).
- [16] J. Wess, B. Zumino, "A Lagrangian Model Invariant Under Supergauge Transformations," Phys. Lett. **B49**, 52 (1974).

- [17] S. Dimopoulos, H. Georgi, "Softly Broken Supersymmetry and SU(5)," Nucl. Phys. **B193**, 150 (1981)
- [18] P. Nath, R. L. Arnowitt, "Generalized Supergauge Symmetry as a New Framework for Unified Gauge Theories," Phys. Lett. **B56**, 177 (1975).
- [19] R. L. Arnowitt, P. Nath, B. Zumino, "Superfield Densities and Action Principle in Curved Superspace," Phys. Lett. **B56**, 81 (1975).
- [20] D. Z. Freedman, P. van Nieuwenhuizen, S. Ferrara, "Progress Toward a Theory of Supergravity," Phys. Rev. **D13**, 3214-3218 (1976).
- [21] S. Deser, B. Zumino, "Consistent Supergravity," Phys. Lett. **B62**, 335 (1976).
- [22] A. H. Chamseddine, R. L. Arnowitt, P. Nath, "Locally Supersymmetric Grand Unification," Phys. Rev. Lett. **49**, 970 (1982).
- [23] L. Girardello, M. T. Grisaru, "Soft Breaking of Supersymmetry," Nucl. Phys. **B194**, 65 (1982).
- [24] S. P. Martin, M. T. Vaughn, "Regularization dependence of running couplings in softly broken supersymmetry," Phys. Lett. **B318**, 331-337 (1993). [hep-ph/9308222].
- [25] B. Altunkaynak, M. Holmes, P. Nath *et al.*, "SUSY Discovery Potential and Benchmarks for Early Runs at  $\sqrt{s} = 7$  TeV at the LHC," Phys. Rev. **D82**, 115001 (2010). [arXiv:1008.3423 [hep-ph]].
- [26] J. Hubisz, J. Lykken, M. Pierini *et al.*, "Missing energy look-alikes with 100 pb<sup>-1</sup> at the LHC," Phys. Rev. **D78**, 075008 (2008). [arXiv:0805.2398 [hep-ph]].
- [27] H. K. Dreiner, M. Kramer, J. M. Lindert *et al.*, "SUSY parameter determination at the LHC using cross sections and kinematic edges," JHEP **1004**, 109 (2010). [arXiv:1003.2648 [hep-ph]].
- [28] H. Baer, A. Lessa, H. Summy, "Early SUSY discovery at LHC via sparticle cascade decays to same-sign and multimueon states," Phys. Lett. **B674**, 49-53 (2009). [arXiv:0809.4719 [hep-ph]].
- [29] J. Dietrich [ ATLAS Collaboration ], "The ATLAS discovery reach for SUSY models with early data," [arXiv:1005.2034 [hep-ex]].
- [30] N. Bhattacharyya, A. Datta, S. Poddar, "SUSY darkmatter at the LHC - 7 TeV," Phys. Rev. **D82**, 035003 (2010). [arXiv:1005.2673 [hep-ph]].
- [31] H. Baer, V. Barger, A. Lessa *et al.*, "Capability of LHC to discover supersymmetry with  $\sqrt{s} = 7$  TeV and 1 fb<sup>-1</sup>," JHEP **1006**, 102 (2010). [arXiv:1004.3594 [hep-ph]].
- [32] J. Alwall, P. Demin, S. de Visscher *et al.*, "MadGraph/MadEvent v4: The New Web Generation," JHEP **0709**, 028 (2007). [arXiv:0706.2334 [hep-ph]].
- [33] T. Sjostrand, S. Mrenna, P. Z. Skands, "PYTHIA 6.4 Physics and Manual," JHEP **0605**, 026 (2006). [hep-ph/0603175].
- [34] Developed by John Conway  
<http://www.physics.ucdavis.edu/~conway/research/software/pgs/pgs4-general.htm>

- [35] Developed by Baris Altunkaynak  
<http://nuweb.neu.edu/ialtunkaynak/heptools.html#parvicursor>
- [36] M. L. Mangano, M. Moretti and R. Pittau, "Multijet matrix elements and shower evolution in hadronic collisions:  $Wb\bar{b} + n$  jets as a case study," Nucl. Phys. B **632**, 343 (2002) [arXiv:hep-ph/0108069].
- [37] M. L. Mangano, M. Moretti, F. Piccinini *et al.*, "ALPGEN, a generator for hard multiparton processes in hadronic collisions," JHEP **0307**, 001 (2003). [hep-ph/0206293].
- [38] J. Pumplin, D. R. Stump, J. Huston *et al.*, "New generation of parton distributions with uncertainties from global QCD analysis," JHEP **0207**, 012 (2002). [hep-ph/0201195].
- [39] G. Aad *et al.* [ The ATLAS Collaboration ], "Expected Performance of the ATLAS Experiment - Detector, Trigger and Physics," [arXiv:0901.0512 [hep-ex]].
- [40] G. L. Bayatian *et al.* [ CMS Collaboration ], "CMS physics: Technical design report,"
- [41] J. Alwall, S. Hoeche, F. Krauss *et al.*, "Comparative study of various algorithms for the merging of parton showers and matrix elements in hadronic collisions," Eur. Phys. J. **C53**, 473-500 (2008). [arXiv:0706.2569 [hep-ph]].
- [42] G. Belanger, F. Boudjema, A. Pukhov *et al.*, "Dark matter direct detection rate in a generic model with micrOMEGAs 2.2," Comput. Phys. Commun. **180**, 747-767 (2009). [arXiv:0803.2360 [hep-ph]].
- [43] A. Djouadi, M. M. Muhlleitner, M. Spira, "Decays of supersymmetric particles: The Program SUSY-HIT (SUSpect-SdecaY-Hdecay-InTerface)," Acta Phys. Polon. **B38**, 635-644 (2007). [hep-ph/0609292].
- [44] P. Z. Skands, B. C. Allanach, H. Baer *et al.*, "SUSY Les Houches accord: Interfacing SUSY spectrum calculators, decay packages, and event generators," JHEP **0407**, 036 (2004). [hep-ph/0311123].
- [45] K Nakamura *et al.* [ Particle Data Group Collaboration ], "Review of particle physics," J. Phys. G **G37**, 075021 (2010).
- [46] A. Djouadi, M. Drees, J. L. Kneur, "Constraints on the minimal supergravity model and prospects for SUSY particle production at future linear  $e^+e^-$  colliders," JHEP **0108**, 055 (2001). [hep-ph/0107316].
- [47] C. Amsler *et al.* [ Particle Data Group Collaboration ], "Review of Particle Physics," Phys. Lett. **B667**, 1-1340 (2008).
- [48] M. Davier, A. Hoecker, B. Malaescu *et al.*, "Reevaluation of the hadronic contribution to the muon magnetic anomaly using new  $e^+e^- \rightarrow \pi^+\pi^-$  cross section data from BABAR," Eur. Phys. J. **C66**, 1-9 (2010). [arXiv:0908.4300 [hep-ph]].
- [49] T. C. Yuan, R. L. Arnowitt, A. H. Chamseddine *et al.*, "Supersymmetric Electroweak Effects on  $G-2(\mu)$ ," Z. Phys. **C26**, 407 (1984).

- [50] D. A. Kosower, L. M. Krauss, N. Sakai, "Low-Energy Supergravity and the Anomalous Magnetic Moment of the Muon," *Phys. Lett.* **B133**, 305 (1983).
- [51] J. L. Lopez, D. V. Nanopoulos, X. Wang, "Large  $(g-2)$ -mu in  $SU(5) \times U(1)$  supergravity models," *Phys. Rev.* **D49**, 366-372 (1994). [hep-ph/9308336].
- [52] U. Chattopadhyay, P. Nath, "Upper limits on sparticle masses from  $g-2$  and the possibility for discovery of SUSY at colliders and in dark matter searches," *Phys. Rev. Lett.* **86**, 5854-5857 (2001). [hep-ph/0102157].
- [53] T. Aaltonen *et al.* [CDF Collaboration], "Search for  $B_s^0 \rightarrow \mu^+ \mu^-$  and  $B_d^0 \rightarrow \mu^+ \mu^-$  decays with  $2 \text{ fb}^{-1}$  of  $p\bar{p}$  collisions," *Phys. Rev. Lett.* **100**, 101802 (2008). [arXiv:0712.1708 [hep-ex]].
- [54] E. Barberio *et al.* [Heavy Flavor Averaging Group Collaboration], "Averages of b-hadron and c-hadron Properties at the End of 2007," [arXiv:0808.1297 [hep-ex]].
- [55] M. Misiak, H. M. Asatrian, K. Bieri *et al.*, "Estimate of  $\mathcal{B}(\bar{B} \rightarrow X_s \gamma)$  at  $\mathcal{O}(\alpha_s^2)$ ," *Phys. Rev. Lett.* **98**, 022002 (2007). [hep-ph/0609232].
- [56] G. Degrandi, P. Gambino, G. F. Giudice, " $B \rightarrow X_s \gamma$  in supersymmetry: Large contributions beyond the leading order," *JHEP* **0012**, 009 (2000). [hep-ph/0009337].
- [57] F. Borzumati, C. Greub, T. Hurth *et al.*, "Gluino contribution to radiative B decays: Organization of QCD corrections and leading order results," *Phys. Rev.* **D62**, 075005 (2000). [hep-ph/9911245].
- [58] M. E. Gomez, T. Ibrahim, P. Nath *et al.*, "An Improved analysis of  $b \rightarrow s \gamma$  in supersymmetry," *Phys. Rev.* **D74**, 015015 (2006). [hep-ph/0601163].
- [59] N. Chen, D. Feldman, Z. Liu *et al.*, "SUSY and Higgs Signatures Implied by Cancellations in  $b \rightarrow s \gamma$ ," *Phys. Lett.* **B685**, 174-181 (2010). [arXiv:0911.0217 [hep-ph]].
- [60] N. Jarosik, C. L. Bennett, J. Dunkley *et al.*, "Seven-Year Wilkinson Microwave Anisotropy Probe (WMAP) Observations: Sky Maps, Systematic Errors, and Basic Results," [arXiv:1001.4744 [astro-ph.CO]].
- [61] Z. Ahmed *et al.* [CDMS Collaboration], "Search for Weakly Interacting Massive Particles with the First Five-Tower Data from the Cryogenic Dark Matter Search at the Soudan Underground Laboratory," *Phys. Rev. Lett.* **102**, 011301 (2009). [arXiv:0802.3530 [astro-ph]].
- [62] Z. Ahmed *et al.* [The CDMS-II Collaboration], "Dark Matter Search Results from the CDMS II Experiment," *Science* **327**, 1619-1621 (2010). [arXiv:0912.3592 [astro-ph.CO]].
- [63] E. Aprile *et al.* [XENON100 Collaboration], "First Dark Matter Results from the XENON100 Experiment," *Phys. Rev. Lett.* **105**, 131302 (2010). [arXiv:1005.0380 [astro-ph.CO]].
- [64] D. N. McKinsey [XENON Collaboration], "The XENON dark matter search," *AIP Conf. Proc.* **870**, 202-204 (2006).
- [65] D. Bauer, "SuperCDMS Development Project,"

- [66] H. Baer, C.-h. Chen, M. Drees *et al.*, “Probing minimal supergravity at the CERN LHC for large  $\tan\beta$ ,” *Phys. Rev.* **D59**, 055014 (1999). [hep-ph/9809223].
- [67] S. Abdullin *et al.* [ CMS Collaboration ], “Discovery potential for supersymmetry in CMS,” *J. Phys. G* **G28**, 469 (2002). [hep-ph/9806366].
- [68] R. L. Arnowitt, B. Dutta, T. Kamon *et al.*, “Detection of SUSY in the stau-neutralino coannihilation region at the LHC,” *Phys. Lett.* **B639**, 46-53 (2006). [hep-ph/0603128].
- [69] D. Feldman, Z. Liu, P. Nath, “The Landscape of Sparticle Mass Hierarchies and Their Signature Space at the LHC,” *Phys. Rev. Lett.* **99**, 251802 (2007). [arXiv:0707.1873 [hep-ph]].
- [70] E. Izaguirre, M. Manhart, J. G. Wacker, “Bigger, Better, Faster, More at the LHC,” *JHEP* **1012**, 030 (2010). [arXiv:1003.3886 [hep-ph]].
- [71] A. Corsetti, P. Nath, “Gaugino mass nonuniversality and dark matter in SUGRA, strings and D-brane models,” *Phys. Rev.* **D64**, 125010 (2001). [hep-ph/0003186].
- [72] U. Chattopadhyay, P. Nath, “ $b - \tau$  Unification,  $g_\mu - 2$ , the  $b \rightarrow s + \gamma$  Constraint and Nonuniversalities,” *Phys. Rev.* **D65**, 075009 (2002). [hep-ph/0110341].
- [73] G. L. Kane, J. D. Lykken, S. Mrenna *et al.*, “Theory motivated benchmark models and superpartners at the Tevatron,” *Phys. Rev.* **D67**, 045008 (2003). [hep-ph/0209061].
- [74] A. Birkedal-Hansen, B. D. Nelson, “Relic neutralino densities and detection rates with non-universal gaugino masses,” *Phys. Rev.* **D67**, 095006 (2003). [hep-ph/0211071].
- [75] H. Baer, A. Mustafayev, S. Profumo *et al.*, “Direct, indirect and collider detection of neutralino dark matter in SUSY models with non-universal Higgs masses,” *JHEP* **0507**, 065 (2005). [hep-ph/0504001].
- [76] S. F. King, J. P. Roberts, D. P. Roy, “Natural dark matter in SUSY GUTs with non-universal gaugino masses,” *JHEP* **0710**, 106 (2007). [arXiv:0705.4219 [hep-ph]].
- [77] A. Birkedal-Hansen, B. D. Nelson, “The Role of Wino content in neutralino dark matter,” *Phys. Rev.* **D64**, 015008 (2001). [hep-ph/0102075].
- [78] D. Feldman, Z. Liu, P. Nath, “Light Higgses at the Tevatron and at the LHC and Observable Dark Matter in SUGRA and D Branes,” *Phys. Lett.* **B662**, 190-198 (2008). [arXiv:0711.4591 [hep-ph]].
- [79] D. Feldman, Z. Liu, P. Nath, “Sparticles at the LHC,” *JHEP* **0804**, 054 (2008). [arXiv:0802.4085 [hep-ph]].
- [80] S. P. Martin, “Exploring compressed supersymmetry with same-sign top quarks at the Large Hadron Collider,” *Phys. Rev.* **D78**, 055019 (2008). [arXiv:0807.2820 [hep-ph]].
- [81] S. Bhattacharya, A. Datta, B. Mukhopadhyaya, “Non-universal gaugino and scalar masses, hadronically quiet tripletons and the Large Hadron Collider,” *Phys. Rev.* **D78**, 115018 (2008). [arXiv:0809.2012 [hep-ph]].

- [82] C. F. Berger, J. S. Gainer, J. L. Hewett *et al.*, “Supersymmetry Without Prejudice,” JHEP **0902**, 023 (2009). [arXiv:0812.0980 [hep-ph]].
- [83] K. Choi, H. P. Nilles, “The Gaugino code,” JHEP **0704**, 006 (2007). [hep-ph/0702146 [HEP-PH]].
- [84] B. Altunkaynak, P. Grajek, M. Holmes *et al.*, “Studying Gaugino Mass Unification at the LHC,” JHEP **0904**, 114 (2009). [arXiv:0901.1145 [hep-ph]].
- [85] B. Altunkaynak, B. D. Nelson, L. L. Everett *et al.*, “Phenomenological Implications of Deflected Mirage Mediation: Comparison with Mirage Mediation,” JHEP **1005**, 054 (2010). [arXiv:1001.5261 [hep-ph]].
- [86] M. Holmes, B. D. Nelson, “Dark Matter Prospects in Deflected Mirage Mediation,” JCAP **0907**, 019 (2009). [arXiv:0905.0674 [hep-ph]].
- [87] D. Feldman, G. Kane, R. Lu *et al.*, “Dark Matter as a Guide Toward a Light Gluino at the LHC,” Phys. Lett. **B687**, 363-370 (2010). [arXiv:1002.2430 [hep-ph]].
- [88] D. Feldman, Z. Liu, P. Nath *et al.*, “Multicomponent Dark Matter in Supersymmetric Hidden Sector Extensions,” Phys. Rev. **D81**, 095017 (2010). [arXiv:1004.0649 [hep-ph]].
- [89] P. Konar, K. T. Matchev, M. Park *et al.*, “How to look for supersymmetry under the lamppost at the LHC,” Phys. Rev. Lett. **105**, 221801 (2010). [arXiv:1008.2483 [hep-ph]].
- [90] I. Gogoladze, R. Khalid, S. Raza *et al.*, “LHC Accesible  $t - b - \tau$  Yukawa Unification with  $\mu < 0$ ,” [arXiv:1008.2765 [hep-ph]].
- [91] D. Feldman, Z. Liu, P. Nath, “Gluino NLSP, Dark Matter via Gluino Coannihilation, and LHC Signatures,” Phys. Rev. **D80**, 015007 (2009). [arXiv:0905.1148 [hep-ph]].
- [92] B. Altunkaynak, “Selecting the Optimal LHC Signatures for Distinguishing Models,” AIP Conf. Proc. **1200**, 766-769 (2010). [arXiv:0909.5246 [hep-ph]].
- [93] P. Nath, B. D. Nelson, H. Davoudiasl *et al.*, “The Hunt for New Physics at the Large Hadron Collider,” Nucl. Phys. Proc. Suppl. **200-202**, 185-417 (2010). [arXiv:1001.2693 [hep-ph]].
- [94] G. Aad *et al.* [ ATLAS Collaboration ], “Search for supersymmetry using final states with one lepton, jets, and missing transverse momentum with the ATLAS detector in  $\sqrt{s} = 7$  TeV  $pp$ ,” [arXiv:1102.2357 [hep-ex]].
- [95] G. L. Kane, J. D. Lykken, B. D. Nelson *et al.*, “Reexamination of electroweak symmetry breaking in supersymmetry and implications for light superpartners,” Phys. Lett. **B551**, 146-160 (2003). [hep-ph/0207168].
- [96] G. L. Kane, A. A. Petrov, J. Shao *et al.*, “Initial determination of the spins of the gluino and squarks at LHC,” J. Phys. G **G37**, 045004 (2010). [arXiv:0805.1397 [hep-ph]].
- [97] S. Yamamoto [ ATLAS Collaboration ], “Strategy for early SUSY searches at ATLAS,” [arXiv:0710.3953 [hep-ex]].

- [98] J. L. Kneur, G. Moultaka, "Inverting the supersymmetric standard model spectrum: From physical to Lagrangian gaugino parameters," *Phys. Rev.* **D59**, 015005 (1999). [hep-ph/9807336].
- [99] N. V. Krasnikov, "The Relation between pole and running masses for gluino and squarks," *Phys. Lett.* **B345**, 25-28 (1995).
- [100] R. L. Arnowitt, P. Nath, "SUSY mass spectrum in SU(5) supergravity grand unification," *Phys. Rev. Lett.* **69**, 725-728 (1992).
- [101] S. Bhattacharya, A. Datta, B. Mukhopadhyaya, "Non-universal gaugino masses: A Signal-based analysis for the Large Hadron Collider," *JHEP* **0710**, 080 (2007). [arXiv:0708.2427 [hep-ph]].
- [102] M. K. Gaillard, B. D. Nelson, Y. -Y. Wu, "Gaugino masses in modular invariant supergravity," *Phys. Lett.* **B459**, 549-556 (1999). [hep-th/9905122].
- [103] J. A. Bagger, T. Moroi, E. Poppitz, "Anomaly mediation in supergravity theories," *JHEP* **0004**, 009 (2000). [hep-th/9911029].
- [104] K. Choi, K. S. Jeong, K. -i. Okumura, "Phenomenology of mixed modulus-anomaly mediation in fluxed string compactifications and brane models," *JHEP* **0509**, 039 (2005). [hep-ph/0504037].
- [105] P. Binetruy, G. L. Kane, B. D. Nelson *et al.*, "Relating incomplete data and incomplete theory," *Phys. Rev.* **D70**, 095006 (2004). [hep-ph/0312248].
- [106] B. C. Allanach, M. Battaglia, G. A. Blair *et al.*, "The Snowmass points and slopes: Benchmarks for SUSY searches," *Eur. Phys. J.* **C25**, 113-123 (2002). [hep-ph/0202233].
- [107] M. Brhlik, G. L. Kane, "Measuring the supersymmetry Lagrangian," *Phys. Lett.* **B437**, 331-336 (1998). [hep-ph/9803391].
- [108] J. G. Branson *et al.* [ ATLAS and CMS Collaboration ], "High transverse momentum physics at the Large Hadron Collider: The ATLAS and CMS Collaborations," *Eur. Phys. J. direct* **C4**, N1 (2002). [hep-ph/0110021].
- [109] B. Altunkaynak, B. D. Nelson, L. L. Everett *et al.*, "Landscape of Supersymmetric Particle Mass Hierarchies in Minimal Supergravity and Deflected Mirage Mediation Models," [arXiv:1011.1439 [hep-ph]].
- [110] S. P. Martin, "A Supersymmetry primer," In \*Kane, G.L. (ed.): Perspectives on supersymmetry\* 1-98. [hep-ph/9709356].
- [111] D. J. H. Chung, L. L. Everett, G. L. Kane *et al.*, "The Soft supersymmetry breaking Lagrangian: Theory and applications," *Phys. Rept.* **407**, 1-203 (2005). [hep-ph/0312378].
- [112] R. Barbieri, S. Ferrara, C. A. Savoy, "Gauge Models with Spontaneously Broken Local Supersymmetry," *Phys. Lett.* **B119**, 343 (1982).

- [113] L. J. Hall, J. D. Lykken, S. Weinberg, "Supergravity as the Messenger of Supersymmetry Breaking," *Phys. Rev.* **D27**, 2359-2378 (1983).
- [114] S. K. Soni, H. A. Weldon, "Analysis of the Supersymmetry Breaking Induced by N=1 Supergravity Theories," *Phys. Lett.* **B126**, 215 (1983).
- [115] H. P. Nilles, "Supersymmetry, Supergravity and Particle Physics," *Phys. Rept.* **110**, 1-162 (1984).
- [116] A. Brignole, L. E. Ibanez, C. Munoz, "Towards a theory of soft terms for the supersymmetric Standard Model," *Nucl. Phys.* **B422**, 125-171 (1994). [hep-ph/9308271].
- [117] A. Brignole, L. E. Ibanez, C. Munoz *et al.*, "Some issues in soft SUSY breaking terms from dilaton / moduli sectors," *Z. Phys.* **C74**, 157-170 (1997). [hep-ph/9508258].
- [118] A. Brignole, L. E. Ibanez, C. Munoz, "Soft supersymmetry breaking terms from supergravity and superstring models," In \*Kane, G.L. (ed.): Perspectives on supersymmetry\* 125-148. [hep-ph/9707209].
- [119] L. Randall, R. Sundrum, "Out of this world supersymmetry breaking," *Nucl. Phys.* **B557**, 79-118 (1999). [hep-th/9810155].
- [120] G. F. Giudice, M. A. Luty, H. Murayama *et al.*, "Gaugino mass without singlets," *JHEP* **9812**, 027 (1998). [hep-ph/9810442].
- [121] M. Dine, W. Fischler, M. Srednicki, "Supersymmetric Technicolor," *Nucl. Phys.* **B189**, 575-593 (1981).
- [122] S. Dimopoulos, S. Raby, "Supercolor," *Nucl. Phys.* **B192**, 353 (1981).
- [123] M. Dine, W. Fischler, "A Phenomenological Model of Particle Physics Based on Supersymmetry," *Phys. Lett.* **B110**, 227 (1982).
- [124] C. R. Nappi, B. A. Ovrut, "Supersymmetric Extension of the SU(3) x SU(2) x U(1) Model," *Phys. Lett.* **B113**, 175 (1982).
- [125] L. Alvarez-Gaume, M. Claudson, M. B. Wise, "Low-Energy Supersymmetry," *Nucl. Phys.* **B207**, 96 (1982).
- [126] S. Dimopoulos, S. Raby, "Geometric Hierarchy," *Nucl. Phys.* **B219**, 479 (1983).
- [127] M. Dine, A. E. Nelson, "Dynamical supersymmetry breaking at low-energies," *Phys. Rev.* **D48**, 1277-1287 (1993). [hep-ph/9303230].
- [128] M. Dine, A. E. Nelson, Y. Shirman, "Low-energy dynamical supersymmetry breaking simplified," *Phys. Rev.* **D51**, 1362-1370 (1995). [hep-ph/9408384].
- [129] M. Dine, A. E. Nelson, Y. Nir *et al.*, "New tools for low-energy dynamical supersymmetry breaking," *Phys. Rev.* **D53**, 2658-2669 (1996). [hep-ph/9507378].
- [130] G. F. Giudice, R. Rattazzi, "Theories with gauge mediated supersymmetry breaking," *Phys. Rept.* **322**, 419-499 (1999). [hep-ph/9801271].

- [131] D. E. Kaplan, G. D. Kribs, M. Schmaltz, "Supersymmetry breaking through transparent extra dimensions," *Phys. Rev.* **D62**, 035010 (2000). [hep-ph/9911293].
- [132] Z. Chacko, M. A. Luty, A. E. Nelson *et al.*, "Gaugino mediated supersymmetry breaking," *JHEP* **0001**, 003 (2000). [hep-ph/9911323].
- [133] P. Langacker, G. Paz, L. -T. Wang *et al.*, "Z'-mediated Supersymmetry Breaking," *Phys. Rev. Lett.* **100**, 041802 (2008). [arXiv:0710.1632 [hep-ph]].
- [134] P. Langacker, G. Paz, L. -T. Wang *et al.*, "Aspects of Z-prime - mediated Supersymmetry Breaking," *Phys. Rev.* **D77**, 085033 (2008). [arXiv:0801.3693 [hep-ph]].
- [135] S. Kachru, R. Kallosh, A. D. Linde *et al.*, "De Sitter vacua in string theory," *Phys. Rev.* **D68**, 046005 (2003). [hep-th/0301240].
- [136] K. Choi, A. Falkowski, H. P. Nilles *et al.*, "Stability of flux compactifications and the pattern of supersymmetry breaking," *JHEP* **0411**, 076 (2004). [hep-th/0411066].
- [137] K. Choi, A. Falkowski, H. P. Nilles *et al.*, "Soft supersymmetry breaking in KKLT flux compactification," *Nucl. Phys.* **B718**, 113-133 (2005). [hep-th/0503216].
- [138] M. Endo, M. Yamaguchi, K. Yoshioka, "A Bottom-up approach to moduli dynamics in heavy gravitino scenario: Superpotential, soft terms and sparticle mass spectrum," *Phys. Rev.* **D72**, 015004 (2005). [hep-ph/0504036].
- [139] A. Falkowski, O. Lebedev, Y. Mambrini, "SUSY phenomenology of KKLT flux compactifications," *JHEP* **0511**, 034 (2005). [hep-ph/0507110].
- [140] H. Baer, E. -K. Park, X. Tata *et al.*, "Collider and Dark Matter Searches in Models with Mixed Modulus-Anomaly Mediated SUSY Breaking," *JHEP* **0608**, 041 (2006). [hep-ph/0604253].
- [141] H. Baer, E. -K. Park, X. Tata *et al.*, "Collider and Dark Matter Phenomenology of Models with Mirage Unification," *JHEP* **0706**, 033 (2007). [hep-ph/0703024].
- [142] K. Choi, K. S. Jeong, "Supersymmetry breaking and moduli stabilization with anomalous U(1) gauge symmetry," *JHEP* **0608**, 007 (2006). [hep-th/0605108].
- [143] K. Choi, K. S. Jeong, K. -I. Okumura, "Flavor and CP conserving moduli mediated SUSY breaking in flux compactification," *JHEP* **0807**, 047 (2008). [arXiv:0804.4283 [hep-ph]].
- [144] K. Choi, K. S. Jeong, T. Kobayashi *et al.*, "Little SUSY hierarchy in mixed modulus-anomaly mediation," *Phys. Lett.* **B633**, 355-361 (2006). [hep-ph/0508029].
- [145] R. Kitano, Y. Nomura, "A Solution to the supersymmetric fine-tuning problem within the MSSM," *Phys. Lett.* **B631**, 58-67 (2005). [hep-ph/0509039].
- [146] O. Lebedev, H. P. Nilles, M. Ratz, "A Note on fine-tuning in mirage mediation," [hep-ph/0511320].
- [147] A. Pierce, J. Thaler, "Prospects for Mirage Mediation," *JHEP* **0609**, 017 (2006). [hep-ph/0604192].

- [148] K. Choi, K. S. Jeong, T. Kobayashi *et al.*, “TeV Scale Mirage Mediation and Natural Little SUSY Hierarchy,” *Phys. Rev.* **D75**, 095012 (2007). [hep-ph/0612258].
- [149] L. L. Everett, I. -W. Kim, P. Ouyang *et al.*, “Deflected Mirage Mediation: A Framework for Generalized Supersymmetry Breaking,” *Phys. Rev. Lett.* **101**, 101803 (2008). [arXiv:0804.0592 [hep-ph]].
- [150] L. L. Everett, I. -W. Kim, P. Ouyang *et al.*, “Moduli Stabilization and Supersymmetry Breaking in Deflected Mirage Mediation,” *JHEP* **0808**, 102 (2008). [arXiv:0806.2330 [hep-ph]].
- [151] K. Choi, K. S. Jeong, S. Nakamura *et al.*, “Sparticle masses in deflected mirage mediation,” *JHEP* **0904**, 107 (2009). [arXiv:0901.0052 [hep-ph]].
- [152] G. L. Bayatian *et al.* [ CMS Collaboration ], “CMS technical design report, volume II: Physics performance,” *J. Phys. G* **G34**, 995-1579 (2007).
- [153] T. Gherghetta, G. F. Giudice, J. D. Wells, “Phenomenological consequences of supersymmetry with anomaly induced masses,” *Nucl. Phys.* **B559**, 27-47 (1999). [hep-ph/9904378].
- [154] A. Djouadi, M. Drees, J. -L. Kneur, “Updated constraints on the minimal supergravity model,” *JHEP* **0603**, 033 (2006). [hep-ph/0602001].
- [155] V. M. Abazov *et al.* [ D0 Collaboration ], “Search for squarks and gluinos in events with jets and missing transverse energy using 2.1 fb<sup>-1</sup> of p anti-p collision data at s<sup>1/2</sup> = 1.96-TeV,” *Phys. Lett.* **B660**, 449-457 (2008). [arXiv:0712.3805 [hep-ex]].
- [156] J. Alwall, M. -P. Le, M. Lisanti *et al.*, “Searching for Directly Decaying Gluinos at the Tevatron,” *Phys. Lett.* **B666**, 34-37 (2008). [arXiv:0803.0019 [hep-ph]].
- [157] D. S. M. Alves, E. Izaguirre, J. G. Wacker, “It’s On: Early Interpretations of ATLAS Results in Jets and Missing Energy Searches,” [arXiv:1008.0407 [hep-ph]].
- [158] E. Barberio *et al.* [ Heavy Flavor Averaging Group (HFAG) Collaboration ], “Averages of b-hadron properties at the end of 2006,” [arXiv:0704.3575 [hep-ex]].
- [159] V. M. Abazov *et al.* [D0 Collaboration], “Search for the rare decay  $B_s^0 \rightarrow \mu^+ \mu^-$ ,” *Phys. Lett. B* **693**, 539 (2010) [arXiv:1006.3469 [hep-ex]].
- [160] J. Dunkley *et al.* [ WMAP Collaboration ], “Five-Year Wilkinson Microwave Anisotropy Probe (WMAP) Observations: Likelihoods and Parameters from the WMAP data,” *Astrophys. J. Suppl.* **180**, 306-329 (2009). [arXiv:0803.0586 [astro-ph]].
- [161] D. Larson, J. Dunkley, G. Hinshaw *et al.*, “Seven-Year Wilkinson Microwave Anisotropy Probe (WMAP) Observations: Power Spectra and WMAP-Derived Parameters,” [arXiv:1001.4635 [astro-ph.CO]].
- [162] P. Salati, “Quintessence and the relic density of neutralinos,” *Phys. Lett.* **B571**, 121-131 (2003). [astro-ph/0207396].
- [163] M. Kamionkowski, M. S. Turner, “Thermal Relics: Do We Know Their Abundances?,” *Phys. Rev.* **D42**, 3310-3320 (1990).

- [164] N. Arkani-Hamed, A. Delgado, G. F. Giudice, "The Well-tempered neutralino," Nucl. Phys. **B741**, 108-130 (2006). [hep-ph/0601041].